DOE/NASA/0181
NASA CR-179559
GARRETT NO. 31-6190

BRAYTON CYCLE SOLARIZED ADVANCED GAS TURBINE

FINAL REPORT

Engineering Staff of
Garrett Turbine Engine Company
A Division of The Garrett Corporation
Phoenix, Arizona 85010

December 1986

Prepared for
NATIONAL AERONAUTICS AND SPACE ADMINISTRATION
Lewis Research Center
Cleveland, Ohio 44135
Under Contract DEN3-181

for
U.S. DEPARTMENT OF ENERGY
Office of Conservation and Solar Applications
Division of Transportation Energy Conservation
Washington, D.C. 20545

DOE/NASA/0181
NASA CR-179559
GARRETT NO. 31-6190

BRAYTON CYCLE SOLARIZED ADVANCED GAS TURBINE

FINAL REPORT

Engineering Staff of
Garrett Turbine Engine Company
A Division of The Garrett Corporation
Phoenix, Arizona 85010

December 1986

Prepared for
National Aeronautics and Space Administration
Lewis Research Center
Cleveland, Ohio 44135
Under Contract DEN3-181

for
U.S. DEPARTMENT OF ENERGY
Office of Conservation and Solar Applications
Division of Transportation Energy Conservation
Washington, D.C. 20545

FOREWORD

The authors wish to acknowledge the efforts of the engineering team at Sanders Associates, Incorporated, Nashua, New Hampshire, without whose cooperation this SAGT program could not have succeeded. Sanders Associates was responsible for the solar receiver, the power conversion assembly (PCA) support structure design and fabrication, and pretest of the receiver on the test bed concentrator. Sanders engineering also performed a checkout of the solar receiver prior to initiation of PCA testing at the Garrett Turbine Engine Company (GTEC) facilities in Phoenix, Arizona. Instructions were transmitted to the GTEC engineering staff for welding of the pipe fittings on the two duct junctions to the pressure vessel and sealing joints located elsewhere on the vessel. These contributions greatly aided successful hardware assembly and kept the program on target.

Government administration of this SAGT program was provided by the National Aeronautics and Space Administration Lewis Research Center (NASA/LeRC). The program was funded by the United States Department of Energy (DOE).

TABLE OF CONTENTS

TABLE OF CONTENTS (Contd)

LIST OF FIGURES

LIST OF FIGURES (Contd)

LIST OF FIGURES (Contd)

LIST OF FIGURES (Contd)

LIST OF FIGURES (Contd)

LIST OF FIGURES (Contd)

LIST OF FIGURES (Contd)

LIST OF TABLES

LIST OF TABLES (Contd)

1.0 SUMMARY

Garrett Turbine Engine Company (GTEC), under Contract DEN3-181 (NASA/DOE), was successful in developing the heat engine (regenerated gas turbine) for a Brayton Engine/Generator Set (BE/G) for solar thermal to electrical power conversion. The program objectives of designing, fabricating, assembling, and testing the SAGT-1A Power Conversion Assembly (PCA) were met. The PCA development was closely tied to the AGT101 development, Contract DEN3-167 (NASA/DOE), since the metal version of this automotive gas turbine was used in the SAGT-1A with only minor modifications. Rotor dynamic problems experienced in the AGT101 delayed the SAGT-1A schedule (at no cost). Prior to this delay, the engine support structure had been designed and procured. Assembly of the PCA, including all engine support systems (air, oil, and fuel system plumbing) and electrical cables and harnesses, had also been completed.

When the metal AGT101 successfully completed its characterization test--a contract milestone completed in January 1985--the SAGT-1A program was given the go-ahead to restart development and ship the PCA to Sandia National Laboratory for test bed concentrator (TBC) tests. The SAGT-1A system was motored for the first time in June of the same year, resulting in excessive belt vibration which caused a foil bearing failure in the engine. Rotor-dynamic bearing problems were subsequently eliminated by adding a stabilizer bar to the PCA to react the higher start torque exerted on the belt drive system. The only other major change made to the PCA was replacing the 110-vac fuel pump electric motor with a 12-vdc motor, which eliminated an intermittent fuel delivery problem.

January of 1986 was a banner month for the SAGT-1A development program as two demonstration tests, 10 hours of run time, and 25 starts were successfully completed. The SAGT-1A and supporting equipment were shipped to Sandia in March 1986.

The metal AGT101 was never intended to meet the performance goals set by the Department of Energy for solar thermal to electrical power conversion systems. Output of the SAGT is estimated to increase up to 20 kW with the ceramic gas turbine, which is currently under development. When available, this ceramic power section will meet the DOE heat engine efficiency goal of 35 to 41 percent.

This Page Intentionally Left Blank

2.0 INTRODUCTION

This final report was prepared and submitted by Garrett Turbine Engine Company (GTEC) in accordance with the requirements of NASA-LeRC/DOE, Contract DEN3-181, Exhibit A, paragraph E, Task V - Report of Work. This report covers the period February 1980 through March 1986. The program objective was to design, fabricate, assemble, and test a small, hybrid, regenerated 20-kW Brayton-engine-powered generator set (BE/G). The generator set, also known as a power conversion assembly (PCA), is designed to operate with solar energy obtained from a parabolic dish concentrator, and/or with fossil energy supplied by burning fuel in a combustor.

This development program was administrated by NASA and funded by the United States Department of Energy (DOE). The DOE is developing the heat engines for solar thermal applications, such as dispersed solar to electric power generation systems like the one shown in Figure 1. These power generation systems use a renewable energy source to decrease United States dependence on depletable energy sources.

Power conversion assemblies would be deployed in the size of about 25 to 50 kW_e, which is consistent with concentrator development in the 11- to 15-meter diameter range.

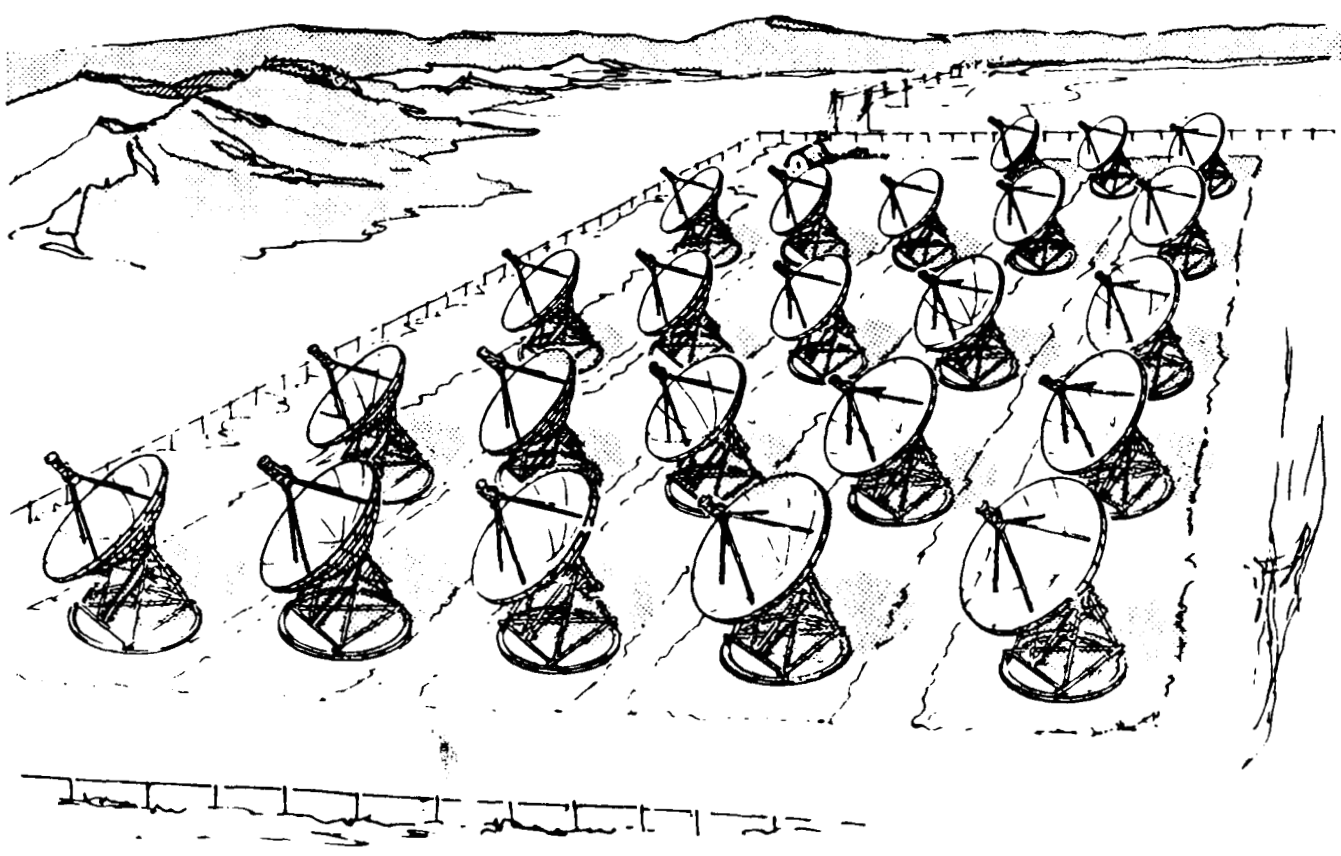

GB6-042-1

Figure 1. Artistic Conception of Dispersed Solar Thermal Power Generation Systems.

The DOE has set heat engine performance and cost goals of 35-percent efficiency and $\$1000/kW_e$ for the interim (circa 1995) and 41-percent efficiency and $\$300/kW_e$ for the long-term (early twenty-first century).

Initially, the contract called for use of the GTEC Model GTP36-51 (recuperated gas turbine) as the power section, which was designated the Mod "O" system. During the design phase of the Mod "O" system, an alternate power section, the AGT101, was selected. The eventual automotive productionizing of this power section would increase the probability of meeting the DOE cost goals for solar thermal heat engines. The Mod "O" system design is presented in this report in Appendix A. The contract redirection to the SAGT-1A (AGT101 power section) was officially completed by Contract Modification No. 5, dated February 4, 1982.

This report covers design and testing of the SAGT power section, and in-house testing of the SAGT-1A PCA system. The design description includes all power section support systems, major components, and performance. It also includes the PCA system performance and support equipment. The testing reported includes power section tests and in-house system tests (fuel mode only).

This report also assesses the ceramic SAGT in terms of its performance, cost, and design life to facilitate NASA and DOE future planning for Brayton heat engines in solar dynamic modules.

3.0 POWER CONVERSION ASSEMBLY DESIGN

The SAGT-1A Power Conversion Assembly (PCA) is designed to generate electricity (480 vac, 3 phase at 60 hertz) from solar energy when installed on an 11-meter-diameter parabolic dish of mirrors (Figure 2), designated a test bed concentrator (TBC). The PCA, shown in Figures 3 and 4, consists of the following major components:

- GTEC SAGT power section, P/N 3609092-1, which uses the AGT101 power section (P/N PA3610110-1) shown in Figure 5, with the combustor adapter installed per Figure 6.
- Sanders solar receiver, Sanders P/N 4024056, which is a ceramic heat exchanger designed to transmit solar thermal energy into the pressurized engine airflow between the regenerator discharge and combustor inlet.
- General Electric 25-kW Induction Motor/Generator, Type No. GE-5KS 286 JL 205, electrically tied into a utility grid and used to start the engine, and then driven to slightly above synchronous speed to generate power into the grid.
- Interconnecting ducts, P/Ns 3608922-1 and 3608922-2, capable of operating at 1600F (see Figure 7) and provided with flexible bellows sections to allow for thermal growth.
- PCA ancillary components to monitor operating conditions, and to supply air, oil, and fuel to the major components.

The assembled PCA weight and the center of gravity (cg) were experimentally determined to be:

Weight = 1665 pounds

cg = 11.5 inches, measured from the PCA mounting surface toward the motor/generator

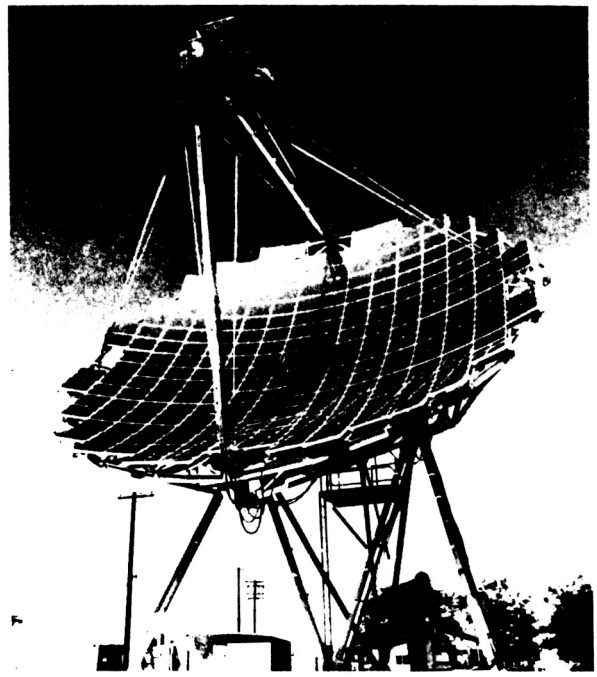

GB6-042-2

Figure 2. Parabolic Dish (11-meter diameter) Used to Demonstrate SAGT-1A Readiness for Solar Thermal Power Conversion.

These components will be discussed in greater detail in the following paragraphs.

3.1 PCA Ancillary Component Design

In general, the PCA ancillary components were procured off-the-shelf and installed on the PCA support structure. Interconnecting lines were installed to service the power section with air, oil, and fuel. To assist in servicing the ancillary components, photographs were taken of these components at the time of the customer demonstration test. These photographs, together with pertinent schematics, are reproduced as figures that accompany the component descriptions provided in the paragraphs that follow.

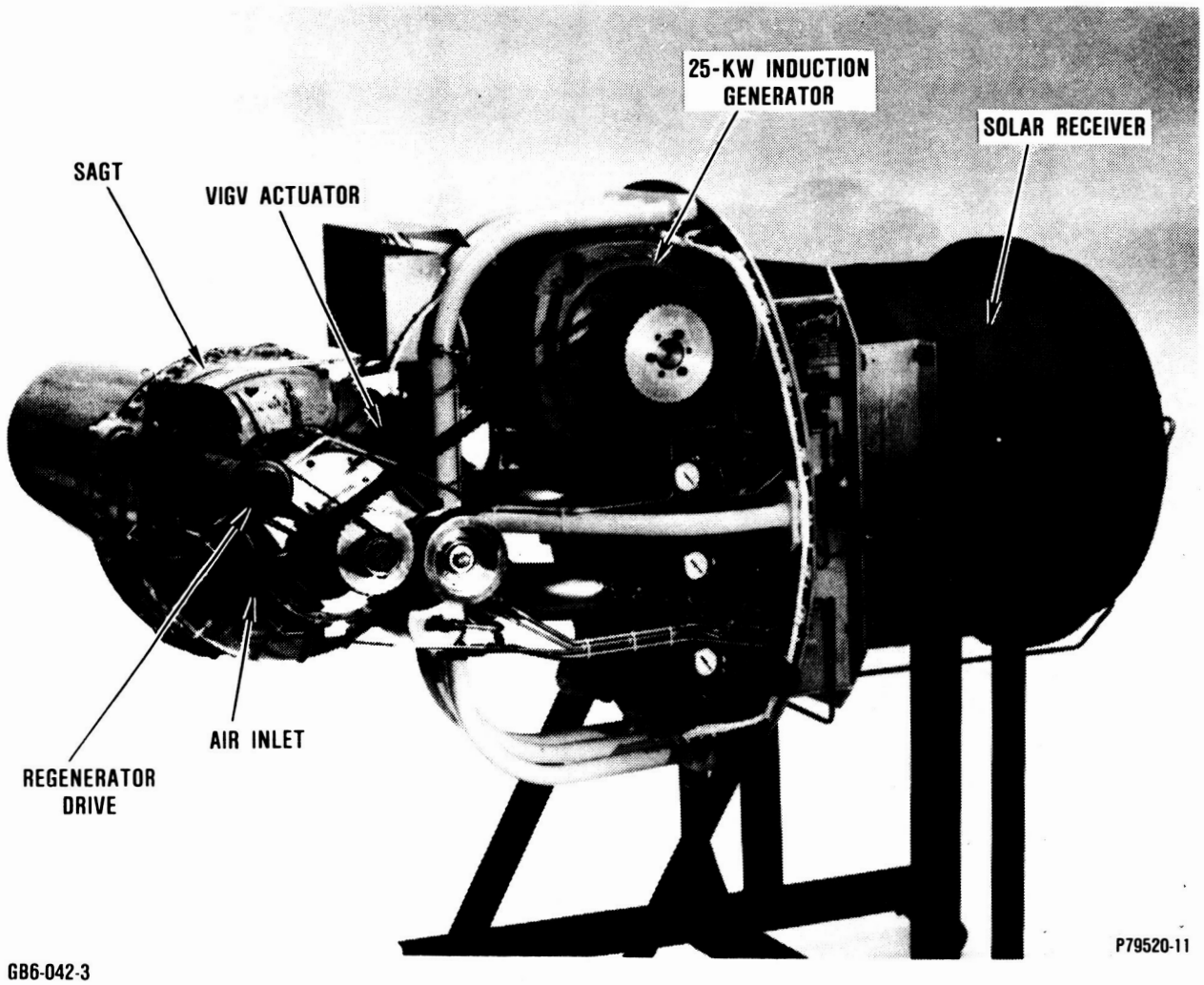

Figure 3. Power Conversion Assembly, Front View.

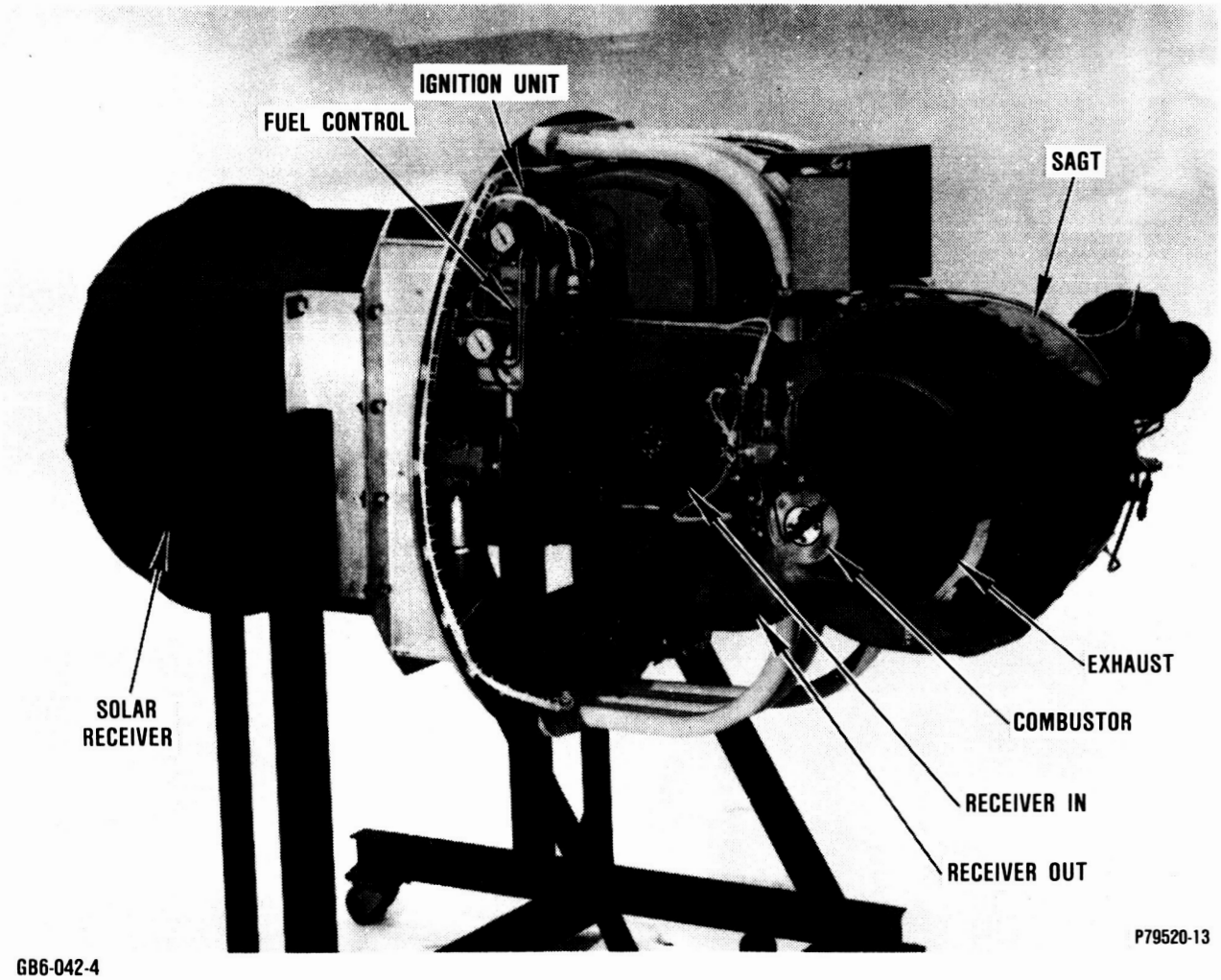

Figure 4. Power Conversion Assembly, Aft View.

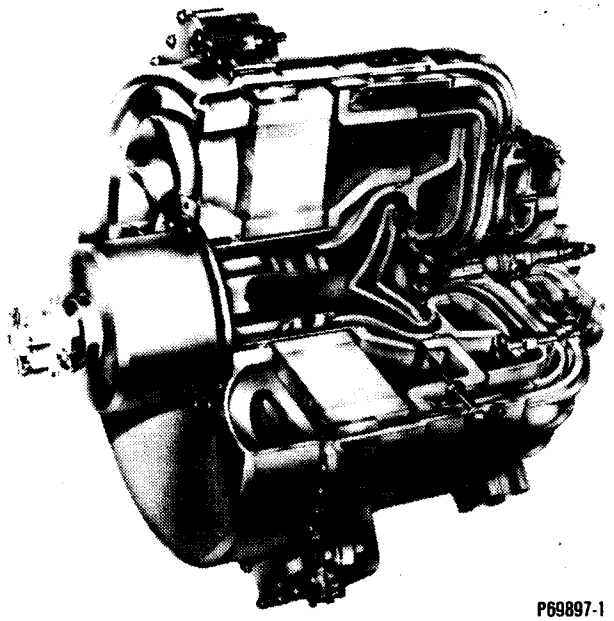

P69897-1

G86-042-5

Figure 5. AGT101 Automotive Gas Turbine Engine.

3.1.1 Power Section Support Systems

3.1.1.1 Air Supply Components

- A supply line (60 psig) into the PCA with a last chance filter at the PCA inlet (Figure 8).
- A regulated supply line to the combustor area teed to air-assist and purge-air locations, both feeding into the fuel nozzle. This line is bias regulated to 5 psig above compressor discharge pressure (Figures 9 and 10).
- A supply line directly into the foil bearing cooling air location (Figure 10).
- A supply line into the gearbox buffer seal area, regulated to 12 psig. Loss of pressure (<5 psig) in this line is cause for automatic system shutdown (Figure 11).
- A supply line for cooling the solar receiver window flange (Figure 12).

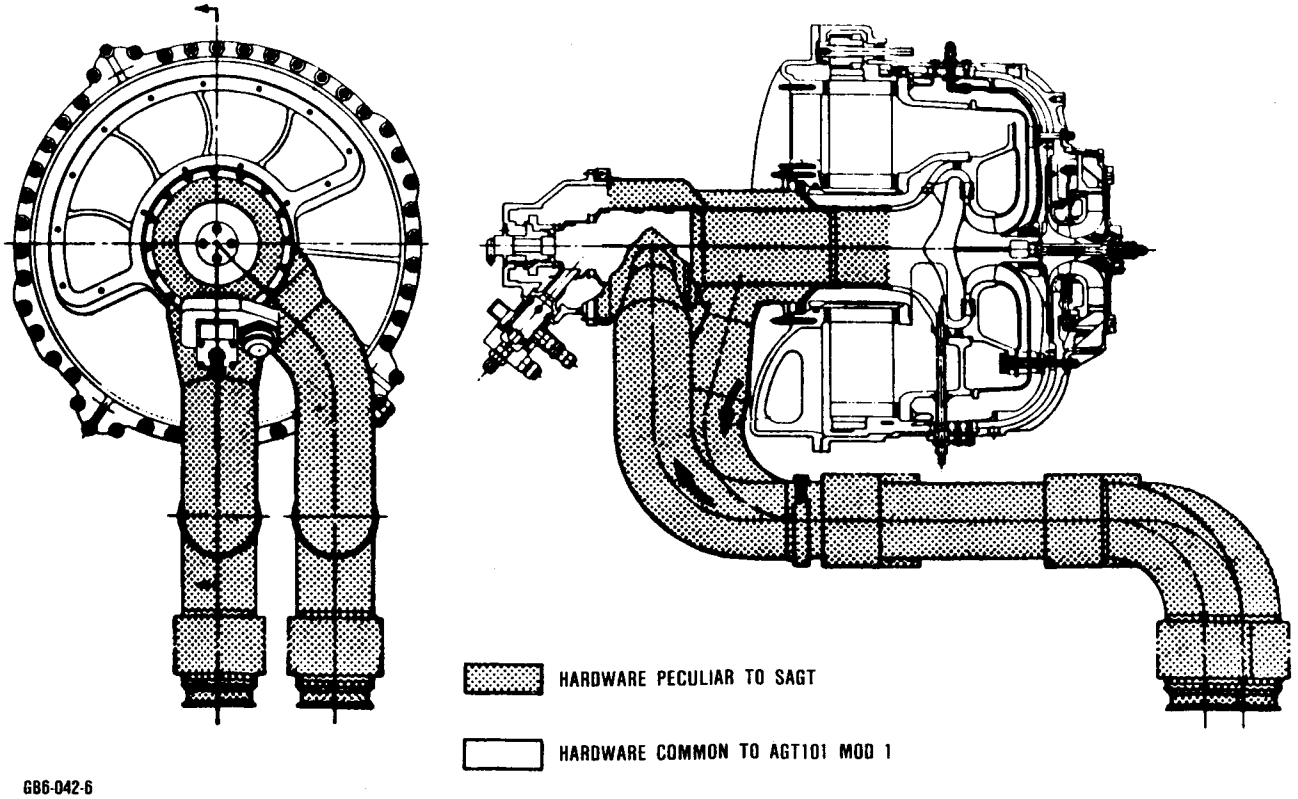

G86-042-6

Figure 6. Minor Changes Required to Adapt the AGT101 Power Section for the SAGT.

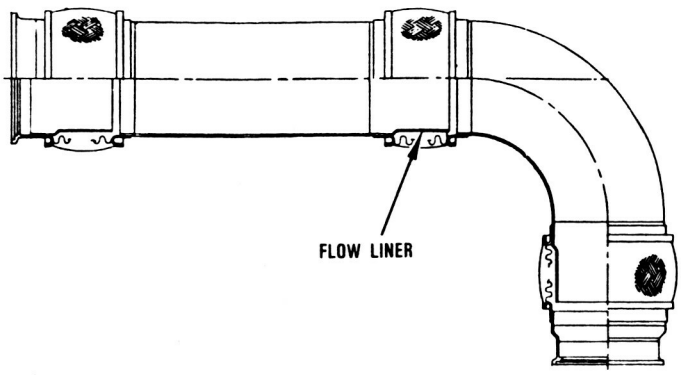

GB6-042-7

Figure 7. Flexible High-Temperature [1600F (871C)] Ducts Allow for Thermal Growth.

GB6-042-9

Figure 9. Fuel Control.

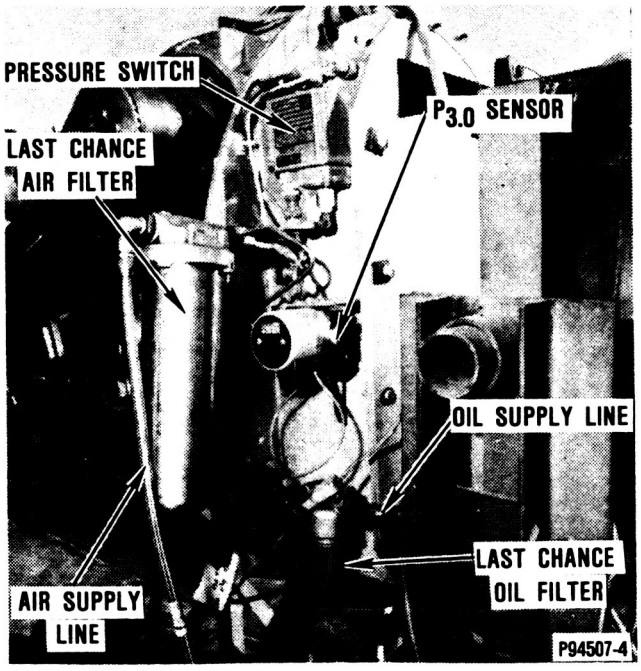

GB6-042-8

Figure 8. Air and Oil Supply Lines.

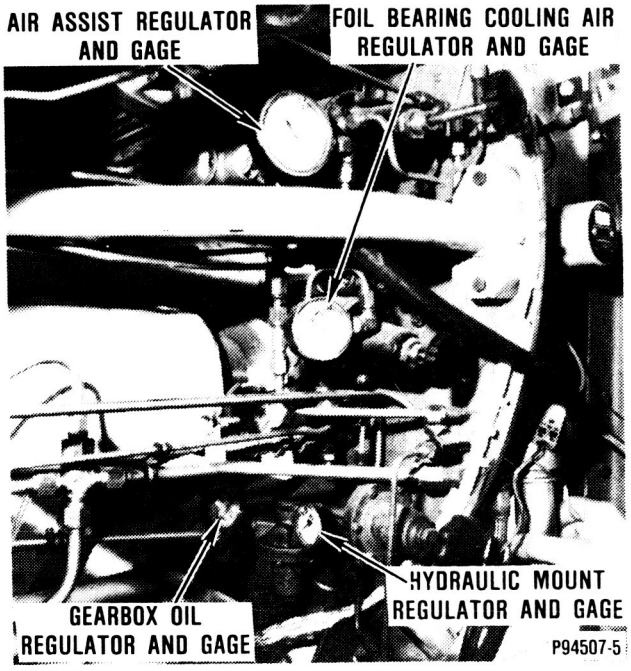

GB6-042-10

Figure 10. Air and Oil Regulators.

GB6-042-13

Figure 11. Oil Supply and Scavenge Lines.

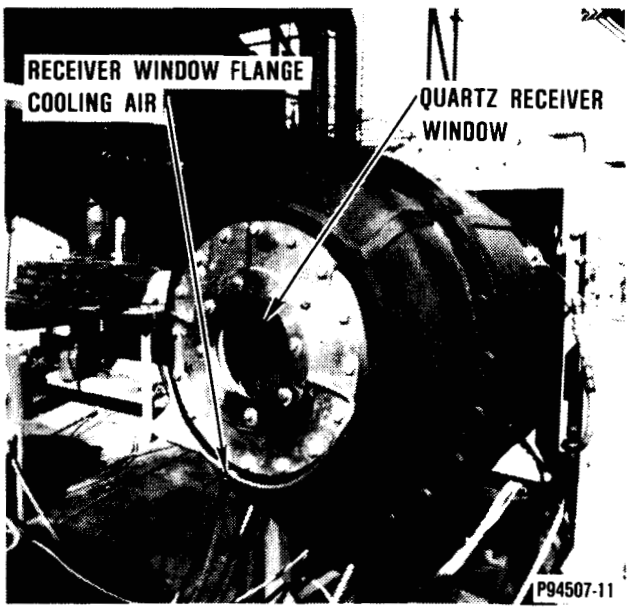

GB6-042-11

Figure 12. Ceramic Solar Receiver.

3.1.1.2 Fuel Supply Components

- Fuel pump and associated control equipment (Figures 9 and 13).

The fuel schematic is shown in Figure 14.

3.1.1.3 Oil Supply Components

The lube schematic is shown in Figure 15.

- A supply line (~25 psig) with a last chance filter (Figure 8).
- A supply line feeding directly into the inlet guide vane (IGV) actuator (Figure 16).
- A 60-psig-regulated lubricant supply line to the hydrodynamic thrust bearing and hydraulic mount line into the gearbox (Figure 15).
- A 25-psig-regulated supply line for gearbox bearing lubrication, with a teed line to

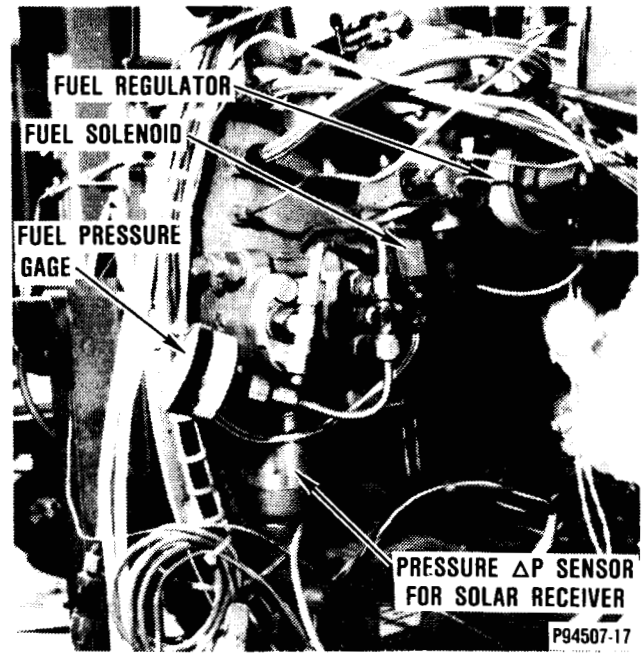

GB6-042-12

Figure 13. Fuel Pump.

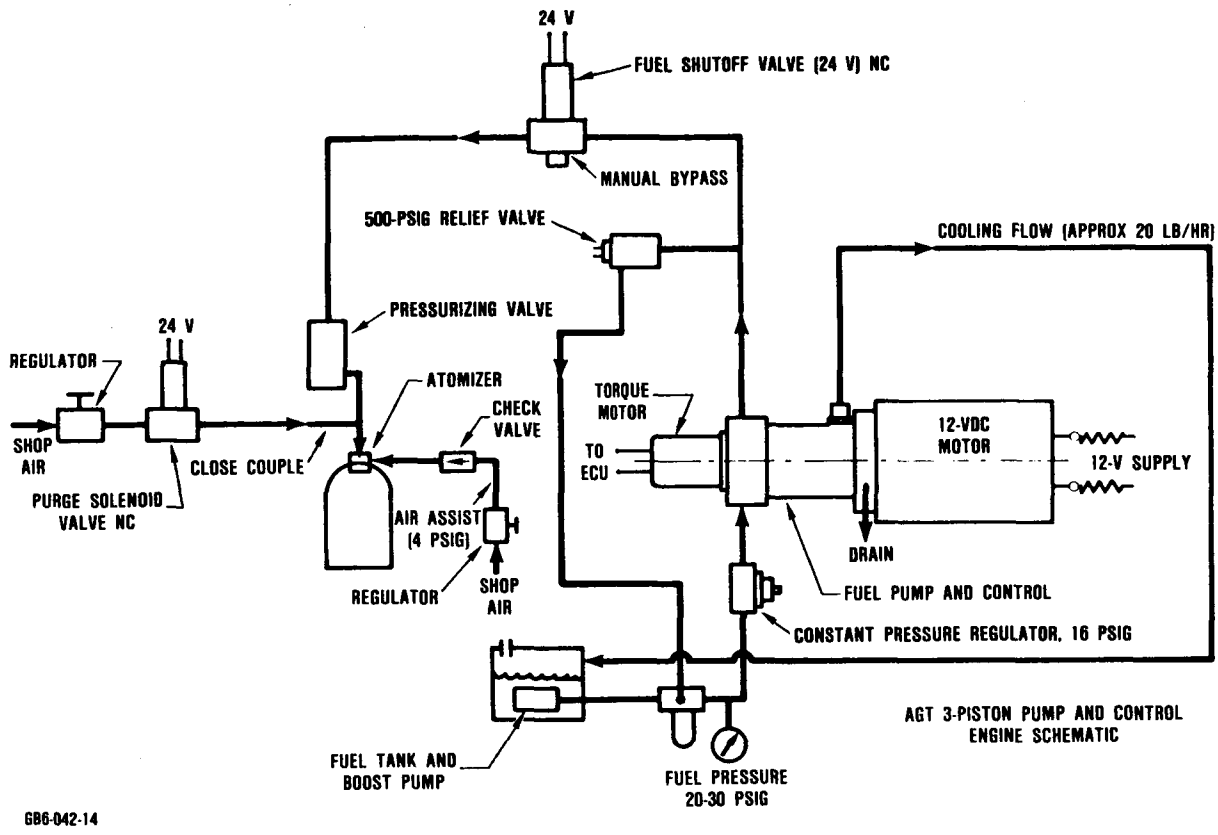

Figure 14. Schematic for Fuel Delivery to the Atomizer (Fuel or Hybrid Mode).

supply rotor ball bearing lubrication (Figure 15).

- A lubrication cart (Figure 17) to be mounted to the alidade.

3.1.1.4 Oil Scavenge Components

- A return line from the IGV actuator (Figure 11).
- Three scavenge lines teed together and covering 90 degrees of the gearbox housing (Figure 11).
- A scavenge line from the hydrodynamic thrust bearing (Figure 11).

3.1.1.5 Vent Components

- Vent lines from the gearbox and regenerator drive gearbox and/or seal drain line from the IGV actuator teed into one line which vents into a collector (Figure 17).

3.1.2 Master Control Panel Components

The numerous features of the master control panel are defined in Table 1 and illustrated in Figure 18. This panel is sufficient to start, operate, and monitor the health of the SAGT-1A PCA during testing. To start the PCA, the operator need only activate the system switches in numerical order as follows:

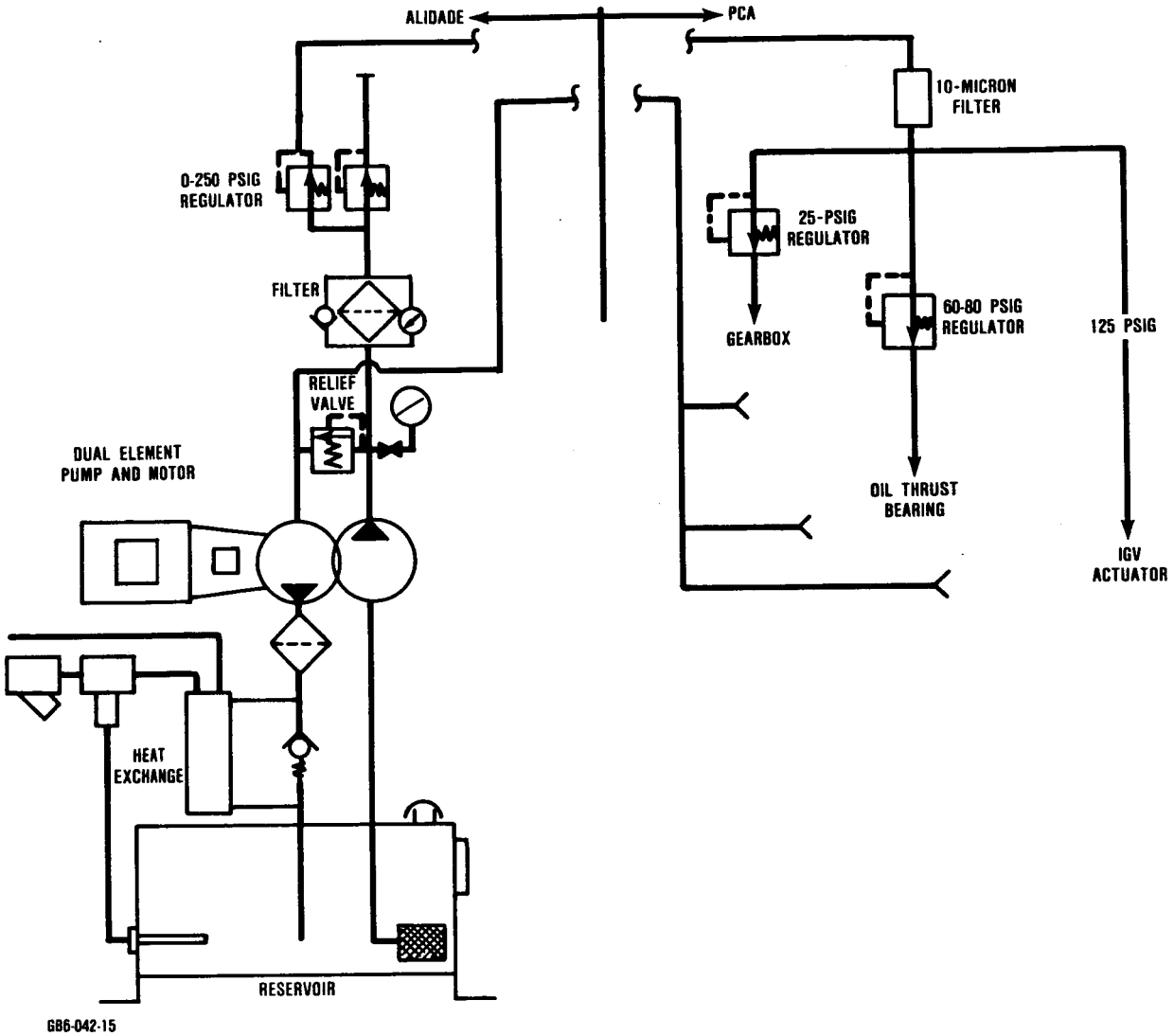

Figure 15. Schematic of Lubrication Cart and Regulation System in the PCA.

1) Select the operating mode: solar mode (switch 1A), fuel mode (switch 1B), or hybrid mode (switches 1A and 1B)

2) Start compressor seal airflow

3) Start lubrication fluid flow

4) Turn on 28-vdc power supply

5) Activate Alarm/Fault Circuits (No fault indicator lights should be on at this point; if any are, resolve problems to clear fault.)

6) Set Run/Stop Switch to Run

7) Start fuel boost pump to supply 25 ±5 psig fuel pressure to fuel control

8) Push start button

9) When engine rotation is indicated on SPEED A or B readouts, open collector door [unless fuel mode (switch 1B) has been selected]

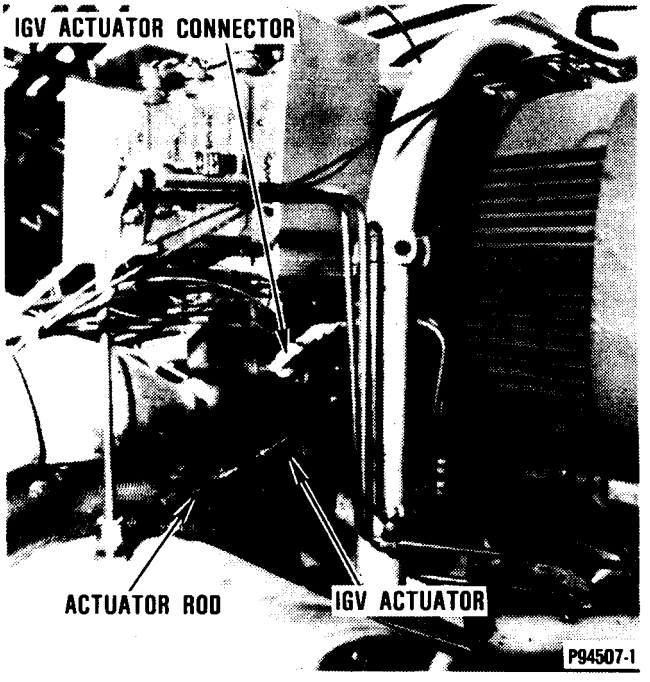

GB6-042-16

Figure 16. VIGV Actuator System.

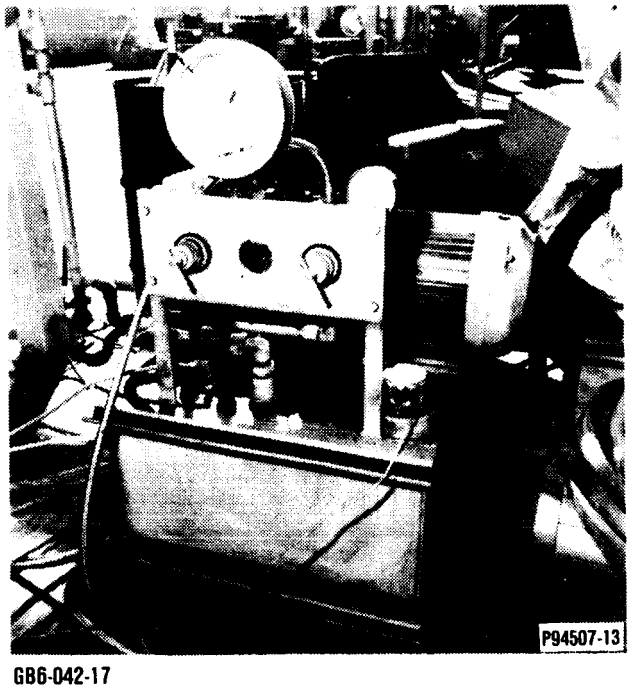

GB6-042-17

Figure 17. Lubrication Cart.

Table 1. Control Panel Features.

1. Instrumentation Readouts

   Speed A, krpm
   Speed B, krpm
   $T_{4.1}$, F
   $T_{5.1}$, F
   $T_{3.7}$, F
   Fuel Command, percent
   $T_{4.1}$ Set Point, F
   $P_{3.0}$, psia
   IGV Position, inches

2. Fault Indicator Lights (left to right)

   Overspeed
   Underspeed
   Overtemperature
   Low oil temperature
   Hot oil temperature
   No flame
   (Spare)
   Compressor seal air

3. Switch Functions

   1A Solar Mode Select
   1B Fuel Mode Select
   2 Compressor seal air
   3 Lubrication pump relay
   4 ECU power
   5 Alarm/start enable
   6 Run/stop
   7 Fuel pump relay
   8 Start
   9 Collector door relay

4. Power Line Test Buttons

   120vac(toptobottom;lefttoright)
   Fuel pump
   Starter/generator
   Compressor seal air

   28 vdc
   ECU power
   Starter/generator relay
   Collector door relay

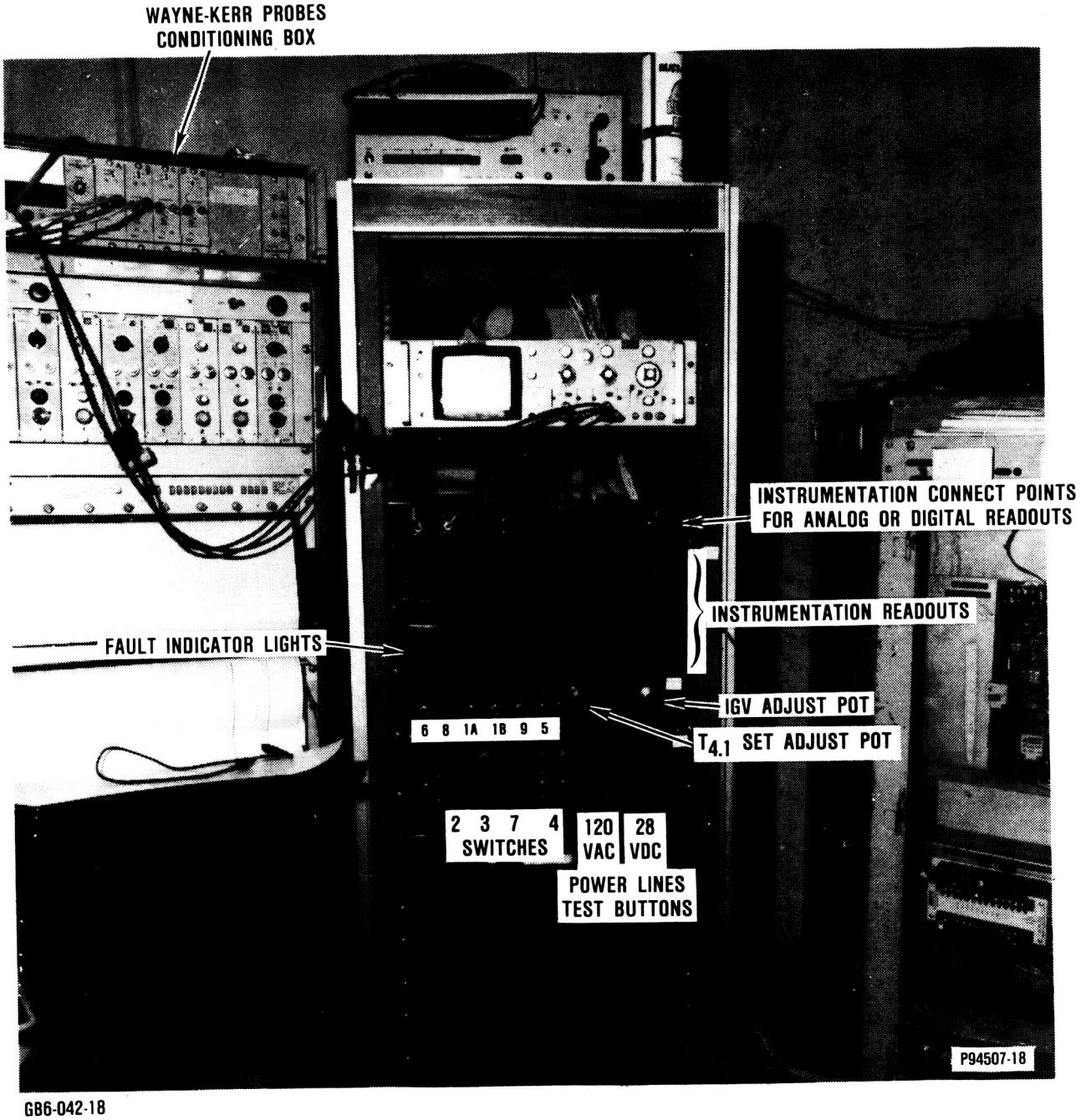

GB6-042-18

Figure 18. Master Control Panel Allows PCA Start, Operation, and Monitoring.

3.1.3 Electrical Enclosure Components

The electrical equipment, including motor starters, circuit breakers, relays, and power supplies, are shown in Figure 19. These components are described in more detail in Table 2. The enclosure and GE induction motor are also described for completeness. The components were wired by GTEC per the wiring diagram, Drawing 305435.

3.2 Power Section Design

Since the SAGT power section is nearly identical to the AGT101 power section (except for the ducting and adapter shown in Figure 6), the latter design will be described herein.

The AGT101 power section (Figure 20) is characterized by a single-stage 5:1 backward-swept centrifugal compressor and a single-stage ceramic radial inflow turbine mounted on a common shaft.

The centrifugal compressor and radial turbine are coupled using proven curvic coupling technology, loaded through an axially stretched tie-bolt. The rotating group is supported at the compressor end by a hydraulically mounted, angular contact, 0.59-inch (15-mm) ball bearing, with the axial rotor load reacted by an oil-film thrust bearing, and by a gas-lubricated foil bearing [1.35-inch (34.3-mm) diameter] between the turbine and compressor. The thickness of each of the seven foils is 0.007 inch (0.18 mm) including coating. At maximum power, the foil bearing load is approximately 2 psi (13.8 kPa) based on a projected area calculated as the product of the diameter and the length. The bearing power loss is 150 watts at maximum power.

AGT critical speed analyses were completed. The first, second, and third critical speeds have been calculated to occur at 5,850; 38,260; and 135,200 rpm. Bearing stiffnesses of 4000 lb/in. (700 N/mm) for the foil bearing and 25,000 lb/in. (4378 N/mm) for the hydraulically mounted ball bearing were used in the analyses. The first and second critical speeds are predominately rigid body modes. GTEC experience shows that with hydraulically mounted bearings, these modes are sufficiently damped to allow transient operation through the first and second critical speeds with acceptable bearing loads and shaft excursions. The third critical speed is 35.2 percent above the maximum operating speed, which gives adequate margins based on GTEC experience.

Structural design of the AGT101 is characterized by simple symmetrical structures (except the flow separator housing) and a flow path arranged to keep the lowest temperature gas outermost to minimize heat loss. Material composition of the structural and rotor components is summarized in Table 3. The structural load path, as depicted in Figure 21, originates at the combustor dome. A mechanical spring load of approximately 150 lb (667 N) is applied to the combustor dome to hold the structural components in position when the engine is not operating. This spring load, combined with the aerodynamic loads across the individual components, is transmitted through the combustor inner liner to the turbine transition duct, across the three struts, through the combustor baffle and turbine backshroud to the turbine stator, across the stator vane leading edge section to the turbine shroud conical webs, through the shroud bolts to the flexmount ring and into the compressor backshroud, and then to the compressor housing. Table 4 summarizes the power section salient features; additional information on the AGT101 program is provided in Appendix B.

3.2.1 Compressor Stage Design

The AGT101 compressor stage comprises a single-stage backward-swept titanium centrifugal impeller having 12 full blades and 12 splitter blades; a three-stage radial diffuser with one stage of diffusion vanes and two stages of deswirl vanes; and an upstream set of 17 variable inlet guide vanes (VIGVs). Current performance predictions of this compressor stage at maximum power operating condition are as follows:

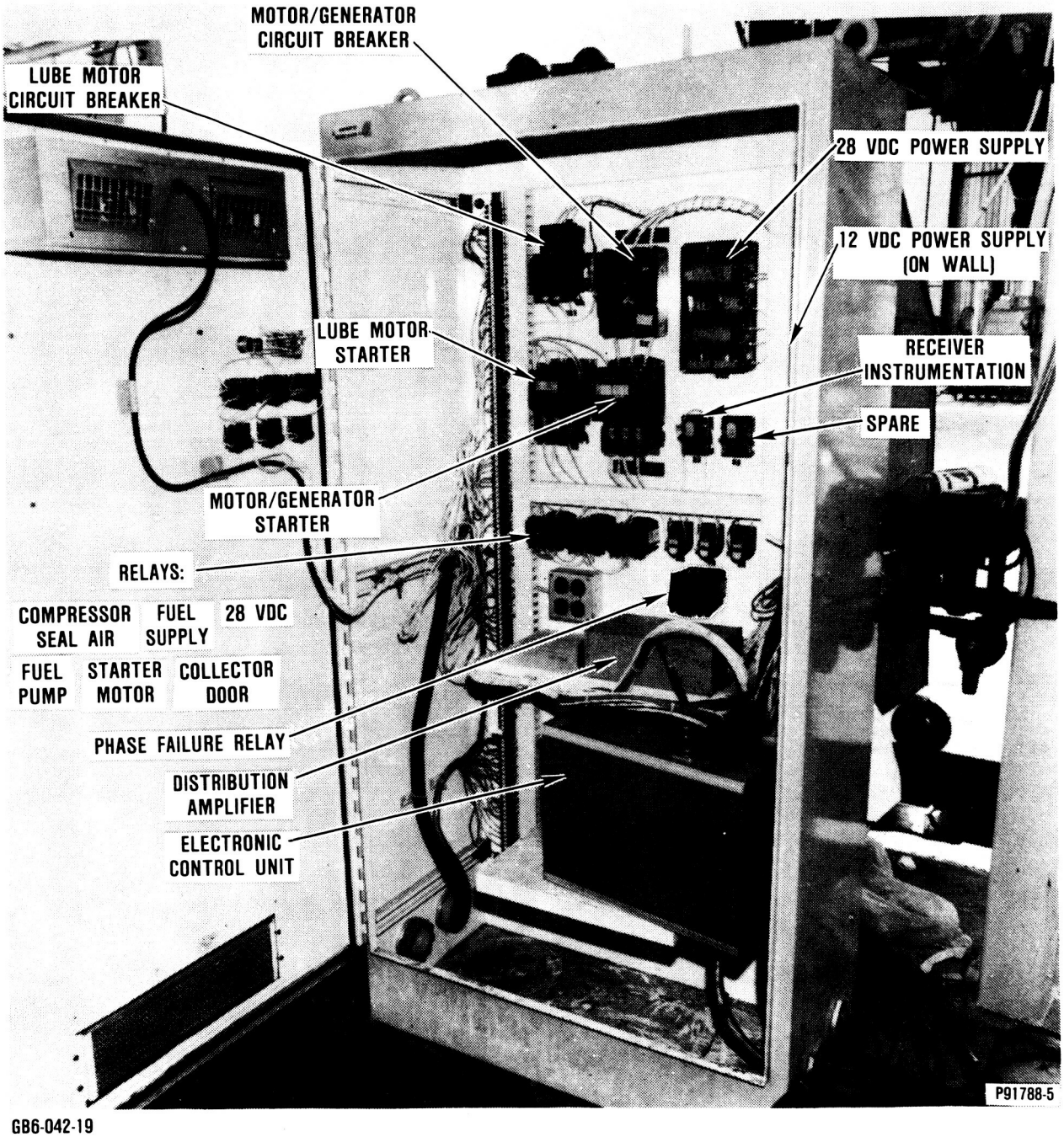

G86-042-19

Figure 19. Electrical Equipment Is Located in Equipment Enclosure.

Table 2. Electrical Equipment Description.

Component	Description	Manufacturer/Part No.
Lube Pump Motor Starter, 460 vac, 3ϕ	NEMA Class, 8536 Type SBO-2 (Size O, 3 pole, open type) 120 vac coil w/3ea B11.5 melting alloy therm units	Square D/SBO-2, Size O
Motor/Starter Induction Motor Starter, 460 vac, 3ϕ	NEMA Class, 8536 Type SDO-1 (Size 2, 3 pole, open type) 120 vac coil w/3ea B79 melting alloy therm units	Square D/SDO-1, Size 2
Lube Pump Motor Circuit Breaker	3 pole, 15 amp, 277/480 vac	Square D/EHB 34015
Motor (Induction) Circuit Breaker	3 pole, 50 amp, 277/480 vac	Square D/EHB 34050
20 vdc Relay ECU Input (K3)	NEMA Class 8501, Type GO-20 w/120 vac coil	Square D/GO-20
Output Control Relay (K4, K5, K6)	NEMA Class 8501, Type CDO-1 w/24 vdc coil	Square D/CDO-1
120 vac Relay (K1, K2)	NEMA Class 8501, Type GO-30 w/120 vac coil	Square D/GO-30
Electrical Enclosure	NEMA Type 12, free-standing single door enclosure 72 x 32 x 18 inches with 60 x 32 inch panel	Hoffman/A723618FS w/A72P36F1
Induction Motor	286 TC aluminum frame 1840 rpm at full load 460v-3 phase-60 Hz rated power 25 kW (33.5 hp) 92 percent efficiency at 0.865 average power factor	General Electric/ GE-SKS 286JL205
Phase Failure Relay	460 vac, 60 Hz 75-100T of rated voltage dropout adjustment 5 amps contact rating solid state sensor	Wilmar/1004X
12 vdc Power Supply (Fuel Pump Motor)	12 vdc, 15 amp overvolt protection 120 vac power input	Delta/EP4E-120V

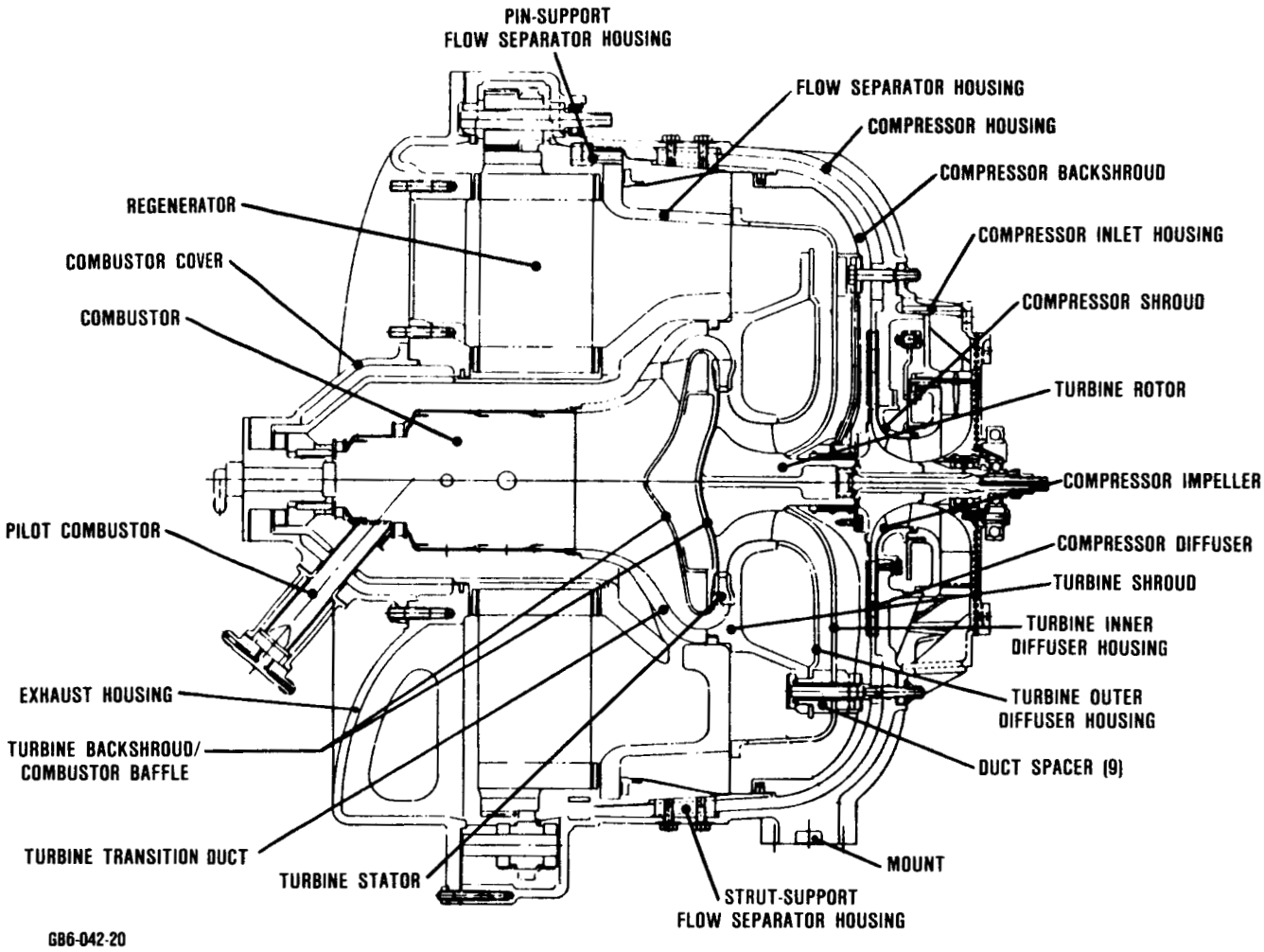

Figure 20. AGT101 Metal Power Section Developed for SAGT Program.

Table 3. AGT101 Metal Engine Materials.

Part Name*	Material
Compressor Inlet Housing	Aluminum 356
Compressor Housing	Cast Ductile Iron**
Compressor Backshroud	Cast Ductile Iron**
Compressor Impeller	Titanium
Compressor Diffuser	Stainless 327
Flow Separator Housing	GMR 235 D
Pin-Support, Flow Separator Housing	Stainless 316
Strut-Support, Flow Separator Housing	Hastelloy X
Turbine Inner Diffuser Housing	Hastelloy X
Turbine Outer Diffuser Housing	Hastelloy X
Turbine Shroud	GMR 235 D
Turbine Backshroud	Hastelloy X
Turbine Transition Duct	Hastelloy S
Turbine Rotor	Astroloy
Turbine Stator	INCO 617
Combustor	Haynes 188
Combustor Baffle	Hastelloy X
Combustor Cover	Cast Ductile Iron**
Exhaust Housing	Cast Ductile Iron**

*Refer to Figure 20 for part locations and descriptions.
**Per ASTM A536.

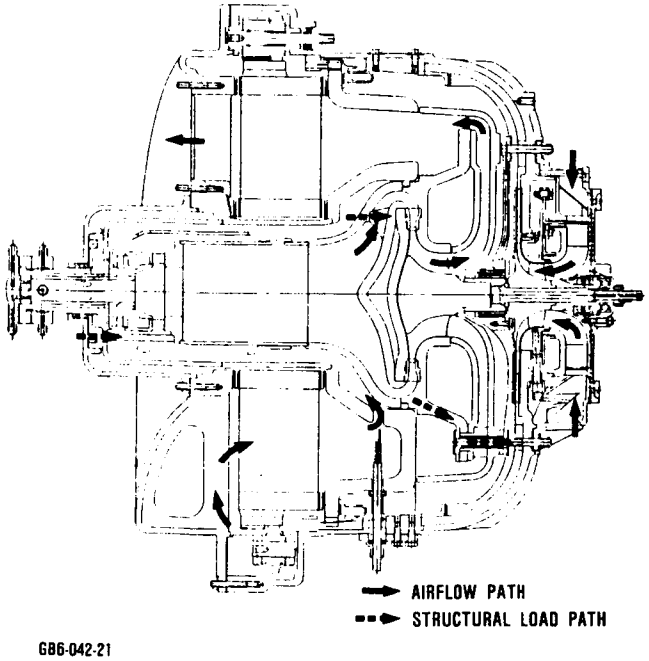

GB6-042-21

Figure 21. AGT101 Structural Loads Are Efficiently Reacted Through Symmetrical Parts.

- Mass Flow 85F (29C), Sea Level — 0.8542 lb/sec (0.3875 kg/sec)
- Stage Pressure Ratio — 5:1
- Stage Efficiency, Total-to-Total — 0.755
- Rotational Speed — 100,000 rpm

Two design iterations were required on the compressor to achieve the desired performance. The first iteration (Test 1 in compressor rig) was low in flow and work. The impeller was modified (shroud recontour and increased tip diameter), then tested with a vaneless diffuser to establish impeller characteristics. Results indicate that, as desired, flow and work increased over Test 1.

In Test 2A, a three-stage diffuser, designed to match the modified impeller, was installed, and full-stage testing was completed at speeds

Table 4. AGT101 Design Summary.

Component	Description
Compressor - Centrifugal	
Material	Titanium
Design flow, lb/sec (kg/sec)	0.85 (0.387)
Number of blades/splitters	12/12
Backward curvature, degrees	50
VIGV type, number of vanes	Articulated, 17
Diffuser type	2D vane island, cascade deswirl
Predicted stage efficiency, percent	75.5
Turbine - Radial Inflow	
Material	Astroloy
Maximum inlet temperature, F (C)	1700 (927)
Maximum tip speed, fps (mps)	2070 (631)
Number of blades	13
Stator type, number of vanes	Radial, 19
Diffuser type	Radial
Predicted stage efficiency, percent	86.5
Regenerator - Rotary	
Material, fabrication process	Aluminum silicate, corrugated
Active matrix diameter, in. (mm)	18.2 (462)
Matrix thickness, in. (mm)	3.3 (84)
Hydraulic diameter, in. (mm)	0.023 (0.6)
Support type, drive	Rim, rim drive
Predicted effectiveness, percent	91.9
Predicted seal leakage, percent	8.0
Combustor - Diffusion Flame Can	
Material	Haynes 188
Outlet temperature, F (C)	1500 to 1700 (816 to 927)
Maximum primary zone temperature, F (C)	3000 (1650)
Ball Bearing - Split Inner Race, Angular Contact	
Material	SAE 52100
Size, in. (mm)	0.59 (15)
Maximum load - radial/axial, lb (N)	9/35 (40/156)
Foil Bearing	
Number of foils	7
Diameter, in. (mm)	1.35 (34.3)
Length, in. (mm)	1.075 (27.3)
Maximum load - steady state, lb (N)	3 (13)
Maximum load - shock, g's	X6

ranging from 40 to 100 percent of design-corrected speed and IGV settings of 0, 20, 40, and 70 degrees. Axial clearance throughout the test was controlled to within 0.003 inch (0.076 mm).

Results of Test 2A are compared with those of Test 1 (original design) in Figures 22 through 24. These data indicate the following:

- Design pressure ratio and flow were attained.
- Speed efficiency, low in Test 1, was significantly increased in Test 2A.
- A desirable efficiency envelope has been achieved, characterized by peak efficiencies increasing at the lower end of the speed range where most driving time occurs. This will effect improvements in overall fuel economy.
- Diffuser performance was very close to predicted levels.

3.2.1.1 Impeller Mechanical Design

Titanium impeller material was selected because of forging availability, good fatigue resistance, and high temperature strength. A change to a powder metal or cast alloy will be accomplished when either material becomes available. Impeller properties are listed in Table 5.

Elastic three-dimensional (3-D) stress and vibration analysis was performed on the final blade configuration. The blade was optimized to provide good aerodynamic performance while maintaining stress levels necessary to assure mechanical integrity. Blade vibrations are confined primarily to the inducer region of low-specific-speed impellers. The exducer short blade height makes this blade region insensitive to aerodynamic excitations. To assure an inducer region vibratory margin, stress levels were limited to 20 ksi (138 MPa), thereby permitting vibratory stress levels of 5 ksi (34.5 MPa) with titanium. Plots showing stress results from a 3-D finite element analysis are presented in Figure 25.

Elastic stress analysis was completed for the impeller hub. Stress results are shown in Figure 26, and isotherms for the 85F (29C) day design point are shown in Figure 27. The burst ratio was calculated to be 1.68. These stress levels and burst ratio are consistent within GTEC experience on similar titanium impeller designs.

The axial and radial displacements of the blade, taking into account maximum temperature, 100-percent operating speed, and centrifugal stiffening, are shown in Figure 28.

Strain gage testing was conducted on the titanium impeller to 80,000 rpm at zero-degree VIGV setting. The full-blade first mode was excited at 73,000 rpm by the four-per-revolution harmonic. Measured strain levels of 500 $\mu\varepsilon$ were observed. The corresponding stress levels are shown in Figure 29 for both titanium and aluminum. No blade problems are anticipated based on these results.

3.2.2 Combustor Design

The AGT101 metal combustor is a scaled version of the GTEC Model GT601 truck engine combustor design as shown in Figure 30. The combustor is designed to operate with a 3.76-percent pressure drop (cold) at maximum power, while allowing a 2.34-percent pressure drop at idle, to provide adequate airblast fuel-nozzle operation. Maximum combustor air inlet and discharge temperatures for this system are 1250F (676C) and 1700F (927C), respectively. Haynes 188 material was used for fabrication, with conventional film cooling used to protect the liner surfaces. Total combustor volume is approximately 0.042 ft^3 (0.0012 m^3), which results in an overall reference velocity of approximately 83 ft/sec (33.5 m/s) and a loading parameter of 0.103 lb/sec/atm·ft^3 (0.0163 kg/s/kPa·m^3). The overall residence time is 0.0057 second at maximum power, which should result in good

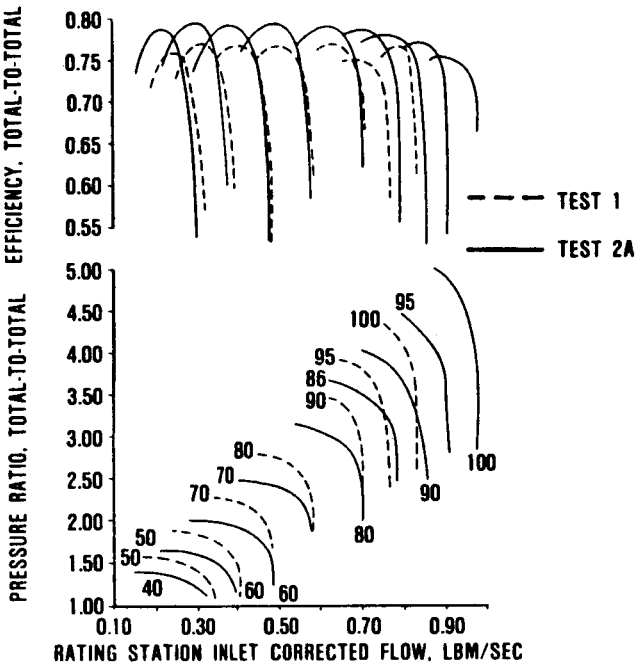

GB6-042-187

Figure 22. Full-Stage Compressor Data, IGVs Open.

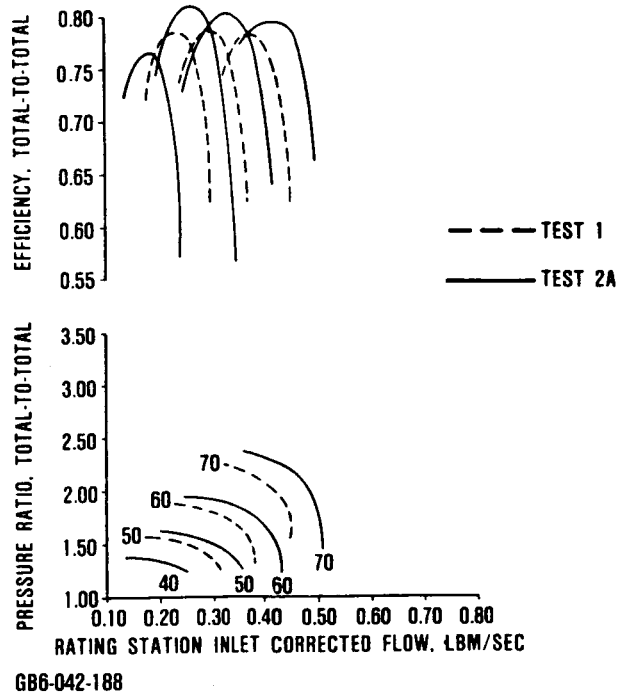

GB6-042-188

Figure 23. Full-Stage Compressor Data, IGV = 40 Degrees.

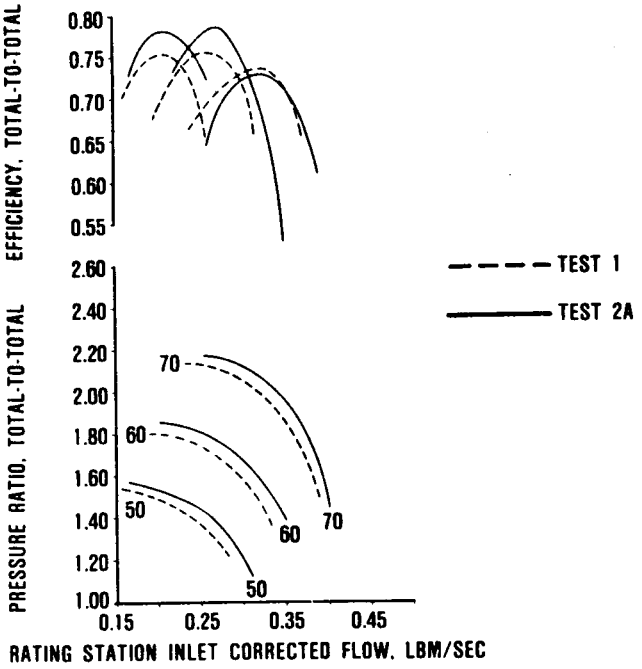

GB6-042-189

Figure 24. Full-Stage Compressor Data, IGV = 70 Degrees.

Table 5. Impeller Properties.

Parameter	Description	
Total Weight, lb (kg)	0.915	(0.415)
Blade Weight, lb (kg)	0.069	(0.031)
I_p, lb-in.-sec^2 (kg-mm-sec^2)	0.0027	(0.031)
I_d, lb-in.-sec^2 (kg-mm-sec^2)	0.023	(0.026)
Hub Area, in.^{2} (cm^2)	1.185	(7.645)
CG, in. (mm) (Forward of Blade Root Exit)	0.277	(7.04)
Kinetic Energy, lb-ft (joules)	10493	(14227)
Density, lb/in.^{3} (kg/cm^3)	0.16	(4.429)

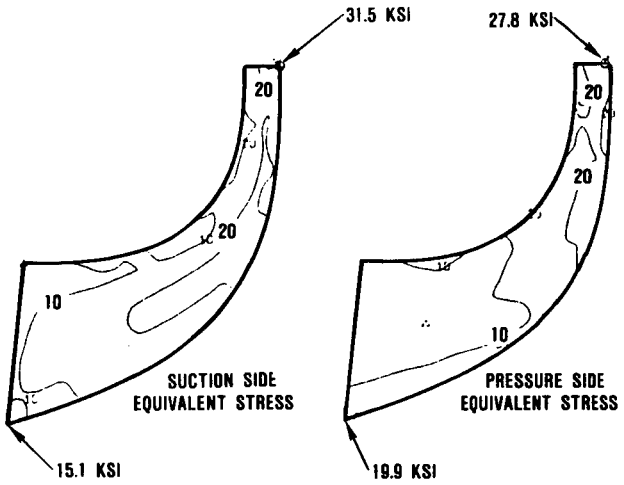

Figure 25. AGT101 3-D Airfoil Elastic Stress at 100,000 rpm.

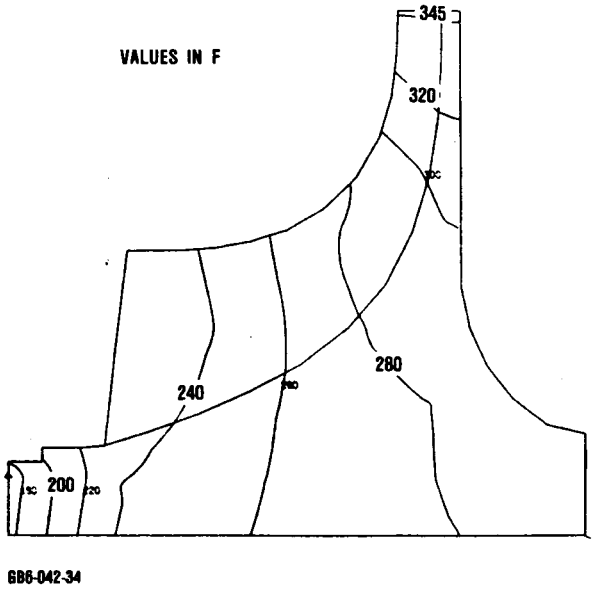

Figure 27. AGT101 Impeller Isotherms for 85F (29C) Inlet Temperature.

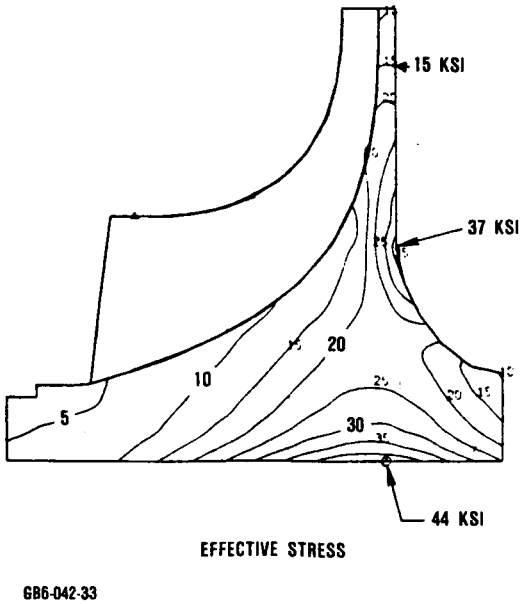

Figure 26. AGT101 Impeller Stress at 100-Percent Speed.

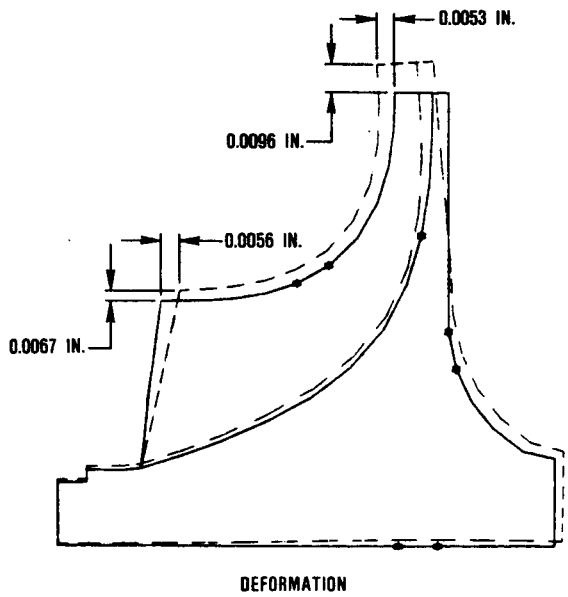

Figure 28. AGT101 Impeller Deformation at 100-Percent Speed.

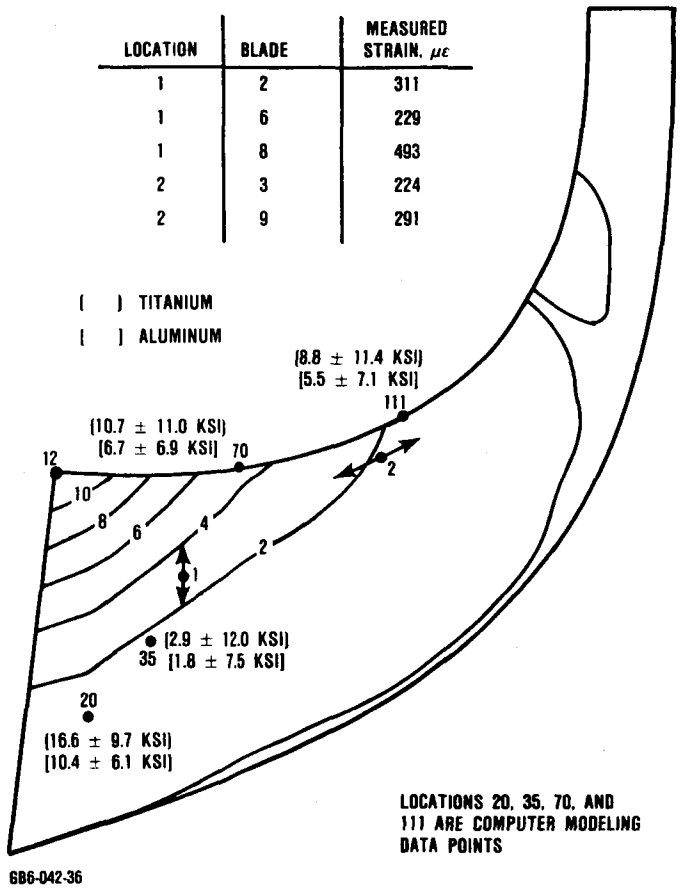

Figure 29. Measured Strains Confirm Analytically Determined Low Stresses.

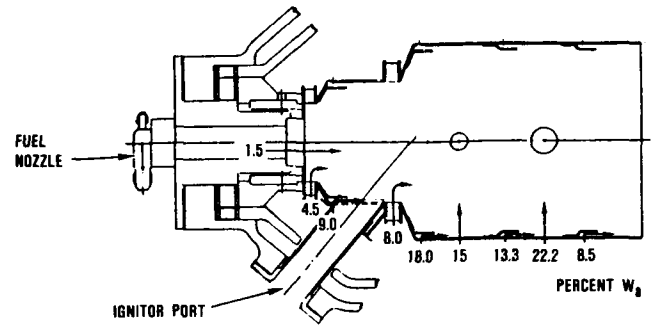

PARAMETER	UNITS	METAL AGT101	GT601
REFERENCE VELOCITY	FT/SEC (M/S)	83 (33.5)	134 (54.1)
LOADING PARAMETER	LB/SEC/ATM·FT^3 (KG/S/KPa·M^3)	0.103 (0.0163)	0.06 (0.0095)
COMBUSTOR VOLUME	FT^3 (M^3)	0.042 (0.0012)	0.176 (0.005)
RESIDENCE TIME	SECONDS	0.0057	0.00645

6B6-042-41

Figure 30. AGT101 Metal Combustor Design Is Scaled Version of GT601.

combustion efficiency values with minimum carbon monoxide, hydrocarbon, and nitrogen oxide emissions. Operating parameters of the metal AGT101 and the GT601 combustors are compared in Table 6. Test results at these conditions are presented in Table 7.

Emission testing was completed on the diffusion flame combustor. Efficiency levels obtained were 98.6 at idle, 99.45 at cruise, and 99.92 at maximum power. Although the metal combustor does not have emission requirements, it meets the carbon monoxide program goals at all power levels and the hydrocarbon goals at cruise and maximum power.

3.2.2.1 Combustor Fuel Nozzle Design

The metal AGT101 fuel nozzle is manufactured by the Delavan Corporation to GTEC Drawing 3830111. A cross section of this fuel nozzle is shown in Figure 31. The design is an air-blast, air-assist, atomizer configuration consisting of several Hastelloy-X parts brazed into an assembly. The air assist supplied by an external air pump is designed to atomize the fuel during light-off when engine airflows are low. Air assist is also used to cool the fuel tube to prevent fuel coking and consequent fouling of the small atomized fuel exit holes. The air blast, using compressor discharge flow, becomes effective for atomization at higher engine speeds, and also for prevention of fuel-nozzle overheating, fuel dribbling, and flame attachment in the primary burning zone of the combustor.

Table 6. Diffusion-Flame Combustor Flow Conditions.

Parameter	Metal AGT101		GT601	
Maximum Power				
Combustor Inlet Temperature, T_{IN}, F (C)	1200	(649)	1220	(660)
Inlet Pressure, P_{IN}, psia (kPa)	63.1	(435)	94.3	(650)
Airflow Rate, W_a, lb/sec (kg/s)	0.841	(0.381)	4.633	(2.102)
Burner Fuel/Air Ratio, F/A	0.0089		0.0139	
Discharge Temperature, T_{out}, F (C)	1786	(974)	2092	(1144)
Idle Point				
T_{IN}, F (C)	1589	(865)	1020	(549)
P_{IN}, psia (kPa)	21.8	(150)	25.8	(178)
W_a, lb/sec (kg/s)	0.204	(0.093)	1.39	(0.631)
Fuel/Air Ratio	0.0031		0.0041	
T_{out}, F (C)	1786	(974)	1286	(697)

Table 7. Combustor Performance Verified Experimentally.

Operating Characteristics					
Power Setting	Idle		Cruise		Maximum
Operating F/A	0.0031		0.0043		0.0089
Lean Blowout F/A	0.0020		0.0024		0.0012
Pattern Factor	0.215		0.130		0.103
Maximum Recorded Wall Temperature, F (C)	1167	(631)	1237	(669)	1332 (722)

Ignition Characteristics					
Engine Speed (%)	20	30	40	50	60
Maximum F/A	0.022	0.022	0.022	0.022	0.022
Light-off F/A	0.0139	0.0091	0.0076	0.0056	0.0046

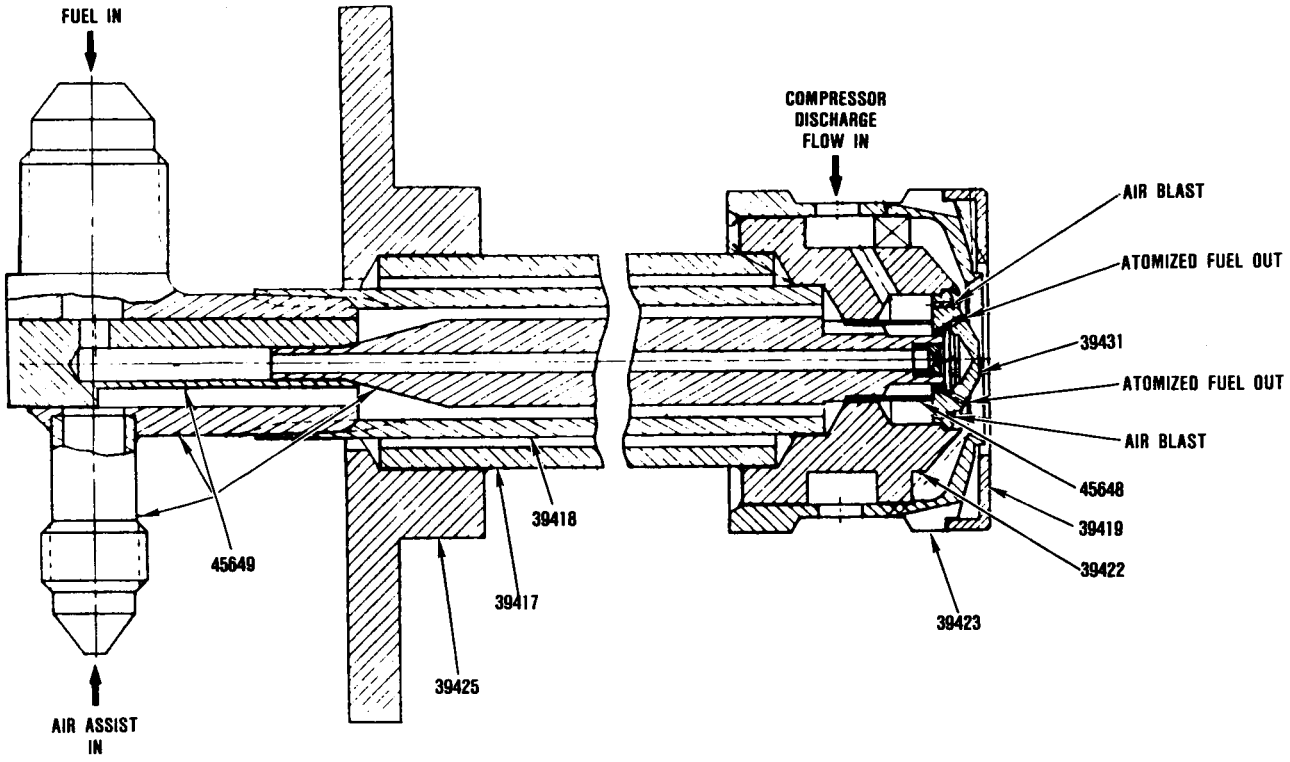

Figure 31. Cross Section of Delavan Fuel Nozzle Used in Metal AGT101.

3.2.3 Turbine Stage Design

The turbine system station designations are shown in Figure 32. The original estimated turbine efficiency summary is presented in Table 8. For cycle analysis purposes, the radial inflow turbine design is rated from combustor exit (station 4.0) to regenerator low-pressure (LP) inlet (station 5.1).

Testing was performed in a test rig that completely replicated the engine flow-path geometry, including the regenerator core. The 1600F (871C) metal turbine stage hardware under evaluation included the transition duct, cast 19-vane contoured endwall stator, machined 13-blade radial inflow turbine, radial exhaust diffuser, and associated ducting. Per-

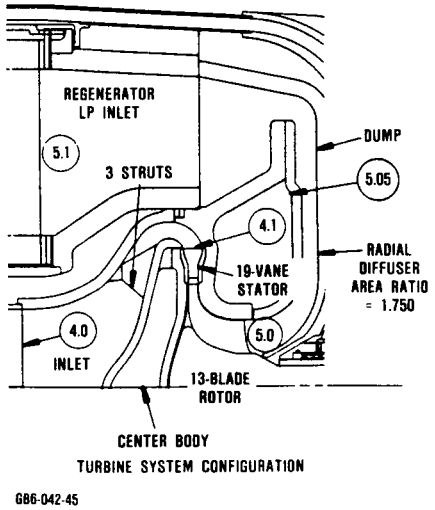

Figure 32. Turbine Stage Design Geometry Shows Designated Performance Stations.

Table 8. Turbine Design Point Efficiency Summary.

U_t = 2070 ft/sec N = 100,000 rpm N_b = 13 Blades Maximum Power		
Parameter	η_{T-T}	$\Delta\eta_{T-T}$*
Base Efficiency from Specific Speed Correlation at $R_e = 3.0 \times 10^5$	0.946	
Reynold's Number Effects from $R_e = 3.0 \times 10^5$ to $R_e = 1.21 \times 10^5$	0.937	-0.96
Rotor Inducer Incidence Effects	0.932	-0.45
Rotor Shroud Clearance Effects at 0.010-Inch Clearance	0.910	-2.21
Rotor Backface Clearance Effects at 0.030-Inch Clearance	0.894	-1.59
Rotor Blade Number Effects	0.888	-0.60
Rotor Backface Disk Friction	0.882	-0.56
Reaction Effects (Rotor Blade Surface Diffusions)	0.882	0.0
Rotor Trailing Edge Blockage Effects (Mixing Loss)	0.878	-0.40
$\Delta P_T/P_T$ Exhaust, Total Pressure Loss from Rotor Exit-to-Regenerator Inlet	0.0312	
η_{T-SYS}, Stator Inlet Total-to-Regenerator Inlet Total	0.864	

*Value cited is percentage points.

formance measurement was based on a high-speed, direct-reading torque sensor. A dummy rotor was used to quantify bearing and gear-train losses prior to performance mapping, and deadweight calibration tests were conducted prior to each performance test.

Aerodynamic performance mapping was conducted over a range of speed and pressure ratios from idle to maximum power conditions. Test results, presented in Figures 33 and 34, indicate that the 1600F (871C) metal turbine system performance level is excellent. An idle efficiency ($\eta_{T-T,SYS}$) of 76.3 percent was achieved, compared with a predicted value of 71.8 percent. At cruise conditions, a performance value of 79.6 percent was attained, compared with a predicted value of 78.2 percent. At maximum power, the predicted efficiency was 87.1 percent, while the test results indicate 86.5 percent.

Automotive application of gas turbine technology requires that the turbine operate over a broad speed range and hence large rotor exit swirl angles. The sensitivity of the radial exhaust diffuser with large rotor exit swirl angle distributions is therefore esssential for determining the turbine system performance levels. Data obtained during cold-air turbine tests and cold-flow regenerator tests indicate that the radial diffuser loss is relatively insensitive to inlet swirl angle. Moreover, losses actually decrease with increasing swirl angles, thereby enhancing the system performance levels at idle and cruise conditions at which the majority of time is spent over the Combined Federal Driving Cycle (CFDC).

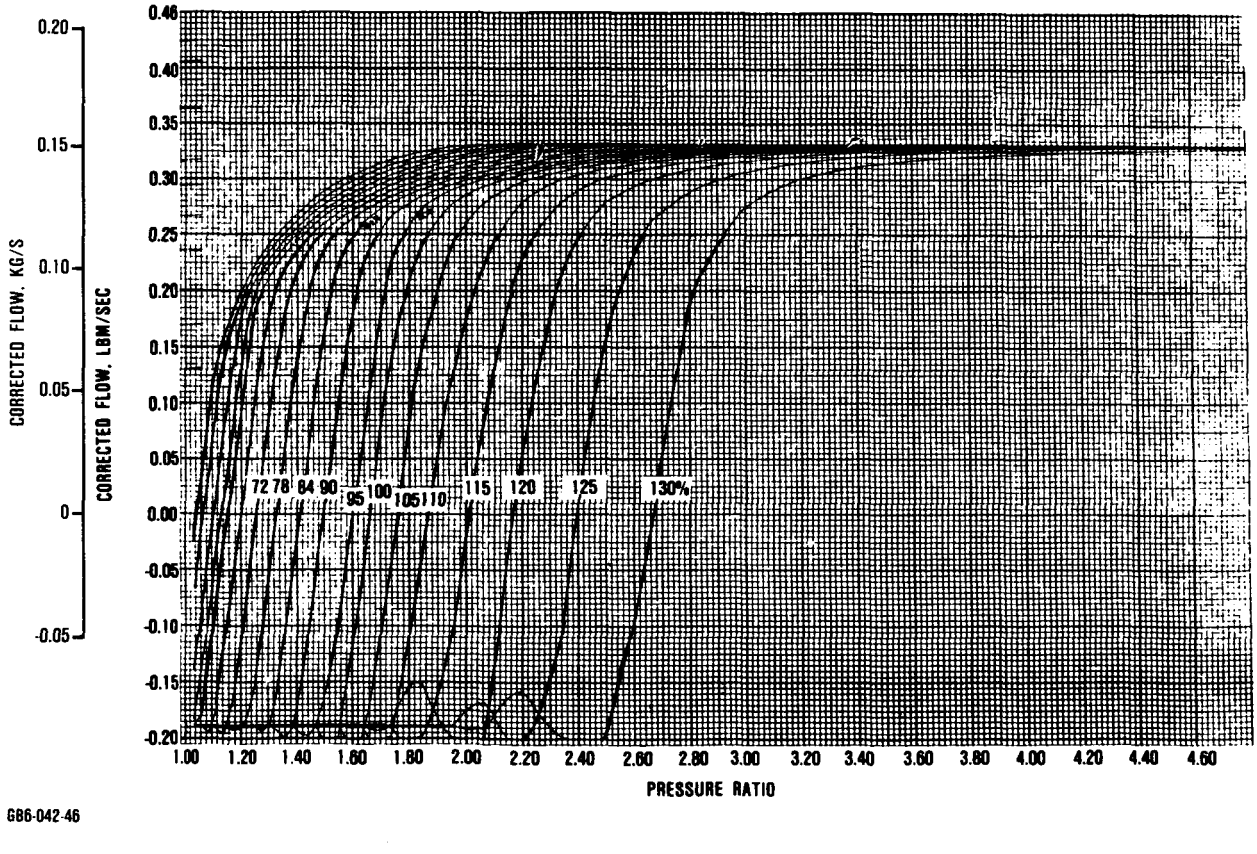

Figure 33. Metal Turbine Performance Map Generated Experimentally.

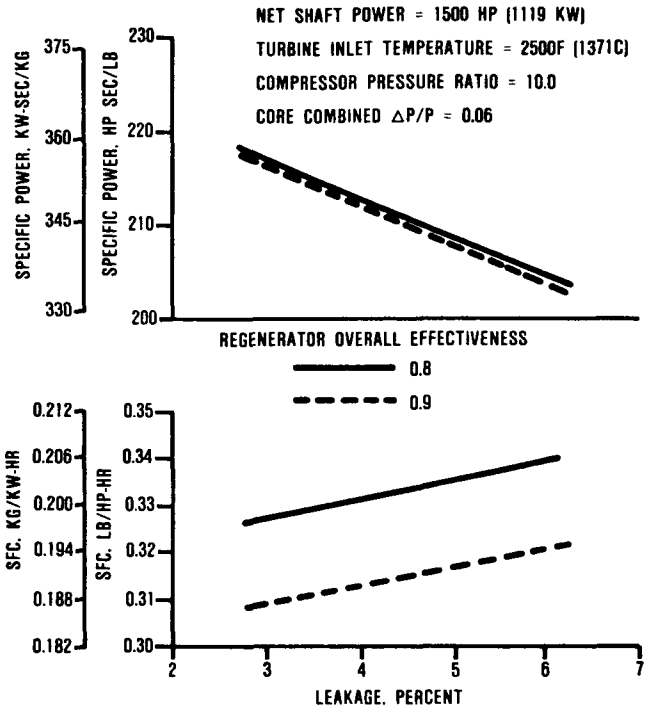

GB6-042-59

Figure 34. Metal Turbine System Efficiency Characteristics.

3.2.4 Regenerator System Design

The regenerator system (Figure 35) includes the following design considerations:

- Regenerator Matrix Performance
- Core Material and Cell Configuration
- Elastomer
- Mount and Drive
- Seal Coatings
- Seal Configuration

3.2.4.1 Regenerator Matrix Performance

The potential benefits of engine exhaust waste heat recovery are well established. The use of a regenerator introduces three performance parameters to the cycle; namely, effectiveness, pressure drop, and leakage.

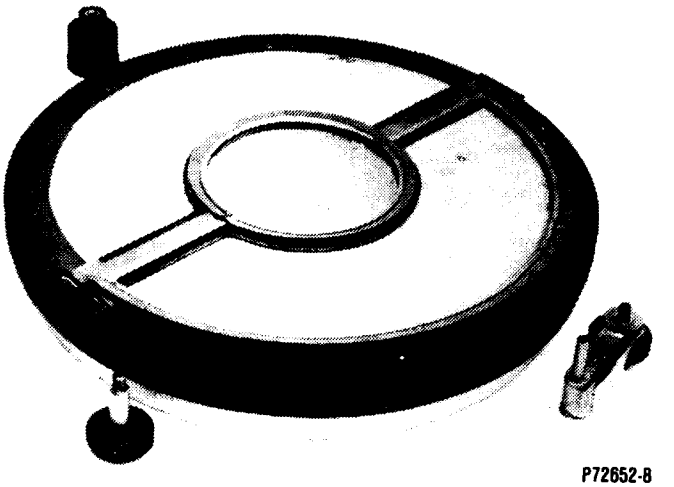

P72652-8

GB6-042-60

Figure 35. AGT101 Regenerator Core, Seals, and Drive System.

Regenerator leakage arises from small gaps occurring between the seal shoe and the rotating core, and between the regenerator seal diaphragms and the housing. Leakage also results from carryover of compressed air as the core passes under the crossarm seals and diaphragm cooling air. Carryover loss cannot be eliminated, even with perfect seals, but is minimized by careful selection of core geometry and rotational speed.

The influence of leakage and effectiveness on design point SFC and specific power is depicted in Figure 36. It is evident that more leakage can be tolerated with higher effectiveness. However, core size increases rapidly as the desired effectiveness approaches unity, and the resulting increase in seal perimeter leads to still more leakage.

Ford Motor Company has made steady progress in reducing static leakage in regenerator seals from the initial Phase III seals (1982) to the latest Phase VI seals (1986). These improvements are shown in Figure 37. Due to program timing, the Phase VA seals were selected for the SAGT-1A power section; how-

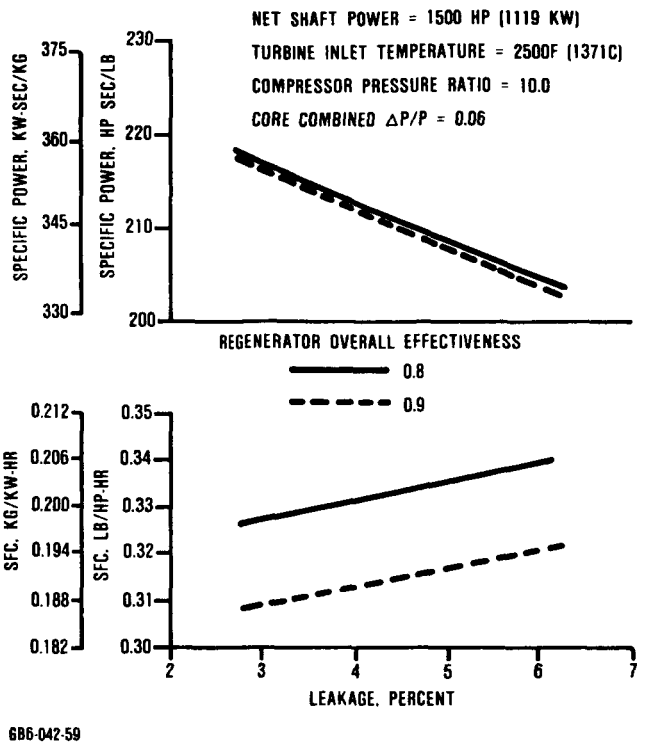

Figure 36. Regenerator Characteristics Strongly Influence Cycle Performance.

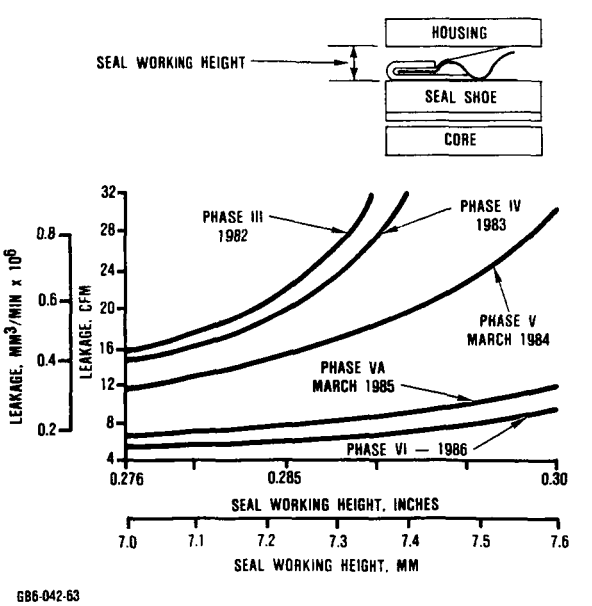

Figure 37. Regenerator Seal Development Continues to Reduce Leakage and Sensitivity.

ever, the option of retrofitting the regenerator with Phase VI seals is available for improved performance.

3.2.4.2 Core Configuration

The core is a flat disk, 3.3 inches (83.8 mm) thick, that contains a finite number of axial flow passages and rotates slowly between ceramic-coated face seals. The axial flow passages are composed of cells (sinusoidal) characterized by wall thicknesses of 0.0025 inch (0.0635 mm) and hydraulic diameters of 0.023 inch (0.6 mm).

The development effort at Ford screened a variety of materials and ultimately focused on three ceramic matrix materials, with feasibility studies conducted on a fourth. This extensive development effort concluded that for core-matrix temperature operation to 2000F (1093C), two candidate core-matrix materials, aluminum silicate (AS) and magnesium aluminum silicate (MAS), are acceptable. Further, these materials are virtually impervious to chemical attack in a turbine exhaust gas environment as demonstrated in the Ford-Regenerator Core Durability Program (References 1 and 2).

The selected regenerator core for the SAGT-1A is a Corning AS material fabricated by the corrugation process.

3.2.4.3 Elastomer Bond Joint

Design of the ring gear that is bonded to the regenerator matrix by an elastomer joint involves two key considerations, namely, elastomer operating temperature and compliancy. The AGT analytically predicted elastomer temperatures at 576F (302C) are lower than those of the Ford 707 engine at 650F (343C). Experience indicates this elastomer has had no difficulty in the AGT thermal environment. Figure 38 shows the configuration selected to optimize compliance, again based on prior Ford experience. 3-D finite-element stress analysis of the AS regenerator outer rim indicates that the lower radial modulus of rupture (MOR) of this material in compression requires the higher compliance elastomer design.

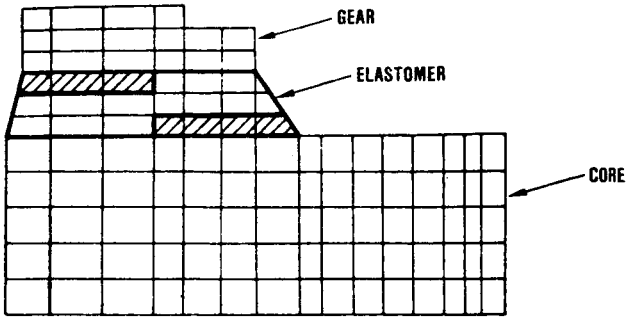

GB6-042-66

Figure 38. Elastomer-Bonded Ring Gear Configuration Optimizes Compliance.

3.2.4.4 Mount and Drive

The regenerator mounting and drive system is a derivative of the Ford 707 engine support system. Support roller locations have been optimized as shown in Figure 39, based on the interacting forces of the system as well as on ring gear flexure.

3.2.4.5 Regenerator Seals

The regenerator seal design was directed by the centerline combustor engine design. The seals wrap around the hub opening on the "hot" and "cold" sides of the regenerator as shown in Figure 40. The low-pressure (LP) side of the seals separates the compressor flow from the turbine exhaust flow through the core and in the bore areas. The high-pressure (HP) side of the seals sees a much smaller pressure differential from compressor flow to regenerator discharge flow, but adds the leakage path from regenerator discharge to the bore opening.

Figure 40 also presents a cross section of the regenerator seals showing the flexible diaphragms and loading spring. The flexible diaphragms offer excellent compliance with the mating part and the seal shoe. The

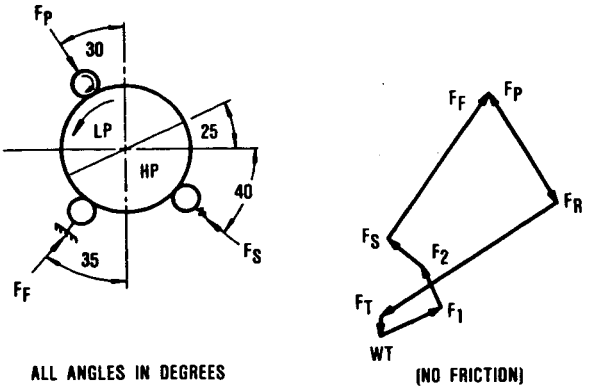

TORQUE = 200 FT-LB (271 N-M)
WT = 20 LB (9.1 KG)
F_R = GEAR SEPARATING FORCE = 86 LB (383 N)
F_T = GEAR DRIVING FORCE = 239 LB (1063 N)
F_1 = PERIPHERAL SEAL REACTION FORCE = 80 LB (356 N)
F_2 = CROSSARM SEAL REACTION FORCE = 48 LB (214 N)
F_S = SPRING ROLLER FORCE = 50 LB (222 N)
F_F = FIXED ROLLER FORCE = 110 LB (489 N)
F_P = PINION ROLLER FORCE = 245 LB (1090 N)

GB6-042-67

Figure 39. Regenerator Support Roller Locations Minimize Fixed Roller Loading.

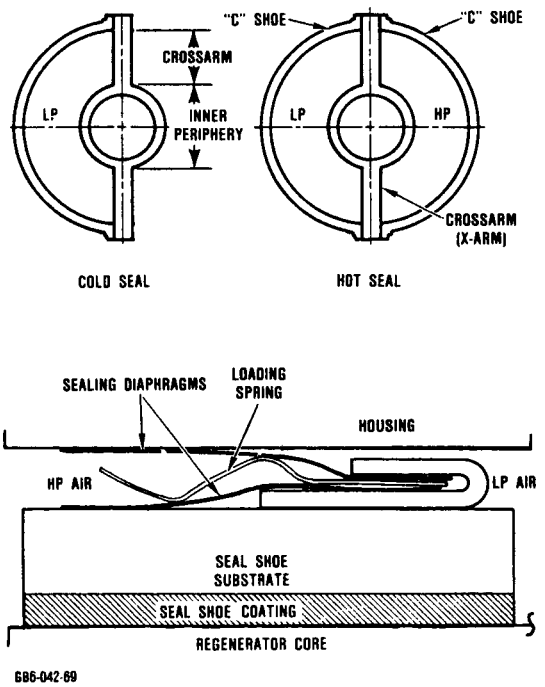

GB6-042-69

Figure 40. SAGT-1A Regenerator Seal Configuration with Cross Section of Phase VA Seals.

diaphragms are forced against the mating parts by increasing pressure to improve their sealing ability, and are used to load the wear and primary sealing surface (the shoe coating surface) against the regenerator core. These Phase VA seals are the configuration used in the SAGT-1A. Work is continuing at Ford to improve these seals. Phase VI seals are now available for retrofit to improve engine performance.

In addition, AGT101 development with respect to the regenerator system is continuing in the following areas:

- Elimination of the hot seal to allow the regenerator core to seal directly against the flow separator housing. Leakage, drive torque, and wear characteristics of candidate coatings on the flow separator housing are being investigated.
- Minimizing distortion in the metal exhaust housing cover by cooling the inner periphery and/or installing a ceramic insert into the exhaust housing to effect a sealing surface that is more thermally stable.

3.2.4.6 Seal Coatings

An extensive evaluation of seal substrate temperatures, involving projections for seals at 2000F (1093C) gas side core temperatures, was performed on a Ford 707 engine system. The test provided temperature data for all critical seal locations and was the basis for the seal-coating selections cited in Table 9.

Table 9. Regenerator Seal Materials and Processes.

Item	Approximate (Extreme) Temp, F (C)	Potential Material	Process Application
Inner Seal			
A. High Pressure "C" Shoe	500 (260)	Substrate: 430 CRES Coating: I85	Photoetch Plasma Spray Coating
B. Low Pressure "C" Shoe	500 (260)	Substrate: 430 CRES Coating: I85	Plasma Spray Coating
C. Crossarm	1300 (704)	Substrate: IN601 Coating: I112	Plasma Spray Coating
D. Peripheral Static Seal/Loading Springs	500 (260)	Retainer: INCOx750 Diaphragms: INCOx750 Springs: INCOx750	
E. Crossarm Static Seal	(cooled)	Retainer: INCOx750 Diaphragms: Waspalloy Springs: Waspalloy	
Outer Seal			
A. Low Pressure "C" Shoe	500 (260)	Substrate: 430 CRES Coating: I85	Plasma Spray Coating
B. Crossarm	800 (427)	Substrate: 430 CRES Coating: I85	Plasma Spray Coating

3.2.5 Structural Design

Thermal and stress analyses were performed on major structural components, and included testing at both steady-state and transient operation. Figure 41 shows the associated static pressure distribution for maximum power. Temperature and stresses were calculated at several different times during the transient to determine peak magnitudes as a function of time.

3.2.5.1 Housing Designs

The major metallic structures analyzed were the compressor housing, compressor backshroud, and exhaust housing (see Figure 42), all constructed of cast ductile iron per ASTM A536. Results of the analyses are described in the paragraphs that follow.

3.2.5.2 Compressor Housing

As shown in Figure 42, the compressor housing is subjected to internal pressurization and axisymmetric blow-off loads acting over the lower half of the exhaust housing/compressor housing bolt flange. Maximum power pressure forces were used for this analysis. Fourier series loads were used to obtain the axisymmetric loading profiles.

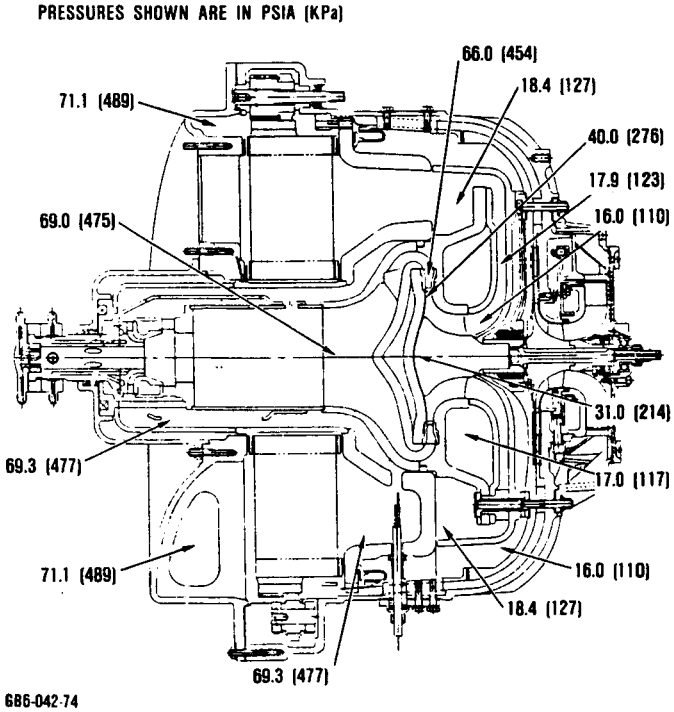

Figure 41. Static Pressure Distribution at Maximum Power Used for Stress Analysis.

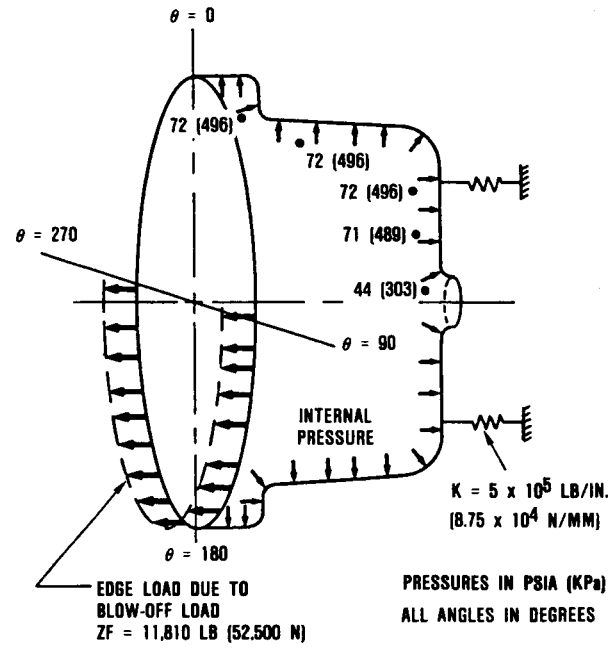

Figure 42. Compressor Housing Free-Body Diagram Showing Pressures and Exhaust Housing Blow-Off Load.

During the structural deflection analysis, external ribs (Figure 43) were added to reduce housing deflections and regenerator distortions (Figure 44).

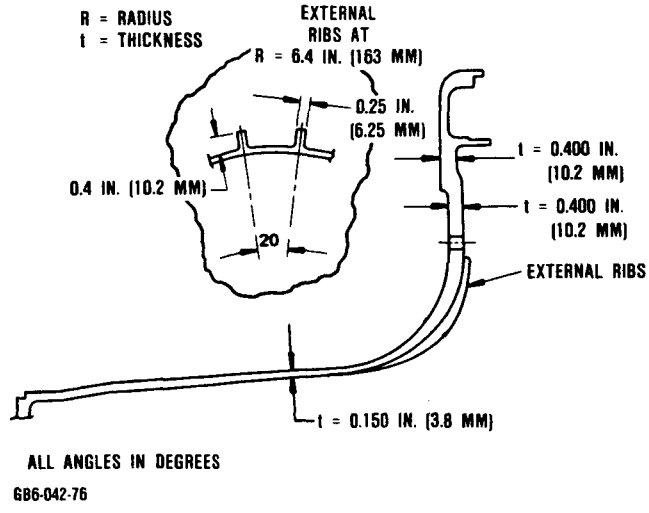

Figure 43. Compressor Housing Deflections Were Decreased with the Addition of External Ribs.

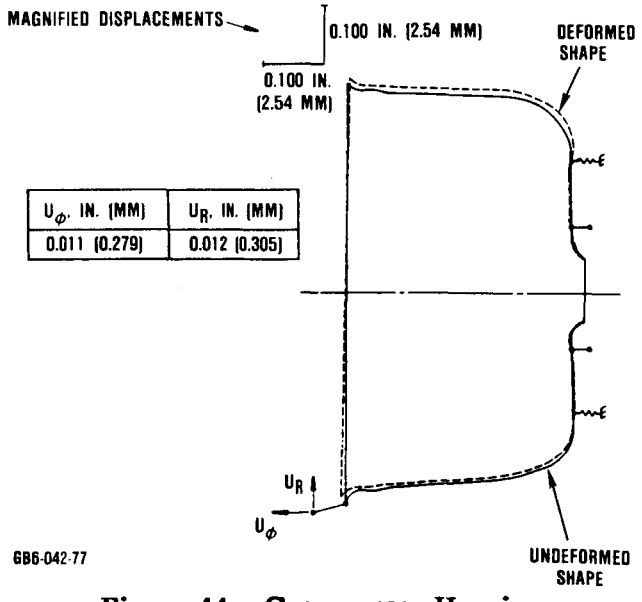

Figure 44. Compressor Housing Deflections Are Reduced.

3.2.5.3 Compressor Backshroud

The compressor backshroud was analyzed at maximum power conditions to determine foil bearing surface deflections. The backshroud is restrained from axial movement at the outer bolt circle and is free to radially deflect. As shown in Figure 45, deflection at the foil bearing surface is approximately 0.003 inch (0.076 mm), which is considered acceptable. No stress or thermal problems are anticipated.

3.2.5.4 Exhaust Housing

Optimization of regenerator pocket dimensional control is critical to engine performance. This optimization includes the compressor housing deflection analysis (see paragraph 3.2.5.2 above), the flow separator housing support, and the exhaust housing. Figure 46 presents the 3-D finite element model of the exhaust housing. Utilizing ribs as effective stiffeners for deflection control, the exhaust housing deflections are minimized. Figure 47 summarizes the exhaust housing deflections. No thermal or stress problems are anticipated.

3.2.6 Foil Bearing Design

The bearing supporting the turbine end of the rotor is a hydrodynamic design requiring no external air supply for operation (except for foil carrier cooling air). Consequently, the bearing must generate a gas film at as low a speed as possible to minimize starting power and foil wear during the start-stop cycle. This film-generation speed must also be compatible with a stable gas film over operating speeds, loads, and temperatures.

The normal bearing operating load was calculated to be 3 pounds (13 N). The foil bearing was designed to also withstand gyroscopic bearing loads resulting from test vehicle maneuvers, as well as short-duration 6-g shock loads.

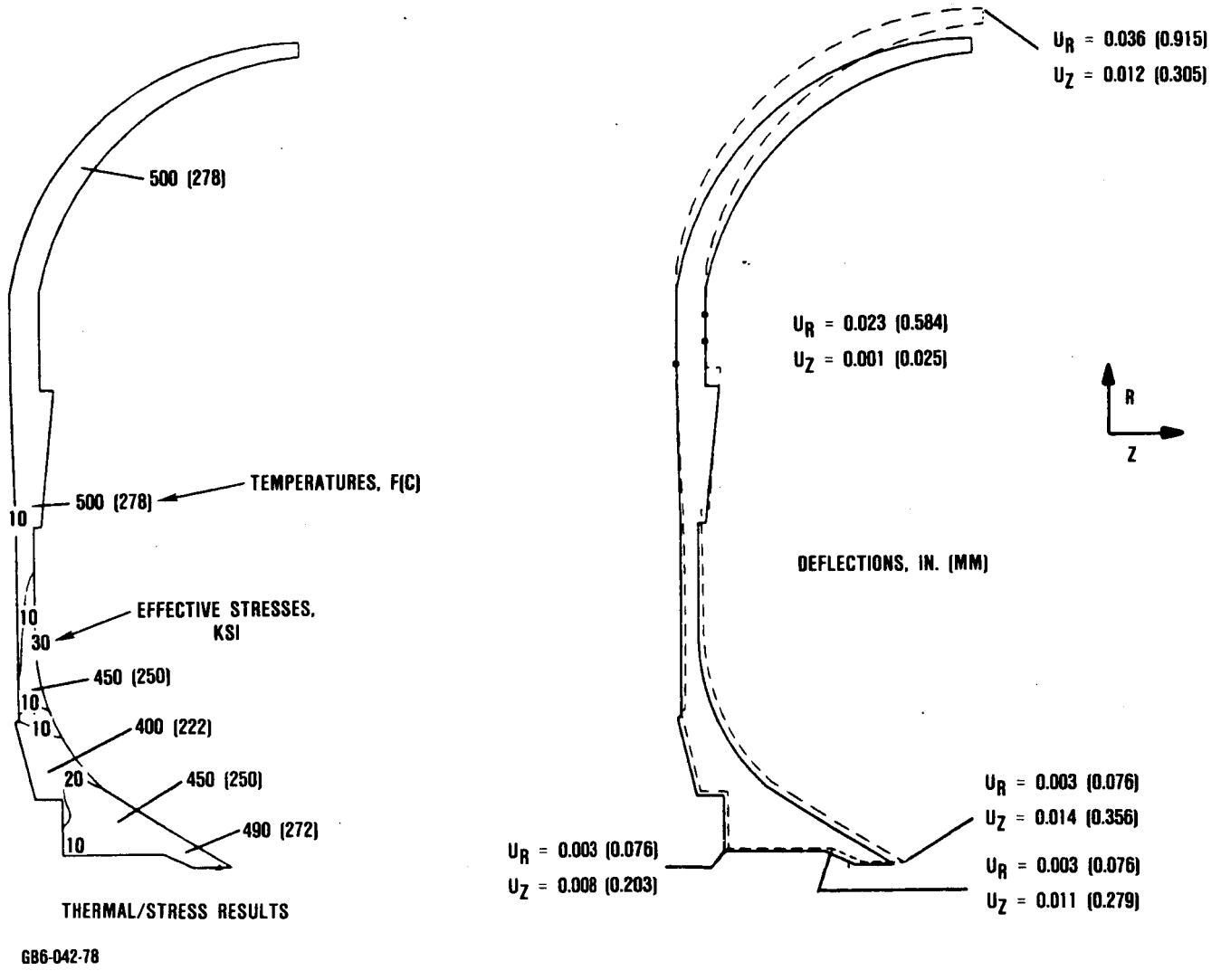

Figure 45. Compressor Backshroud Thermal Stress and Deflections Are Acceptable.

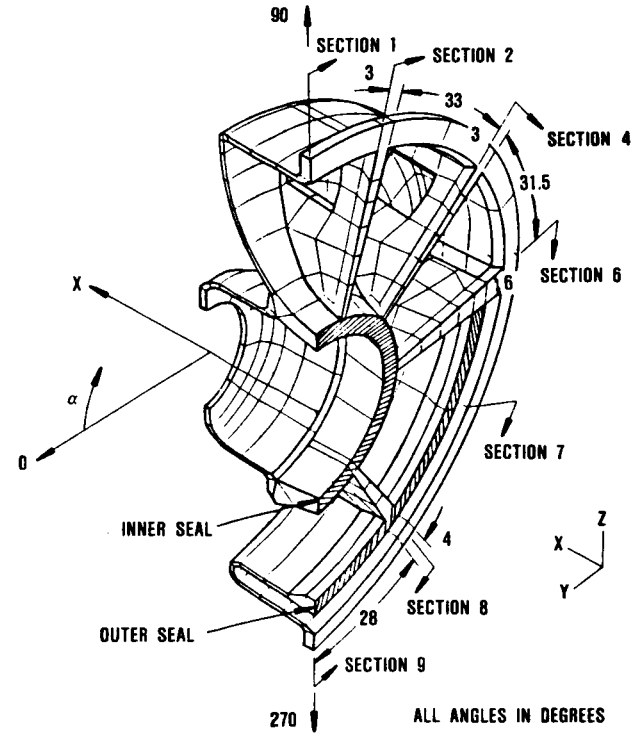

Figure 46. 3-D Finite Element Model of the Exhaust Housing.

3.2.7 Bearing and Seal Design

The high-speed pinion bearing and floating ring seals are shown in Figure 48. The pinion bearing is a 0.59-inch (15-mm) 202 series ball bearing designed to carry a maximum predicted radial load of 9 pounds (40 N) and a thrust load of approximately 35 pounds (156 N) at 100,000 rpm.

The bearing was designed to meet the following design conditions:

- Speed: 55,000 to 100,000 rpm
- Radial loads: 9.5 to 41 pounds (42 to 182 N)
- Thrust loads: 70 to 250 pounds (311 to 1112 N)
- Life: 3900 hours - variable speed and load
- Lubricant: automotive transmission fluid (ATF)
- Lubricant Temperature: 100 to 250F (38 to 121C)

The high-speed ring seal assembly (see Figure 49) consists of two floating carbon rings designed to permit flow of buffer air between the carbon elements.

Bearing component details are summarized in Table 10.

3.3 Performance Calculations

The calculations to predict PCA electrical power output are based on extensive GTEC experience with gas turbine performance analysis. The basic program used is a GTEC-developed computer program called PSPROC, which synthesizes separate models of different gas turbine engine configurations. The model used for the SAGT-1A analysis is a regenerated, single-shaft gas turbine with no load compressor. This model is modified for the particular engine operating conditions and the external combustor (Sanders receiver), in series with the fuel combustion chamber, to make it useful for analyzing the solarized version of the AGT101. Next, the parasitic losses are applied (simple adder in negative direction) to the aerodynamic power calculated by the program. Finally, the losses resulting from converting engine mechanical power to electrical power are assessed and the calculation is completed.

3.3.1 Engine Performance

The engine performance analysis starts with an engine model of the AGT101, known as AGT TCM. This computer program uses the familiar thermodynamic laws to calculate the inlet and exit state points for each aerodynamic component of the engine (compressor, turbine, combustor, and regenerator). It incorporates actual component performance maps (Figures 33 and 34), and applies multipliers to account for differences between the impeller/shroud clearance in the test engine

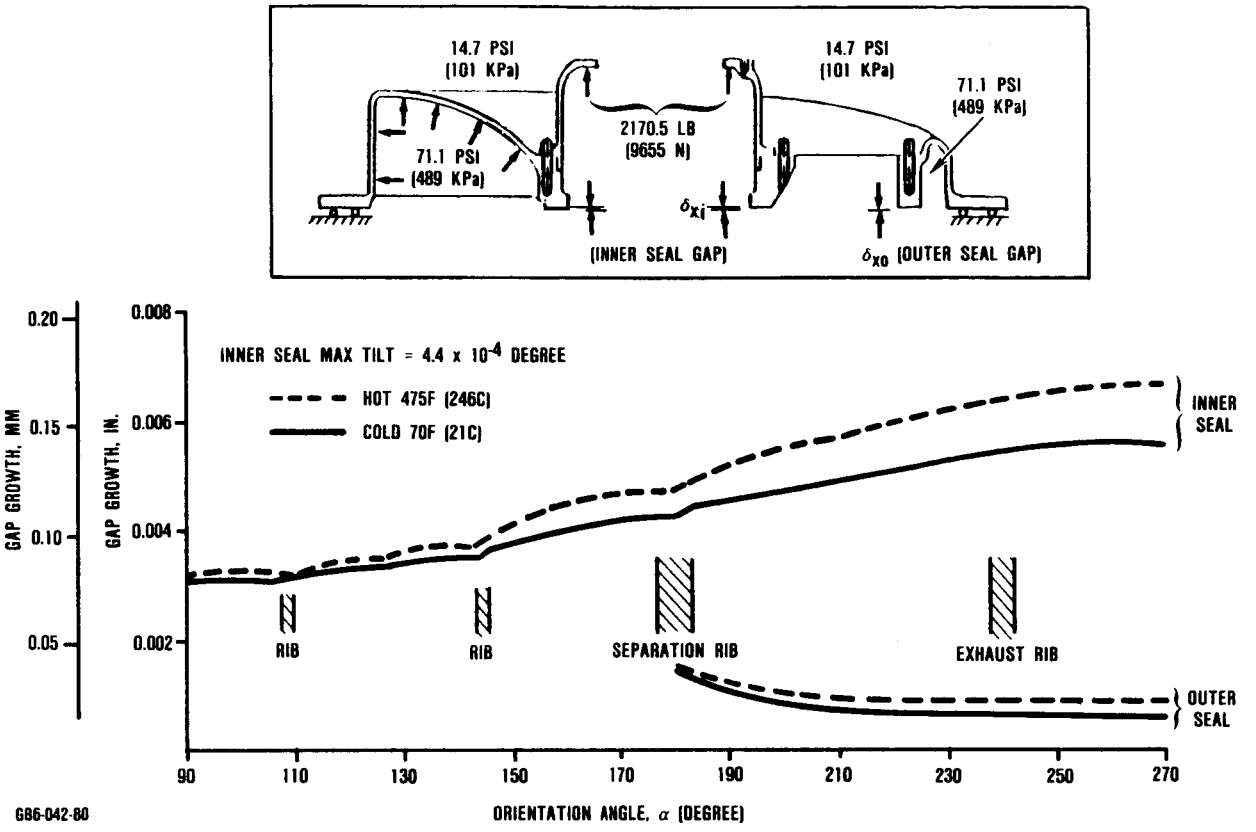

Figure 47. Exhaust Housing Regenerator Header Seal Gap Growth.

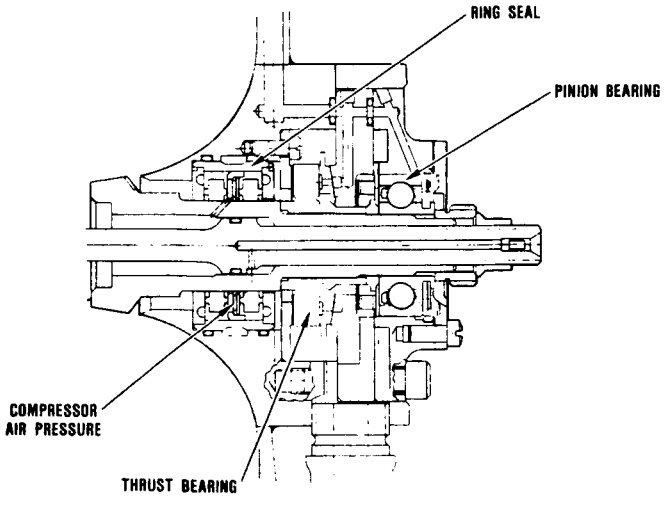

Figure 48. High-Speed Pinion Bearing and Floating Ring Seals.

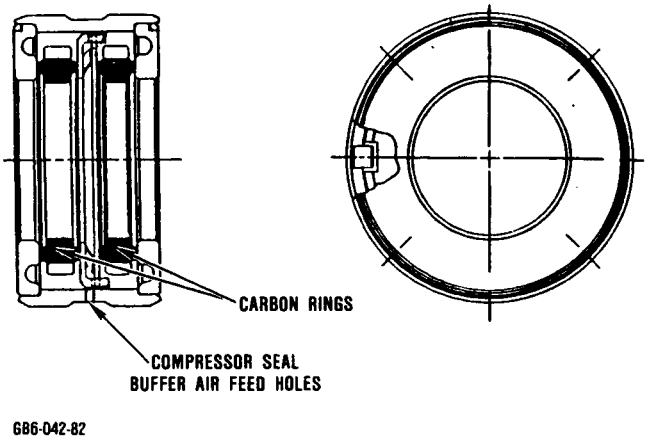

Figure 49. High-Speed Ring Seal Assembly.

Table 10. Pinion Bearing Component Detail.

Bearing Description - Ball, Split-Inner-Race, Series 202; Grade 5	
Inner Ring	**Outer Ring**
Material - SAE 52100 Steel-Rc 58-64 Bore - 0.5904-0.5906 in. (15 mm) Width - 0.525-0.535 in. (13.42 mm) Race Depth - 24 min % of Ball/Roller Diameter Race Curvature - 51.6-52.4% of Ball/Roller Diameter Separator Pilot Land to Groove Runout - TIR, 0.0005 in. (0.0127 mm)	Material - SAE 52100 Steel-Rc 58-64 OD - 1.3778-1.3780 in. (35 mm) Width - 0.4281-0.4331 in. (11 mm) Race Depth - 16 min % of Ball/Roller Diameter Race Curvature - 50.6-51.4% of Ball/Roller Diameter Separator Pilot Land to Groove Runout - TIR, 0.0005 in. (0.0127 mm)
Separator	**Rolling Elements**
Material - SAE 4340 Steel-Rc 34-38 Silver Plated, 0.001 in. (0.0254 mm) Thick per AMS 2410 Construction - Machined Assembly - One Piece Pilot Surface - Outer Ring Lands Pilot Clearance - 0.010-0.016 in. (0.254-0.406 mm)	Material - SAE 52100 Steel-Rc 58-64 Elements per Row - 10 Element Diameter - 0.25 in. (6.35 mm)

versus the optimum clearance used to generate the compressor performance map. The program assesses heat losses between components and static structures based on calculations for the specific insulations used. It also estimates leakage flows and iterates on these flows to find the best match with measured gas temperatures. The schematic of internal engine leakage is presented in Figure 50; the complexity of the many leakage paths and the extreme difficulty of trying to experimentally determine the leakage through each area are evident from this figure.

The parameters input to the program are the following:

- Ambient Air Temperature (T_{cell})
- Ambient Air Pressure (P_{BAR})
- Engine Speed (N_e)
- Inlet Guide Vane Angle (IGV)
- Fuel Type [to ensure use of the correct lower heating value (LHV)]

The values assigned to these parameters for the test case are listed below:

- T_{cell} = 111F (43.9C)
- P_{BAR} = 14.065 psia (96.9 kPa)
- N_e = 90,290 rpm
- IGV = 0 degree
- Fuel Type = JP-4 with LHV of 18,700 Btu/lb (43,550 kJ/kg)

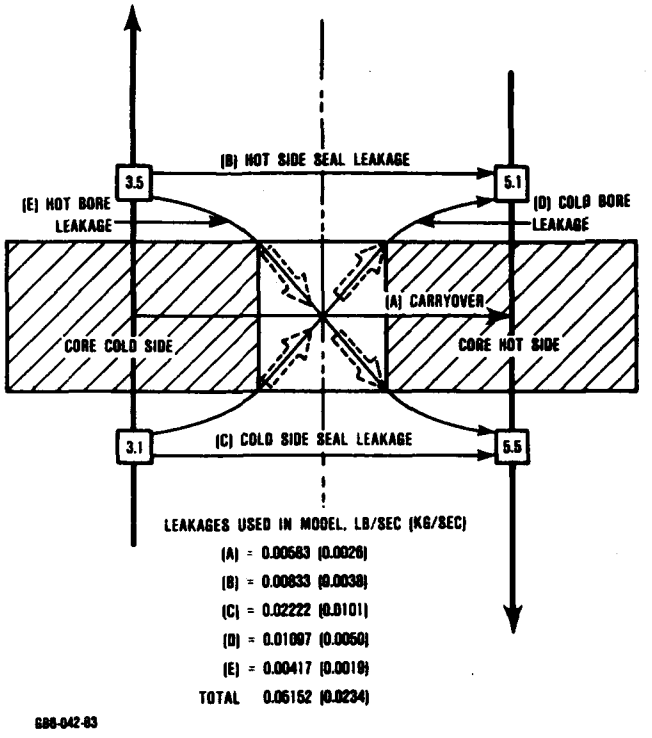

Figure 50. Complex Regenerator Leakage Model Is Required in Computer Engine Simulation.

Program output for this test case is shown in Figure 51, which can be compared with results of an actual engine test as described in Section 4.1.2.

3.3.2 System Performance

Based on the engine performance predictions described in the previous section, additional losses experienced by the system are calculated. These system losses include receiver and conversion losses occurring between the mechanical output of the engine and the electrical output of the induction motor/generator. Figure 52 depicts the various system losses. Sanders Associates supplied the data on thermal and pressure losses in the receiver system and thermal input into the engine duct at the interface.

The system performance analysis addresses the loss resulting from conversion of thermal input power to mechanical power at the engine output gear, as well as a series of subsequent mechanical and power conversion losses, as shown in Figure 53. The gearbox loss was measured in a bench test; the belt-drive and generator efficiencies were based on data provided by the suppliers of this equipment; and the regenerator drive power was estimated based on the nominal drive torque in the range in which it operates. Figure 53 shows the estimated design point performance at 72.7 kW thermal input. Figure 54 presents the estimated performance for the test at Sandia.

3.4 Support System Design

The electrical and electronic support systems described herein assure safe starts and controlled operation of the SAGT-1A PCA. The central part of these systems is the full-authority electronic control unit (ECU) shown connected to the electrical equipment in Figure 55. The electrical cables and harnesses connect the PCA to the enclosure and then to the control panel. In addition, the PCA is monitored by an extensive instrumentation network to assess operation of the engine and receiver and initiate automatic shutdowns in response to any out-of-limit conditions.

3.4.1 Electronic Control System

As a full-authority control unit, the ECU operates the relays and solenoids to accomplish the following:

- Engage the start motor
- Turn on ignition and fuel for light-off
- Open the variable inlet guide vanes (VIGVs) to produce power
- Control the fuel flow to hold the turbine inlet temperature ($T_{4.1}$) at the selected value
- Close the VIGVs to hold $T_{4.1}$ at the selected value

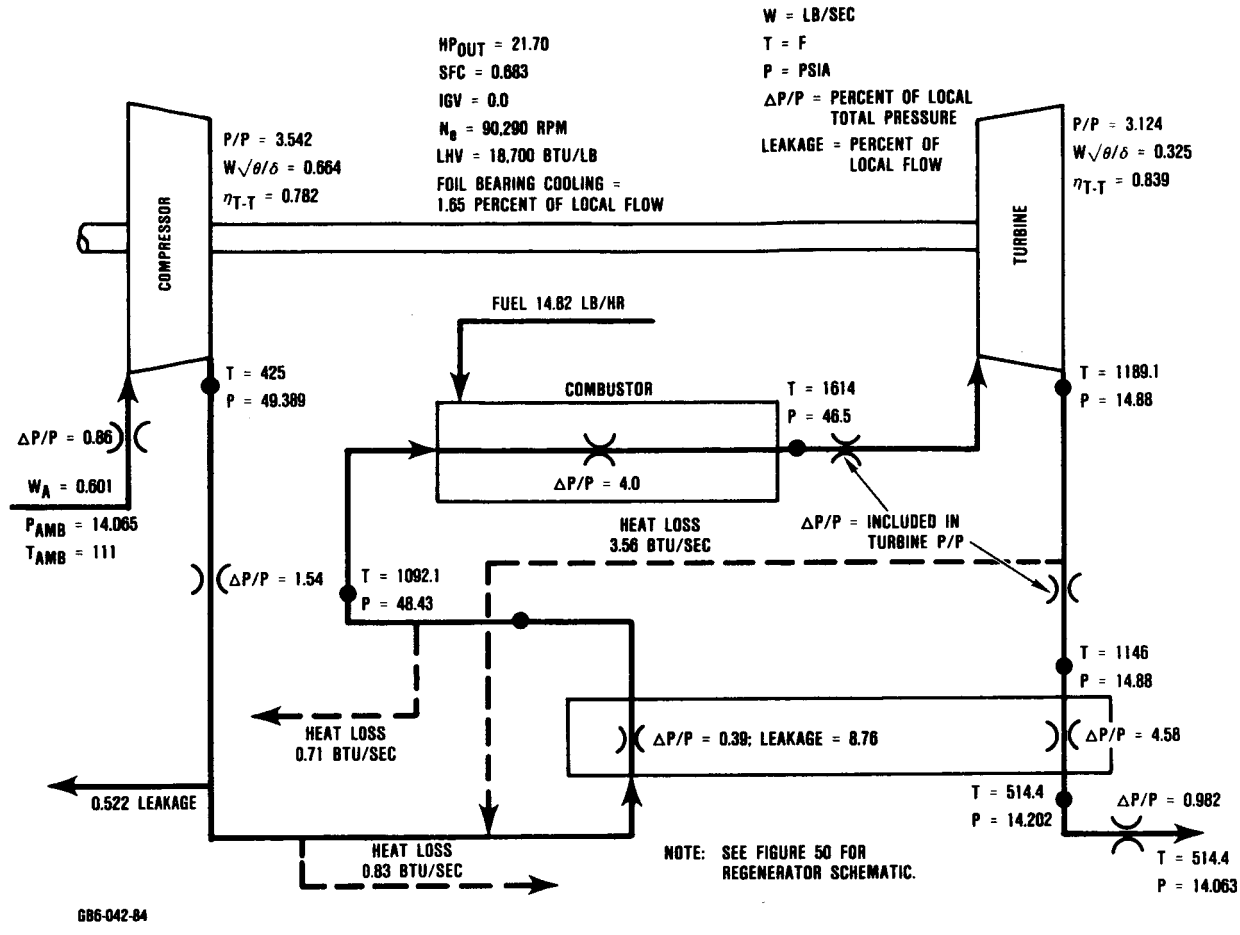

Figure 51. Computer Model Cycle Schematic.

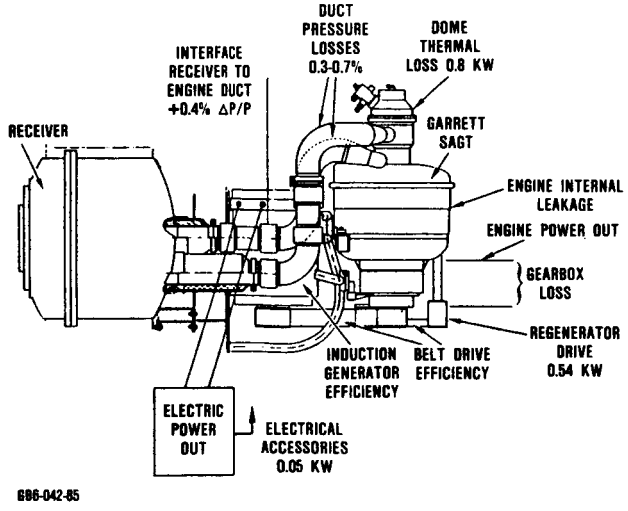

Figure 52. SAGT System Losses.

The ECU also executes a shutdown (S/D) by de-energizing the fuel solenoid and the purge-air solenoid, which blows the fuel out of the fuel nozzle to prevent coking. This S/D sequence is triggered automatically when the ECU recognizes any of the following faults: no light-off within 15 seconds, low oil pressure, high oil temperature, engine overspeed, or overtemperature.

The ECU logic diagram is shown in Figure 56. The parameters in the left-hand column are operator command inputs and sensor inputs; the parameters in the right-hand column are the ECU outputs to the relays, solenoids, and torquemotor.

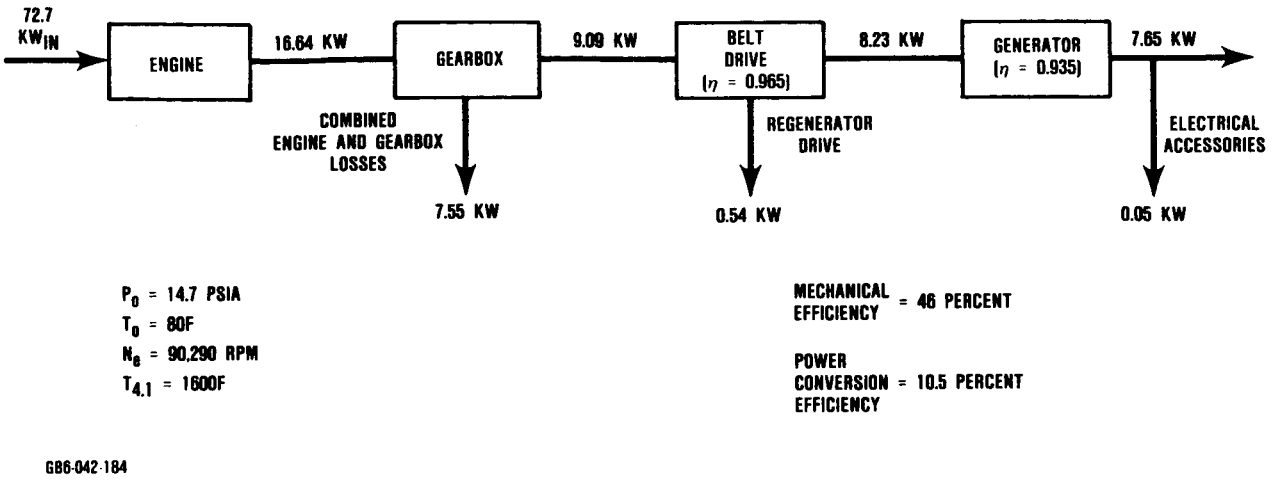

Figure 53. SAGT-1A Design Point Performance.

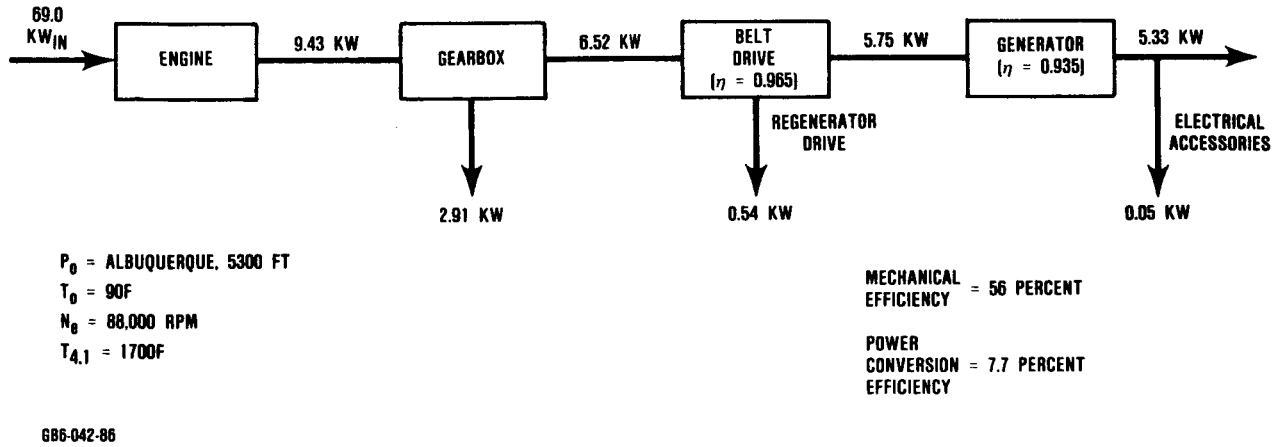

Figure 54. Predicted SAGT-1A Performance at Sandia.

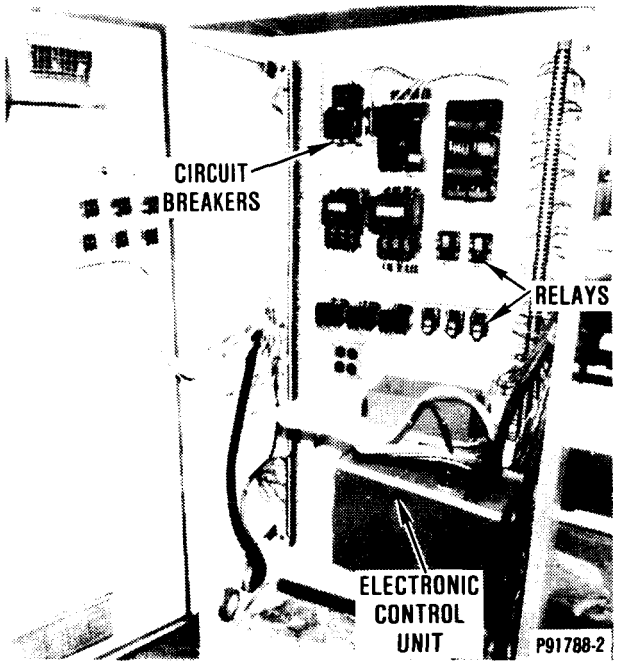

GB6-042-87

Figure 55. Electrical Enclosure Components.

The following logic statements are intended to clarify the control functions of the ECU.

a) The starter is turned on when both of the following conditions occur:

   1) Start switch is high (on) and low oil pressure (LOP) switch is low after 2-second delay.

   2) No shutdown (S/D) signal is present.

b) The solar receiver door (RCVR) is opened when both of the conditions cited above (a1 and a2) occur.

c) The atomizer purge solenoid is activated when:

   1) The BURN ENABLE signal is low or shut down, and engine speed is equal to or greater than 8 percent. (The solenoid is shut off 10 seconds later.)

   NOTE: The BURN ENABLE signal is high when in fuel mode only.

d) The fuel solenoid is turned on when all of the following conditions occur:

   1) In fuel mode.

   2) Two-second delay has elapsed.

   3) Shutdown circuit has not been activated.

   NOTE: Start fuel flow is calculated using the equation

$$Wf_{START} = 7.0 - (T_{3.5}/500)$$

e) The fuel solenoid is shut off when:

   1) The BURN ENABLE signal is low with no time delay.

f) The fuel pump is started when both of the following conditions occur:

   1) In fuel mode.

   2) Shutdown circuit has not been activated.

g) The ignitor is turned on when both of the following conditions occur:

   1) In fuel mode.

   2) Shutdown circuit has not been activated.

h) The ignitor is shut off when any one of the following conditions occurs:

   1) Ten seconds have elapsed since fuel mode was activated, speed is greater than 75 percent, and $T_{3.5}$ is greater than 500F (260C).

   2) Shutdown circuit has been activated.

   3) Fuel mode was not selected.

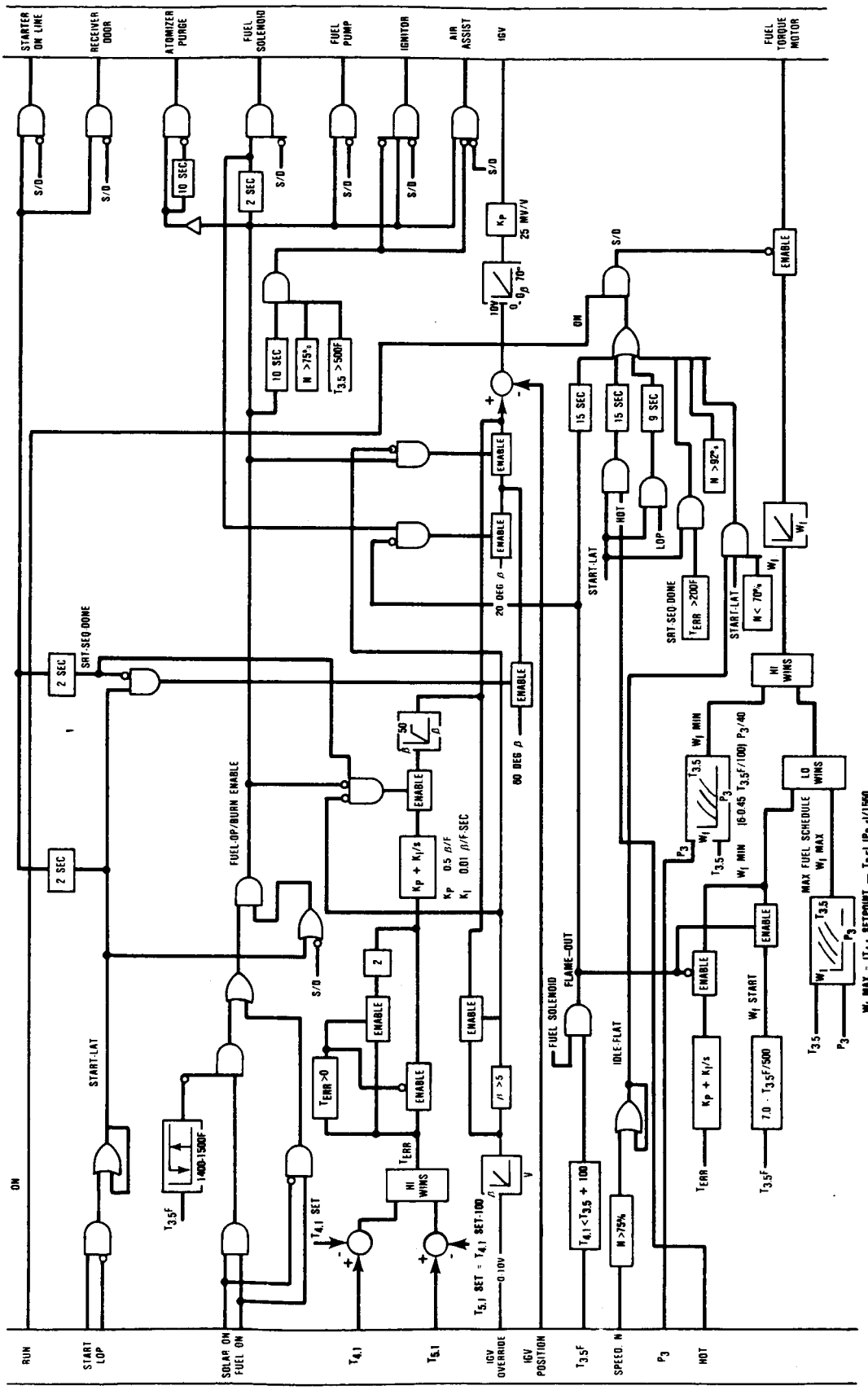

Figure 56. SAGT-1A Logic Diagram Shows ECU Control of Engine Functions.

i) The 0-degree IGV position is held when all of the following conditions occur:

1) In fuel mode.

2) The BURN ENABLE signal is high for 2 seconds.

3) The manual override is set at less than 5 degrees.

NOTE: The 60-degree IGV position is vanes closed.

j) The 20-degree IGV position is selected when:

1) The fuel solenoid is turned on.

k) The IGVs are modulated by the closed-loop temperature control when both of the following conditions occur:

1) The fuel mode has been turned off.

2) Two seconds have elapsed since activation of the starter.

NOTE: The temperature error of $T_{5.1}$ or $T_{4.1}$, whichever is higher, is operated on by an integral and proportional controller which opens the IGVs if either $T_{5.1}$ or $T_{4.1}$ is too high.

l) The fuel control is modulated by the closed-loop control when:

1) In fuel mode only.

NOTE: The temperature error of $T_{5.1}$ or $T_{4.1}$, whichever is higher, is acted on by an integral and proportional controller which changes fuel flow to maintain set-point temperature. Whenever the fuel flow is on the maximum or minimum schedules, the integrater is held to a fixed output.

m) The shutdown circuit is activated when any one or more of the following conditions occur:

1) Fifteen seconds have elapsed since flame-out began. (Flame-out occurs when $T_{4.1}$ is less than $T_{3.5}$ + 100 and the fuel solenoid is on.)

2) Both the high oil temperature and start switches are ON.

3) The start switch is ON and low oil pressure has been high for 9 seconds.

4) The start switch is ON and the $T_{5.1}$ or $T_{4.1}$ temperature error is greater than 200F (95C).

5) Engine speed exceeds 95,000 rpm.

6) The engine is overloaded, i.e., speed has exceeded 75 percent, start sequence has been completed, and engine speed falls below 70 percent.

3.4.2 Electrical Systems

The electrical systems for starting and operating the PCA are contained in three major pieces of equipment: the control panel (Figure 18), the electrical enclosure (Figure 19), and the PCA (Figure 3). The wiring diagrams for these components are defined in GTEC drawings SKP4745, 305435, and 305437, respectively.

The major equipment is interconnected with cables. A 120-foot (36.6-meter) cable connects the electrical enclosure and the PCA harnesses. There are separate cables for sensor/control functions and power extraction (utility grid connection). The cables reach from the enclosure housed on the alidade (the support base for the TBC which rotates with the parabolic solar dish) up the structure to the dish focal point support for the PCA. Pin connectors at the ends of the cables attach to the mating connectors on the PCA. A 360-foot (110-meter) cable connects the electrical enclosure with the control panel.

3.4.3 Instrumentation

The power section and receiver are instrumented adequately to allow comparison of each major component's performance with the computer model (described in Section 3.3.1) and previous test results. The instrumentation locations are shown in Figures 57 and 58 for the power section and receiver, respectively. Table 11 lists the parameters of system instrumentation, together with identifying numbers, symbols, ranges, and units.

Power section speed, temperatures, and pressures are for monitoring performance, while shaft and rotor motion are for monitoring the rotor dynamic health of the high-speed engine rotor. Lubricant and thrust washer temperatures are monitored to assure adequate lubricant cooling and to verify oil-thrust-bearing power loss. Generator electrical parameters of power, current, voltage, and frequency are used to monitor net output and proper interconnection with the utility grid. Receiver pressures and temperatures are used for estimating effectiveness, pressure losses, and thermal input into the engine.

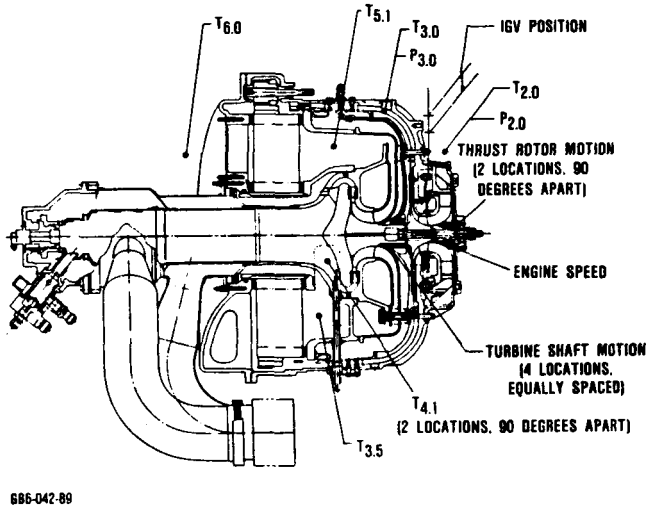

Figure 57. SAGT-1A Power Section Instrumentation Locations.

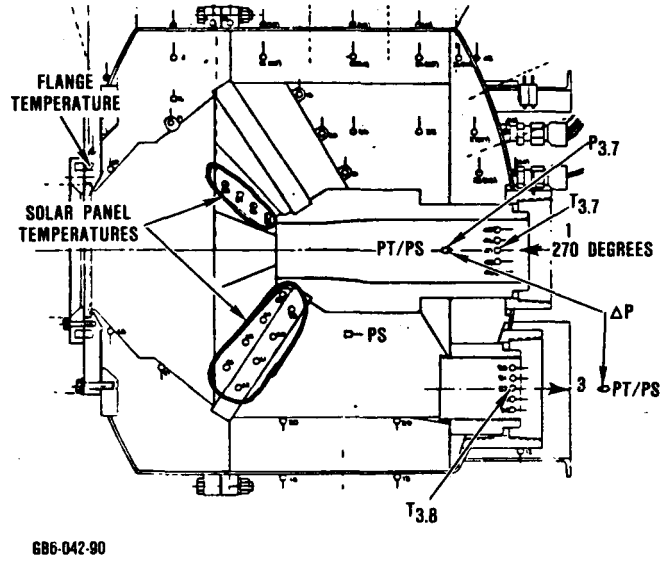

Figure 58. SAGT-1A Receiver Instrumentation Locations.

Table 11. System Test Instrumentation.

Data System*				Master Number	Parameter	Symbol	No. of Sensors	Range	Units
1	2	3	4						
X	X	X		1	Engine Speed	NE	2	0-100	krpm
X	X			5	Barometric Pressure	$P_{2.0}$	1	13-16	psia
X	X	X		51	IGV Position	VIGV	1	0-100	percent
X	X			548	Comp Disch Pressure	$P_{3.0}$	1	0-50	psig
X				148	Comp Disch Temperature	$T_{3.0}$	1	0-500	F
X	X			185	Regen Disch Temp (HP)	$T_{3.5}$	1	0-2000	F
X	X	X		208	Turbine Inlet Temperature	$T_{4.1}$	2 Avg.	0-2000	F
X	X			256	Regen Inlet Temp (LP)	$T_{5.1}$	1	0-2000	F
X				299	Exhaust Gas Temperature	$T_{6.0}$	3 Avg.	0-1000	F
X				401	Engine Inlet Temperature	$T_{2.0}$	1	0-100	F
			X	601	Turbine Shaft Motion	SMTB	4 (2)	0-5	mils
			X	701	Thrust Rotor Motion	SMTR	2	0-5	mils
	X	X		801	Fuel Command	FULC	1	0-100	percent
X				2501	Thrust Washer Temperature	TWOD	2	0-500	F
X				3506	Oil Inlet Temperature	TOILI	1	0-500	F
X				3507	Oil Out Temperature	TOILO	1	0-500	F
X				4326	Scavenge Temperature	SCOT	2	0-500	F
X				5101	Receiver Inlet Pressure	$P_{3.7}$	1	0-500	psig
X				5201	Receiver Pressure Drop	DPREC	1	0-10	in.H_2O
X				5301	Receiver Inlet Temp	$T_{3.7}$	5 (2 Avg)	0-2000	F
X				5401	Receiver Exit Temperature	$T_{3.8}$	5 (2 Avg)	0-2000	F
X				5555 through 5566	Solar Panel Temperature	TSOLP	12	0-2000	F
X		X		5701	Receiver Flange Temp	TRECF	1	0-500	F
X		X		6001	Generator Power	WATTS	1	±25	kW
X		X		6002	Generator Current	GENA	1	±250	amps
X				6003	Generator Voltage	GENV	1	0-500	volts
X				6010	Generator Frequency	GENF	1	0-100	Hz

*Data System

1. Data Logger
2. Control Panel Meter
3. Analog Chart
4. Oscilloscope

4.0 DISCUSSION OF TEST RESULTS

The SAGT-1A test program comprised two phases: engine or power section testing, and power conversion assembly (PCA) or system testing. These tests and the results are described in this section. Also included herein is a discussion of the metal engine characterization test (a program milestone), since the SAGT-1A test program was closely linked to the AGT101 program. In fact, the decision to go ahead with the SAGT-1A test program followed the successful completion of the characterization test.

4.1 Power Section Test Results

The total test history of the S/N 003 power section is summarized below:

Test	Hours	Starts
SAGT Power Section	6.8	32
SAGT-1A System	11.0	29
AGT101 Engine	100.2	272
Total of all Builds of S/N 003 Power Section	118.0	333

This total experience represents a relatively mature engine (for a nonproduction class engine) and indicates a readiness for testing on the solar test bed concentrator (TBC).

4.1.1 Metal Engine Characterization Test

The metal engine characterization test was completed on Build 48B of the S/N 003 power section in January 1985. Performance was measured at various speeds and variable inlet guide vane (VIGV) positions as defined in Table 12. During this test, the engine accumulated 5.6 hours and 4 starts.

Table 12. Performance Measured to Complete Metal Engine Characterization.

Data Point	Speed,* rpm	VIGV Position,** degrees
1	70,000	0
2	80,000	0
3	80,000	20
4	80,000	40
5	80,000	60
6	90,000	0
7	95,000	0

*±200 rpm
**±2 degrees

4.1.1.1 Metal Engine Configuration

Build 47 test results indicated excessive leakage in several engine sealing areas. These areas are shown in Figure 59. Improvements to reduce leakage were made in all areas except the flipper seals and exhaust housing "C" seal, these last two areas having already exhibited very low leakage rates. The regenerator seals were improved by Ford as part of its planned development program (see Figure 37). When the Phase VA seals became available, they showed a significant improvement at pressure simulating 80,000 rpm. These data are plotted in Figure 60, along with data resulting from the other improvements. The foil-bearing leakage was reduced by adding a baffle adjacent to the bearing on the upstream side. This baffle is a thin shim, 0.005 in. (0.127 mm) thick, with a radial clearance to the shaft equal to its thickness. It is piloted in the foil-bearing carrier to keep it centered relative to the shaft. The baffle is shown installed in the engine in Figure 61.

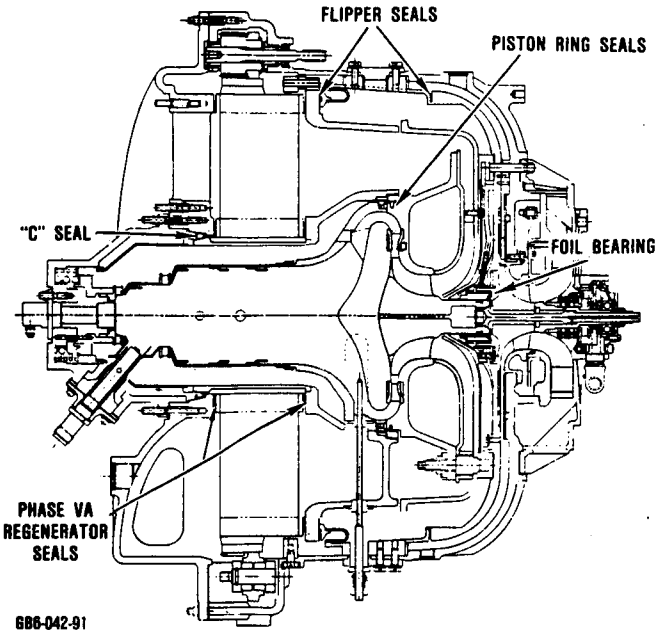

Figure 59. Seal Leakage Areas Were Individually Tested.

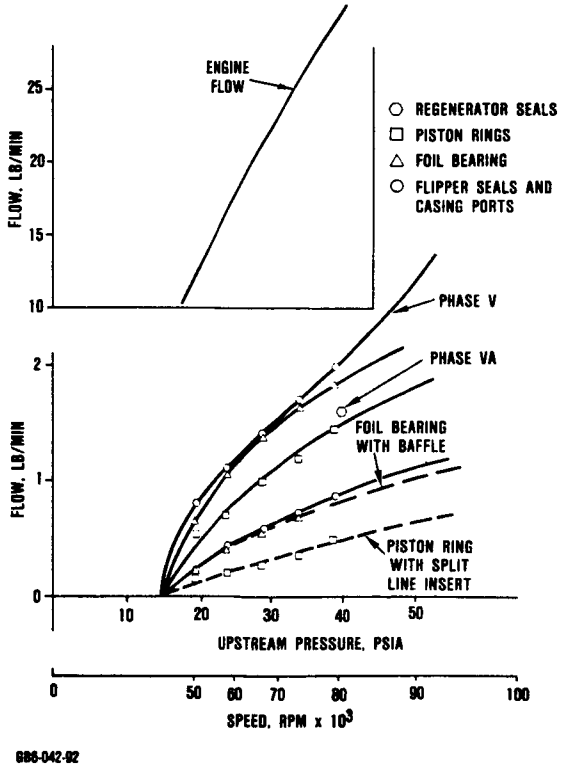

Figure 60. S/N 003 Build 48B Engine Leakage Improvements Were Measured.

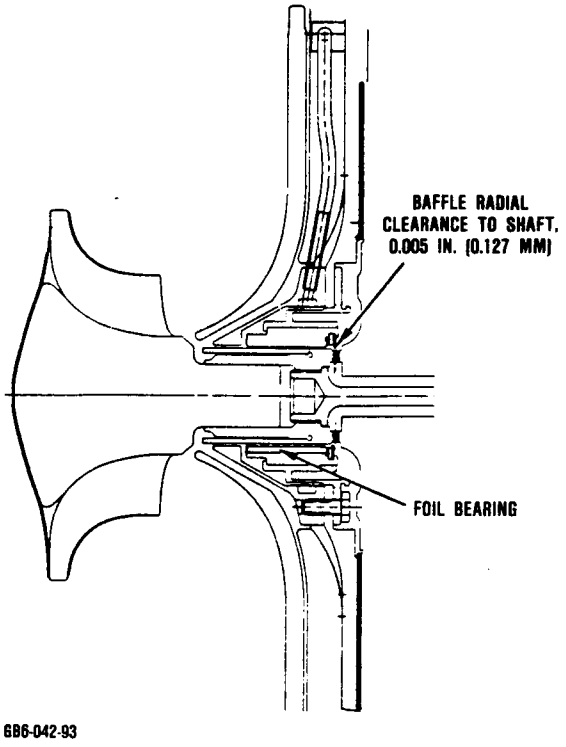

Figure 61. Foil Bearing Baffle Was Installed to Reduce Leakage.

The piston rings were also modified with a sheet-metal insert. The split line of each of the three rings creates leakage areas as shown (shaded) in Figure 62. A Hastelloy-X insert was installed in the ring to cover the split-line gap. With this insert installed, the leakage rate decreased to 1.5 percent.

With these sealing areas improved, the engine was built per AGT101 assembly drawing PA3610110.

4.1.1.2 Test Results

Performance was measured at 70,000, 80,000, 90,000, and 95,000 rpm with the IGV position at O degree; measurements were also made at variable IGV positions (20, 40, and 60 degrees) at 80,000 rpm (Data Points 3, 4, and 5 in Table 12).

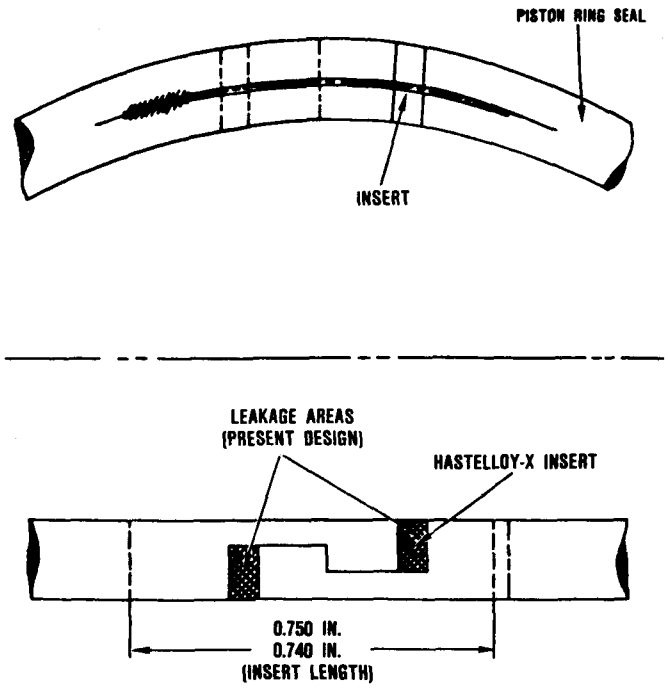

Figure 62. Piston Ring Seal Showing Added Inserts at Split Line to Decrease Leakage.

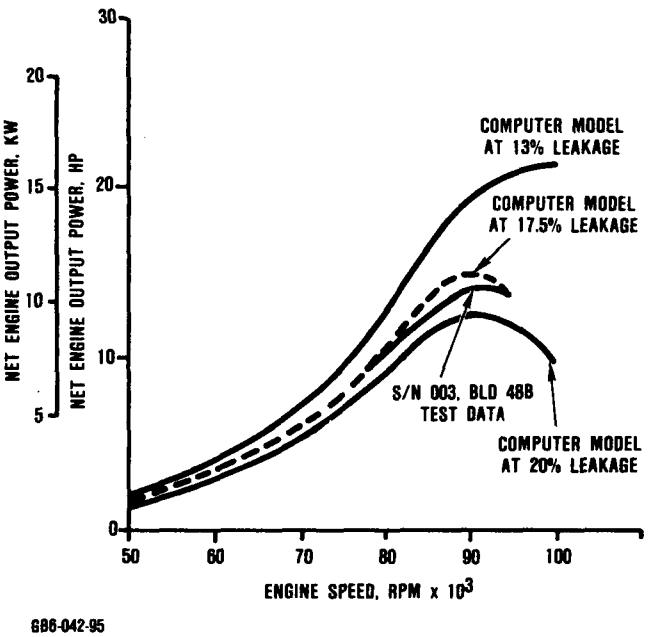

Figure 63. Engine Performance as a Function of Speed.

The drag torque applied to the hydraulic load motor was measured at each operating condition. The resulting net power output is plotted as a function of engine speed in Figure 63 and as a function of IGV position in Figure 64.

4.1.1.3 Analysis of Results

To calculate the aerodynamic power output (neglecting losses) for comparison with the computer performance model, the parasitic losses were measured and are shown in Figure 65. Figure 66(a) shows the total parasitic losses versus speed. This curve represents a summation of the five curves shown in Figure 65. Adding the power-train loss [Figure 66(b)] to the measured output yields bare engine power, i.e., the power available at the high-speed output gear of the engine (the input to the gearbox).

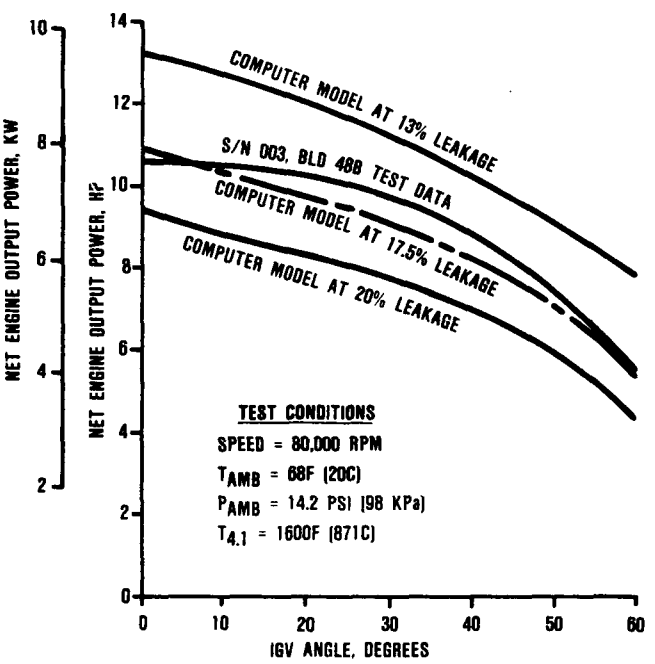

Figure 64. Engine Performance as a Function of IGV Position.

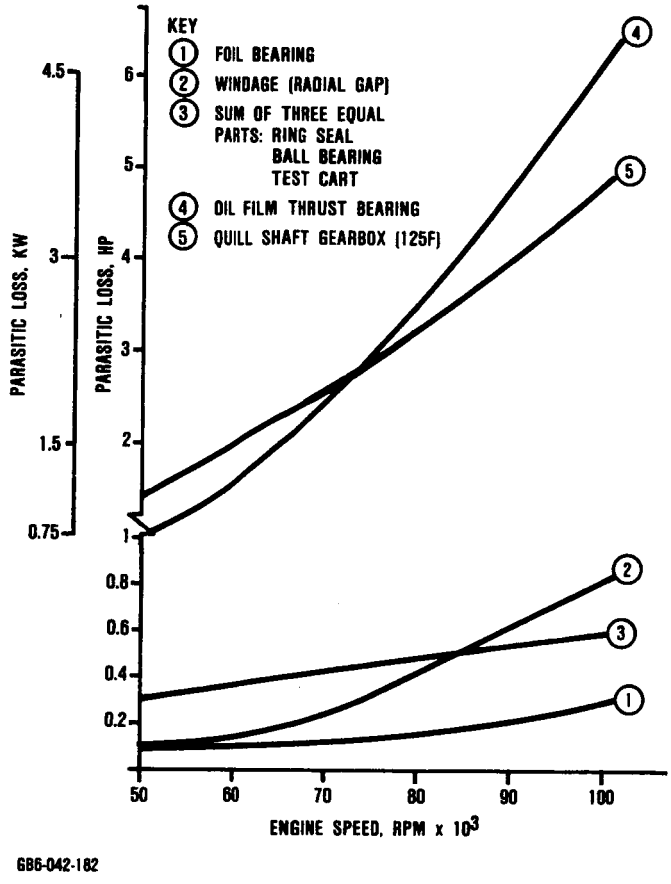

Figure 65. Parasitic Losses Versus Engine Speed Were Measured.

Adding the power loss from the curve in Figure 66(a) to the dynamometer-measured power output yields a "measured" aerodynamic power to compare with the computer modeling results. Comparison of these values at 70,000, 80,000, and 90,000 rpm (±200 rpm) is shown in Table 13. The instrumentation locations referenced in Table 13 are shown in Figure 57. Component efficiencies at these operating conditions are plotted on the performance maps in Figures 67 and 68.

The comparisons show excellent agreement between the computer model and the test

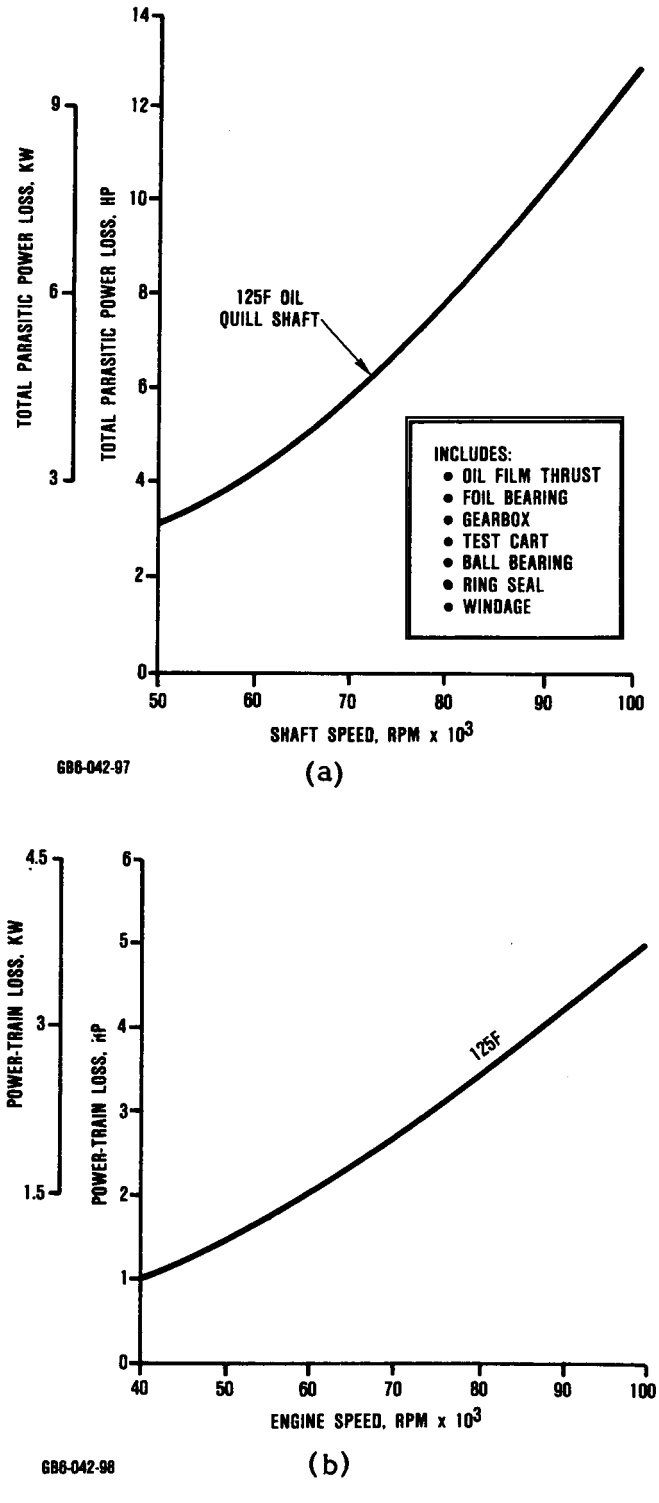

Figure 66. Parasitic Power Losses Were Determined Between Aero and Dynamometer (a) and Back to the Engine Output Gear (b).

Table 13. AGT101 S/N 003 Engine Test/Computer Model Comparison.

Parameter	Engine Test 1-11-85		Computer Model		Δ	Engine Test 1-14-85		Computer Model		Δ	Engine Test 1-11-85		Computer Model		Δ
N_e, rpm	69,000		69,000		0	80,060		80,060		0	90,150		90,150		0
N_{reg}, rpm	12.5		12.5		0	18.6		18.6		0	20.2		20.2		0
IGV, degrees	0		0		0	0		0		0	0		0		0
$P_{ambient}$,psia (kPa)	14.17	(97.7)	14.17	(97.7)	0	14.186	(97.8)	14.186	(97.8)	0	14.17	(97.7)	14.17	(97.7)	0
$P_{3.0}$, psia (kPa)	34.88	(240.5)	32.58	(224.6)	+2.3	43.95	(303.0)	42.73	(294.6)	+1.22	54.21	(373.8)	52.9	(364.7)	+1.31
T_{cell}, F (C)	74	(23)	74	(23)	0	68	(20)	68	(20)	0	76	(24)	76	(24)	0
$T_{3.0}$, F (C)	293	(145)	270	(132)	+23	330	(166)	332	(167)	-2	394	(201)	401	(205)	-7
$T_{3.1}$, F (C)	318	(156)	314	(152)	+4	352	(178)	359	(182)	-7	419	(215)	418	(214)	+1
*$T_{3.5}$, F (C)	1100	(593)	1203	(651)	-103	992	(533)	1129	(609)	-137	958	(514)	1070	(577)	-112
$T_{4.1}$, F (C)	1603	(873)	1603	(873)	0	1611	(877)	1611	(877)	0	1622	(883)	1622	(883)	0
$T_{5.0}$, F (C)	1280	(656)	1325	(718)	-45	1210	(654)	1237	(669)	-27	1215*	(657)	1172	(633)	+43
$T_{5.1}$, F (C)	1212	(656)	1256	(680)	-44	1146	(619)	1187	(642)	-41	1108	(598)	1134	(612)	-26
$T_{6.0}$, F (C)	417	(214)	394	(201)	+23	450	(232)	440	(227)	+10	510	(266)	500	(260)	+10
Gross Power, hp (kW)	---	---	10.4	(7.76)	---	---	---	18.35	(13.7)	---	---	---	24.7	(18.42)	---
Parasitic Loss, hp (kW)	---	---	5.6	(4.18)	---	---	---	7.8	(5.82)	---	---	---	10.2	(7.61)	---
Net Power, hp (kW)	5.3	(3.95)	4.8	(3.58)	+0.5	10.56	(7.87)	10.55	(7.87)	+0.01	14.1	(10.51)	14.5	(10.81)	-0.4
Power-Train Loss, hp (kW)	---	---	2.65	(1.98)	---	---	---	3.45	(2.57)	---	---	---	4.25	(3.17)	---
Bare Engine, hp (kW)	---	---	7.45	(5.56)	---	---	---	14.0	(10.44)	---	---	---	18.75	(13.98)	---
Bare Engine [at SL, 59F (15C)], hp (kW)	---	---	9.07	(6.76)	---	---	---	16.0	(11.93)	---	---	---	22.40	(16.70)	---
Fuel Flow, lb/hr (kg/hr)	---	---	7.53	(3.42)	---	12.5	(5.67)	12.2	(5.53)	+0.3	---	---	17.4	(7.89)	---
Total Leakage, percent	---	---	15.4	---	---	---	---	16.2	---	---	---	---	16.6	---	---
	NOTE: Leakage and/or parasitic losses may be lower at low speeds.					NOTE: Best match.					NOTE: Leakage and/or parasitic losses may be higher at high speeds.				

*Bad reading.

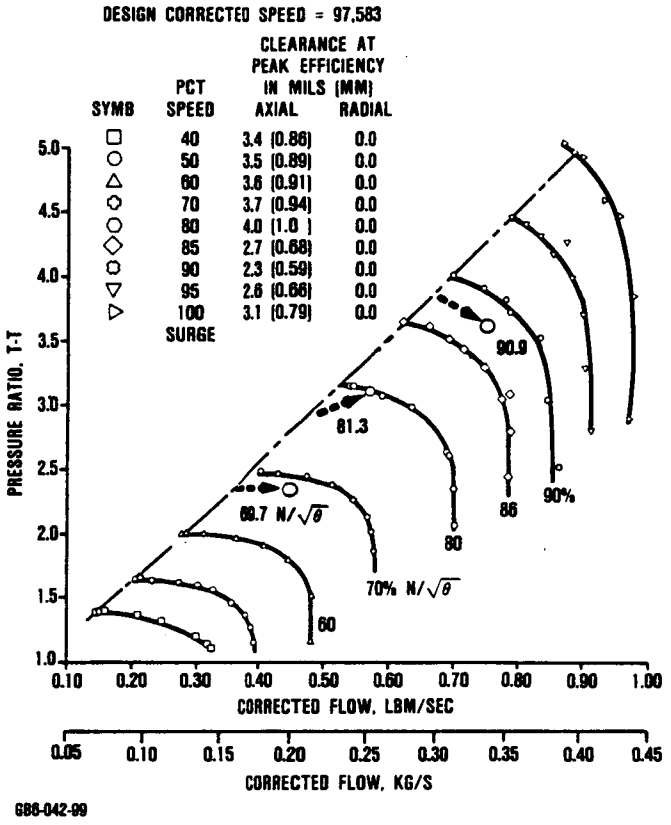

Figure 67. Engine S/N 003 Build 48B Compressor Performance (updated corrected flows).

results, except for the noted bad readings (Table 13). The thermocouple measuring $T_{3.5}$ was inspected after the test, and a secondary junction was found at the connector outside the engine. This would cause "averaging" to occur between the ambient temperature and the internal engine temperature, which explains the significantly lower temperatures in the test data as compared with those for the computer model.

Table 14 compares component leakage measured for pretest cold static state with component leakage estimated by the computer model for hot operating engine, all at 80,000-rpm pressures. Examination of the data reveals that predicted hot-engine leakage is significantly higher than measured cold-static leakage, indicating that the thermal and/or pressure distortion of the housings with the sealing surfaces causes increased leakage.

4.1.2 SAGT Power Section Performance Test

The AGT101 power section, S/N 003, was reconfigured to the SAGT configuration with the addition of an external flow loop in series with the combustor. The engine is shown set up in the test cell in Figure 69. The special test duct, STE276075, was used to simulate the expected pressure drop that the regenerator discharge flow will experience through the Sanders solar receiver before it reenters the combustor. In addition, the effects of reduced compressor and turbine clearances on SAGT performance were measured. A total of 21 starts and 3.1 hours of run time were accumulated in this power section test.

The power section was then installed on the PCA for system testing as described in paragraph 4.2.1.

4.1.2.1 SAGT Configuration

The engine test configuration designated Build 49 included all of the features tested in Build 48B. These features included:

- The baseline "6+1" foil bearing from the motoring tests, Builds 45 and 46
- The Phase VA regenerator seals
- The baffle, P/N PA3610675-1, installed upstream of the foil bearing to reduce leakage
- The sheet-metal insert installed on each of the three piston rings to block leakage at the split line

In addition, certain changes were made to Build 48B for this SAGT-1A application. These modifications of the rotating group and combustor ducting are described below:

ORIGINAL PAGE IS
OF POOR QUALITY

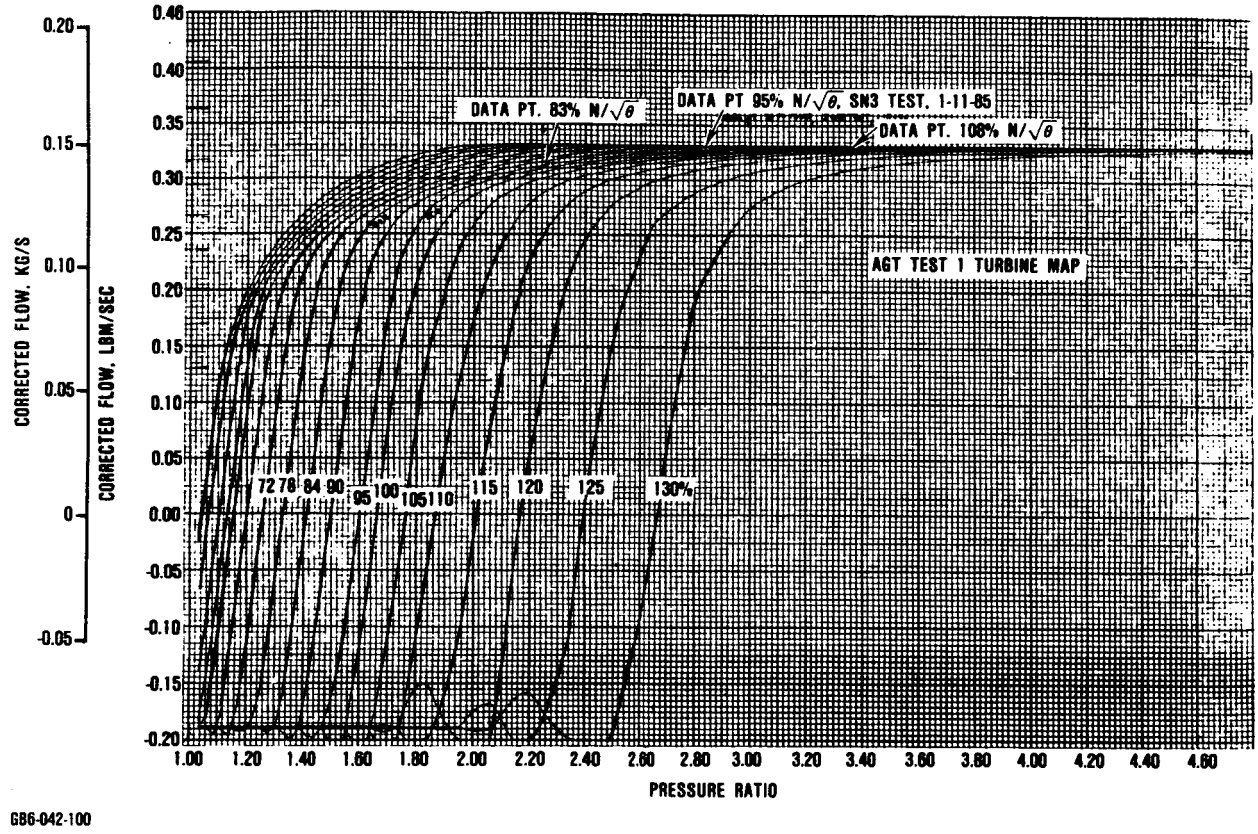

G86-042-100

Figure 68. Engine S/N 003 Build 48B Turbine Performance Plotted on Component Map.

Table 14. Component Leakage Compared Between Measured Cold Static and Estimated Hot Operating Engine (all data for 80,000-rpm pressures).

Component	Cold Static Test Data, percent*	Hot Operating Engine Data,** percent local flow
Piston Rings	1.8	4.5
Foil Bearing	2.8	1.65
Flipper Seals and Overboard	3.1	0.53
Regenerator System	4.3	11.5
Total	12	18.18 = 17.5*

*Percent of total engine flow.
**Estimated via computer model.

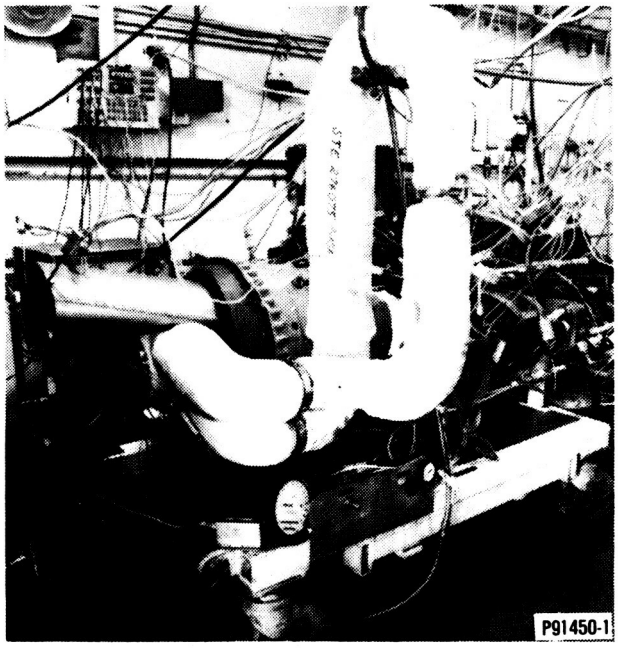

GB6-042-101

Figure 69. SAGT-1A Power Section Test Setup.

- The compressor shroud was set at the minimum clearance, 11 mils (0.279 mm) within adjustment range. This represents a decrease in clearance from Build 48B of approximately 4 mils (0.10 mm), which is allowable since the speed is limited to 10,000 rpm less than AGT101 full speed.

- The turbine shroud clearance also was decreased from 45 to 35 mils (11.4 to 8.9 mm).

Rotor Clearance Data

Figure 70 summarizes a typical turbine axial clearance transient during a cold start to 50,000 rpm. Compressor axial, knee, and radial clearance data were obtained to 100,000 rpm. Steady-state turbine and compressor data are summarized in Figure 71. This figure represents an envelope of observed thermal

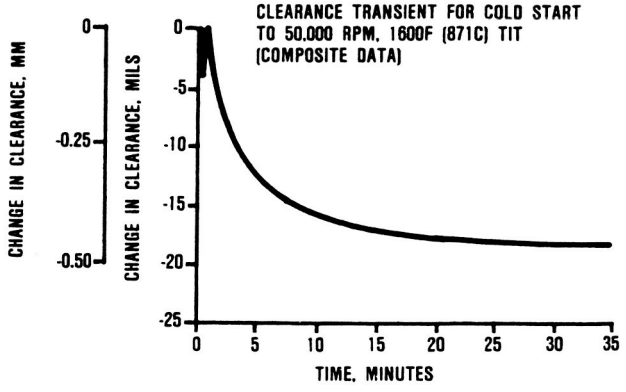

GB6-042-102

Figure 70. Typical Turbine Axial Clearance Transient for Cold Start.

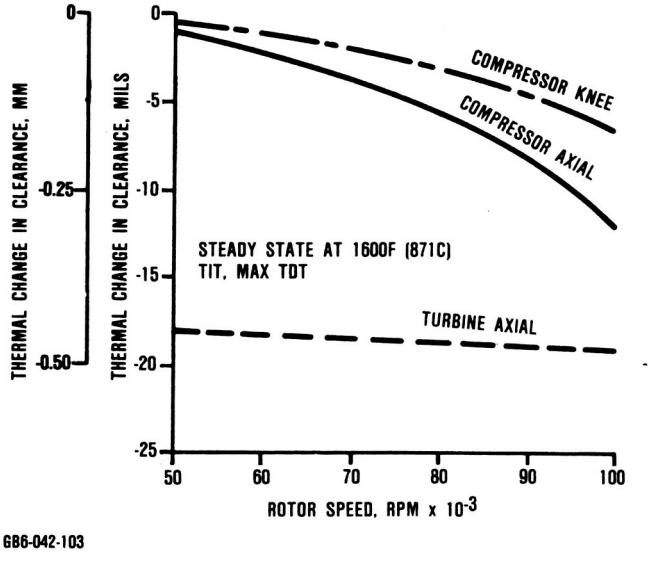

GB6-042-103

Figure 71. Compressor and Turbine Clearance Loss Due to Thermal Growths.

closure at steady-state operation. These data have been used as the basis for establishing the SAGT clearance at 90,000 rpm. The clearances were determined as described below.

Compressor Knee

Thermal/Centrifugal	0.004 in. (0.102 mm)
Rotor Droop Allowance	0.001 in. (0.025 mm)
Minimum Running Clearance	0.003 in. (0.076 mm)
Minimum Knee Build Dimension	0.008 in. (0.203 mm)

Turbine Axial

Thermal/Centrifugal	0.018 in. (0.457 mm)
Rotor Droop Allowance	0.003 in. (0.076 mm)
Worst Transient	0.003 in. (0.076 mm)
Worst Excursion	0.004 in. (0.102 mm)
Build Tolerance	0.002 in. (0.051 mm)
Minimum Running Clearance	0.005 in. (0.127 mm)
Minimum Turbine Axial Build Dimension	0.035 in. (0.889 mm)

The anticipated compressor axial build dimension is 0.0125 inch (0.318 mm)--larger than the knee build dimension by 0.0045 inch (0.114 mm). This difference is incorporated in the blade/shroud profile such that when the blade knee is touching the shroud, there exists a clearance of approximately 0.004 inch at the blade tips. This profile allowance accounts for "flowering" of the wheel due to thermal/centrifugal effects (see Figure 28). Build axial measurements are based on the knee clearance.

As noted above, the minimum compressor axial clearance should have been 0.008 inch (0.204 mm) at the knee, plus 0.0045 inch (0.114 mm) for "flowering," for a total of 0.0125 inch (0.318 mm). The actual measured clearance (cold-static) was 0.011 inch (0.279 mm); however, the oil-film thrust bearing develops a 0.001-inch (0.025-mm) thick film which increases the compressor (and turbine) shroud clearance by the same amount, for a total of 0.012 inch (0.304 mm). This results in an estimated minimum running clearance of 0.0025 inch (0.063 mm).

The engine was assembled per Drawing PA3610110 and the associated parts list. The external ducts and combustor adapter were added as defined in Drawing 3609092.

4.1.2.2 Test Results

All but two of the test points shown in Table 15 were successfully completed. Test Points 4 and 8 (both at the nearly closed IGV position) were omitted because they are representative of transient and not steady-state conditions. The engine was run at each test-point condition long enough to reach steady state thermally, or for a minimum of 10 minutes. Data were recorded every 60 seconds.

Table 15. SAGT Power Section Test Points Cover Range of Planned TBC Tests.

Test Point	Speed,* rpm	VIGV Position,** degrees
1	80,900	0
2	80,900	20
3	80,900	40
4	80,900	70
5	85,500	0
6	85,500	20
7	85,500	40
8	85,500	70
9	90,300	0
10	90,300	20
11	90,300	40

*±50 rpm
**±2 degrees

After the performance test was successfully completed, a start test was also run. For this test, the speed command was preselected to full speed (80,000 to 90,000 rpm), and the starter was manually disengaged at approximately 55,000 rpm during acceleration to full speed. Starts were successfully made to 90,000 rpm and IGVs closed to as low as 80 degrees. Because of the anticipated difference in the start characteristics of the hydraulic starter (engine test) that was disengaged at 55,000 rpm versus the electric motor/generator (system test) that remains engaged continuously, additional testing was performed during the system test to evaluate engine start characteristics and control parameters.

An overspeed test was also run. The electronic control unit (ECU) shut the engine down at 94,000 rpm due to an overspeed fault. This represents a 2-percent error from the requested set point (92,000 rpm) for the total speed control loop plus the readout system.

4.1.2.3 Analysis of Results

The measured performance data were input to the computer model. The results are compared with the actual measured data in Table 16. Good correlation exists for Test Point 9, i.e., 90,300 rpm and 0-degree IGV position (see Table 15).

Table 17 presents the power output for all nine test points. The internal engine losses (representing $hp_{Aero} - hp_{Bare}$) and external losses (representing $hp_{Bare} - hp_{Dyno}$) are based on the measured losses presented in Figure 66.

The most significant effect noted from this test is the influence of the compressor/shroud clearance change on compressor efficiency. Figure 72 shows the compressor efficiencies as a function of corrected flow for both the Build 48B test and this test [Build 49 with a 4-mil (0.10-mm) reduction in clearance]. These data show a 4-point improvement as a result of decreasing the clearance to the levels used in the component performance test.

4.1.3 Power Section Green Runs Prior to System Test

4.1.3.1 Build 50

After the bearing failure in the first system test (Section 4.2.1), the power section was rebuilt (Build 50) to the same configuration as Build 49, except the combustor adapter duct was not installed. Instead the combustor was directly mounted to the exhaust housing.

The engine was run for 42 minutes at speeds up to 90,000 rpm. The proximity probes tracking the turbine shaft indicated excessive synchronous (1/revolution) motion and the engine was shut down. The analog chart trace shown in Figure 73 shows the turbine rotor vertical runout, as well as other parameters. The runout parameter read 1.5 mils (0.038 mm) at 90,000 rpm, which is right at the limit. However, the probe located 90 degrees from the one recorded on the analog chart indicated a turbine shaft motion of 2.6 mils (0.066 mm). Since this is significantly higher than the 1.5-mil (0.038-mm) limit, the engine was returned to assembly and completely torn down.

Teardown did not reveal any problem. A closer examination of the shaft motion data indicated that the eccentric motion may actually have been much less. First, the proximity probe calibration data were plotted (see Figure 74). This plot shows extreme nonlinearity, possibly due to the 125-foot cable between the probe and the amplifier. The slope changes by a factor of 7:1 from a gap of 1 to 17 mils (0.025 to 0.431 mm). This gap can vary during the test by the shaft changing position and/or the probe changing electrically as it heats up.

For these reasons, the gap was continuously monitored during the next test. The dc voltage was recorded on the tape recorder along with the ac voltage to permit thorough reduction of the recorded data by adjusting the slope of the motion (Figure 74 slope) based on the actual gap measured at the same time (the dc amplitude).

Table 16. SAGT-1A Engine Test/Computer Model Comparison of Various Parameters.

Parameter	Engine Test, 5-15-85	Computer Model
N_e, rpm	90,290	90,290
N_{reg}, rpm	21	21
IGV, degrees	0	0
$P_{ambient}$, psia (kPa)	14.065 (96.9)	14.065 (96.9)
$P_{3.0}$, psia (kPa)	48.011 (331)	49.389 (340)
T_{cell}, F (C)	111 (43.9)	111 (43.9)
$T_{3.0}$, F (C)	407 (208)	425 (218)
$T_{3.1}$, F (C)	--	444 (228.8)
$T_{3.5}$, F (C)	1022 (550)	1097 (591)
$T_{4.1}$, F (C)	1614 (879)	1614 (879)
$T_{5.0}$, F (C)	--	1187 (642)
$T_{5.1}$, F (C)	1122 (606)	1146 (619)
$T_{6.0}$, F (C)	509 (263)	514 (267.5)
Fuel Flow, lb/hr (kg/hr)	--	14.82 (6.71)
Net Power, hp (kW)	10.56 (7.88)	11.33 (8.46)
Gross Power, hp (kW)	20.78 (15.5)	21.70 (16.2)
Bare Engine, hp (kW)	14.64 (10.92)	15.59 (11.62)
Leakage, percent	--	15.0

Table 17. SAGT-1A Engine Test/Computer Model Comparison of Power Output.

Engine Speed, rpm	Compressor IGV, degrees	Power Output, 5-15-85 Test			Power Output, Computer Model	Leakage, percent
		hp_{Dyno} (kW_{Dyno})	hp_{Bare} (kW_{Bare})	hp_{Aero} (kW_{Aero})	hp_{Aero} (kW_{Aero})	
80,900	0	8.57 (6.39)	12.07 (9.00)	16.67 (12.42)	16.7 (12.47)	11.3
80,900	20	8.03 (5.99)	11.53 (8.61)	16.13 (12.04)	15.6 (11.64)	11.3
80,900	40	6.65 (4.96)	10.15 (7.57)	14.75 (11.0)	14.0 (10.44)	11.3
85,450	0	9.19 (6.75)	13.04 (9.73)	18.29 (13.62)	18.5 (13.80)	13.1
85,500	20	8.96 (6.68)	12.81 (9.56)	18.06 (13.48)	17.4 (12.98)	13.1
85,440	40	6.6 (4.92)	10.45 (7.80)	15.70 (11.71)	15.5 (11.57)	13.0
90,290	0	10.56 (7.88)	14.64 (10.91)	20.78 (15.50)	21.7 (16.18)	15.0
90,340	20	10.24 (7.65)	14.50 (10.82)	20.64 (15.40)	18.5 (13.80)	14.9
90,380	40	7.22 (5.39)	11.48 (8.57)	17.62 (13.15)	17.9 (13.36)	14.9

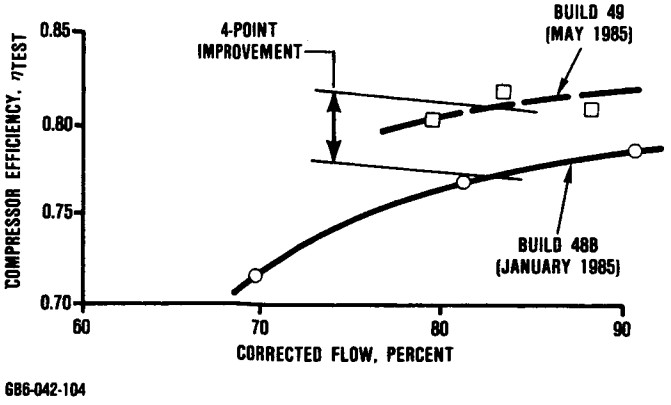

Figure 72. Compressor/Shroud Clearance Effects on Efficiency Are Significant.

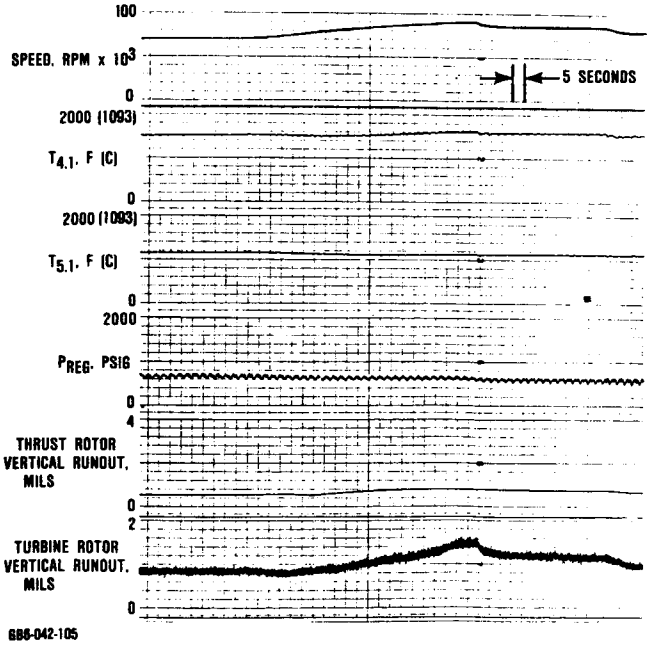

Figure 73. Engine S/N 003 Build 50 Rotor Motion at Maximum Speed.

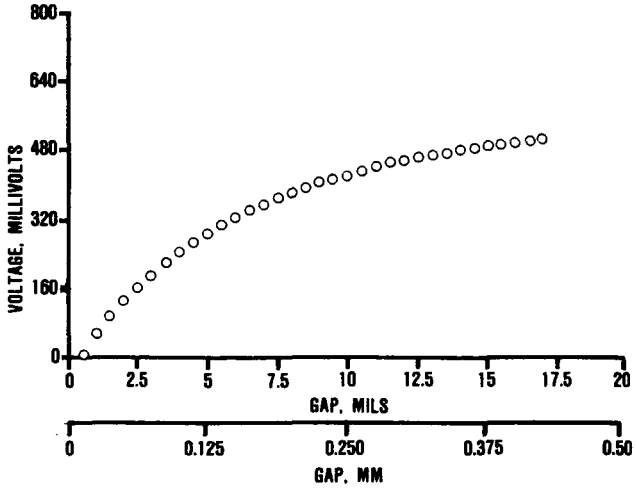

Figure 74. Horizontal Proximity Probe (Turbine Motion) Calibration Curve.

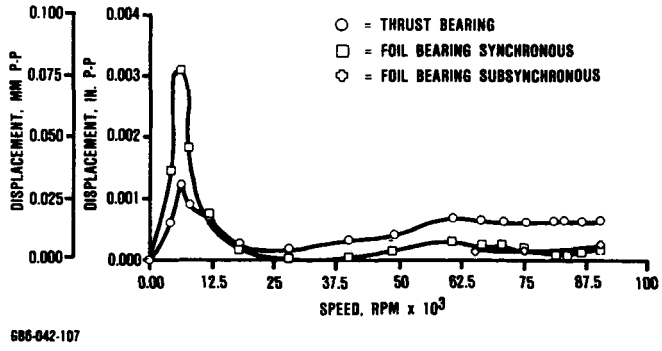

Figure 75. Engine S/N 003 Build 51 Dynamic Response Shows Much Lower Displacement Than Build 50.

4.1.3.2 Build 51

For Build 51 of the S/N 003 engine, the two rotor support bearings were replaced as a precautionary measure; neither the foil bearing nor the ball bearing was damaged in the previous test of this engine. The objectives of this test were to check the rotor dynamic signature up to full speed and to check performance at 80,000 to 90,000 rpm.

The rotor dynamic signature was taken and recorded up to 90,000 rpm. The data show significantly lower displacement levels than those observed for Build 50. Figure 75 plots the synchronous and subsynchronous motion of the rotor turbine end as a function of speed for Build 51. The figure shows the dynamic response to be lower than 0.001 inch (0.025 mm) peak-to-peak (P-P) along the entire speed range, except for the first critical rotor motion where the displacement peaks at 0.0031 inch (0.079 mm). However, this is normal behavior and is a transient condition during the start, which does not damage the rotor/support system.

The other objective--the performance check--was not so successful. Performance was significantly lower than that observed in the previous performance test (Build 49). The engine was returned to assembly and partially torn down. During teardown, the exhaust housing was found to be significantly distorted in the regenerator seal and mounting flange areas (see Figure 76). The part measured 0.009 inch (0.228 mm) out of flat, whereas the blueprint tolerance is only 0.002 inch (0.051 mm). Consequently, the out-of-flat surfaces of the exhaust housing were remachined to conform to the blueprint.

4.1.3.3 Build 51A

After the exhaust housing was remachined and ground, inspection indicated the flatness of the mounting and sealing surfaces to be 0.001 inch (0.025 mm) and 0.0008 inch (0.02 mm), respectively. The engine was reassembled, installed in the test cell, and run at operating temperature and at speeds of 80,000 to 90,000 rpm for approximately 30 minutes. However, the output power was only 10 percent higher than that of Build 51, and was still below the required power. The engine was therefore returned to the assembly area for modification.

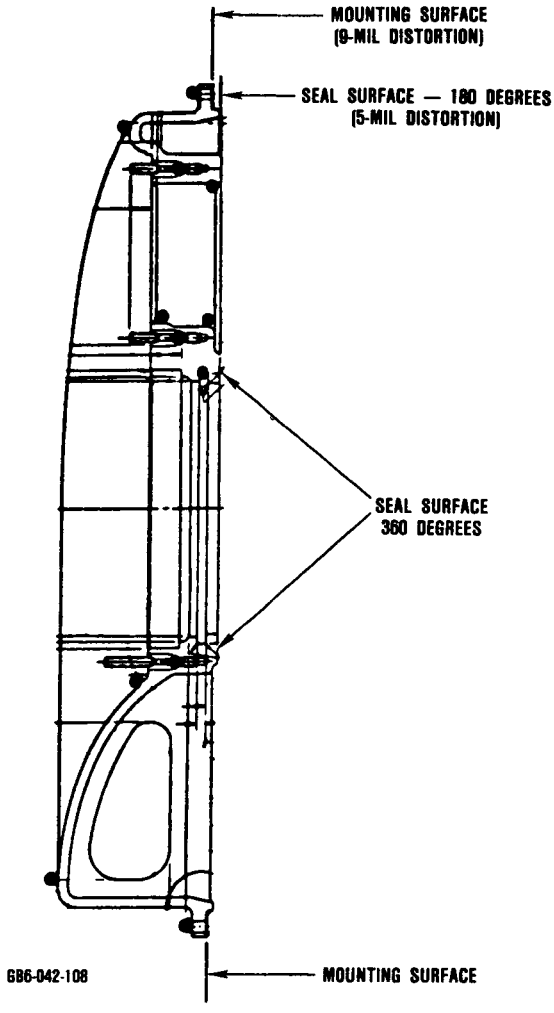

Figure 76. Exhaust Housing Distortion.

4.1.3.4 Build 51B

The regenerator was suspected to be a source of the performance deterioration observed in Build 51A. Accordingly, the regenerator core and the hot and cold seals (Figure 77) were replaced for the next test, designated Build 51B. The core was replaced with a new magnesium-aluminum-silicate (MAS) core. In addition, the engine was shimmed so that the regenerator breakaway torque was at the high limit of the allowable

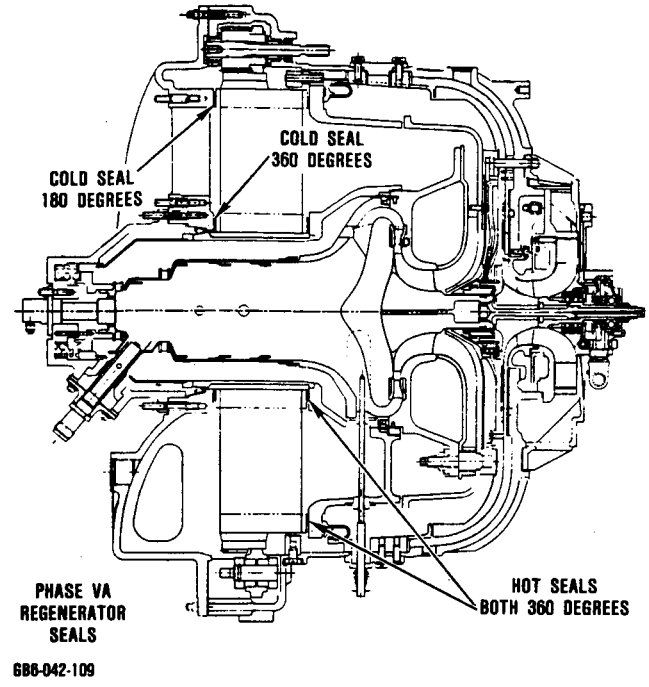

Figure 77. Power Section Showing Regenerator Seal Locations.

range, thereby creating the lowest leakage condition possible.

The engine was tested using the same parameters as Build 51A. Seven minutes into the run, the regenerator locked up. The monitored power output during the test was 11.75 hp (8.76 kW) at 80,000 rpm. This was approximately 12 percent higher than the Build 48B test results and represented a marked improvement over the previous (Build 51A) test. However, partial teardown revealed that the regenerator core was cracked in two locations and had to be replaced.

4.1.3.5 Build 51C

The regenerator core that had been installed in the engine up to and including Build 51A (made of aluminum silicate) was reinstalled for Build 51C. Shimming was also adjusted to decrease regenerator breakaway

torque from 175 lb-in. (19.8 N-m) to 150 lb-in. (17 N-m).

After reassembly with the reconfigured regenerator system, the engine was installed in the test cell and tested for 23 minutes at speeds of 80,000 and 90,000 rpm. The measured power output at these speeds was 7.9 hp (5.89 kW) and 12.7 hp (9.47 kW), respectively. The engine was then run at lower speeds and higher temperatures for 90 minutes in an attempt to wear in or glaze the regenerator seals. A second performance measurement was then taken at the same conditions as the first run, i.e., higher speeds and lower temperatures. This time, the power output was 9.5 hp (7.09 kW) and 14.4 hp (10.73 kW) at 80,000 and 90,000 rpm, respectively. These data are plotted on the performance curve (Figure 78), and show that the data for Build 51C are essentially the same as that for Build 48B. The data for Builds 51A and 51B are also presented in Figure 78 for comparison.

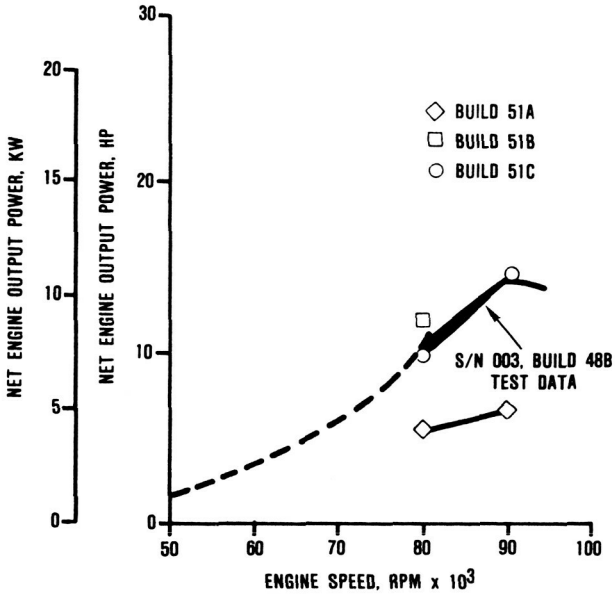

GB6-042-110

Figure 78. Build 51C Engine Performance Achieves Characterization Test Levels.

4.2 System Test Results

The power conversion assembly (PCA or system) test was initiated in June 1985, with the Build 49 engine assembled to the PCA as shown in Figure 79. SAGT-1A development, during which the PCA was readied for the TBC test at Sandia National Laboratory, is summarized in Table 18. The PCA/system was started 29 times and accumulated 11 hours of running time. The individual tests are discussed in the following paragraphs.

4.2.1 System Checkout Test

Initially, the engine was motored by energizing the starter/generator to determine if the speed signal and other engine monitoring instrumentation were operational and correctly calibrated. Five successful starts were made to an engine speed of 55,000 rpm. However, visual observation of the belt drive system during these starts indicated significant deflection in the belt and/or engine support structure. This sequence was the first time the belt drive system was used to start the engine. Belt deflections during engine starting

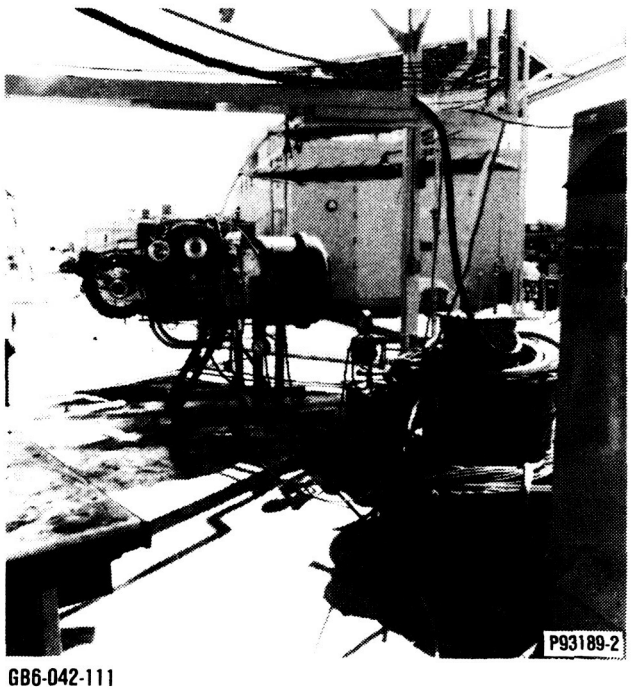

GB6-042-111

Figure 79. First PCA Test Setup.

Table 18. SAGT-1A Development Summary

Engine Build	Test Results*	Problem	Solution
49	F/B failure; turbine and compressor rub (D107E)	Belt vibrations transmitted through gearbox to engine rotor	Install stabilizer bar and move idler to start side of belt.
50	High vibrations noted during accel from 70 to 90K rpm (C-102)	Bad instrumentation (probe calibrations changed)	Recalibrate probes.
51	Performance low (C-102)	High leakage; distorted exhaust housing	Remachine exhaust housing flat.
51A	Performance low (C-102)	High leakage	Replace regenerator parts (hot and cold seals and regenerator core).
51B	Regenerator core locked up (C-102)	Regenerator core cracked	Replace core with one from Build 51A.
51C	Good run; intermittent light-offs (D-107E)	Maximum fuel schedule	Modify maximum fuel schedule.
51C	Starter overpowered	Contamination in air system caused high torque in foil bearing	Install better air filter.
52	Intermittent light-offs	Fuel control motor (poor application for selected motor)	Replace with AGT101 motor.

*Test site locations in parentheses; e.g. (D107E, Test Cell shown in Figure 79).

were transmitted through the gearbox at the gear passing frequencies. The belt vibration is transmitted as subsynchronous motion that can be observed in the turbine shaft at the foil bearing. This is not a new problem; this rotor dynamic configuration showed high sensitivity to output shaft dynamic inputs during the AGT101 development program.

On the sixth start, which was intended to check fuel flow and ignition, the engine attained a speed of 75,000 rpm. Strip chart recordings of the last two starts (5 and 6) are shown in Figure 80. At 75,000 rpm, the shaft motion was significantly higher, and before the starter could be disengaged, the foil bearing failed and a shutdown was executed. The engine was removed from the PCA and disassembled. Teardown revealed a heavily rubbed, unserviceable foil bearing, a radial turbine shroud rub, and a slight axial compressor rub.

4.2.1.1 Belt System Development Test

To isolate the belt deflection problem which was observed in the Build 49 system test, a simple belt load/deflection test was conducted. The belt motion could have been caused by belt deflection and/or by deflection of the engine support structure under the increased start load transmitted through the belt.

From the strip chart data shown in Figure 80, peak torque can be determined. The electric generator/starter peak output is 16 kW at 5000 rpm. This translates to 340 pounds (1513 N) of tensile load in the lower portion of the belt (see Figure 81). In the simple belt load/deflection test, which puts belt tension on both sides of the pulleys, the test load must be doubled.

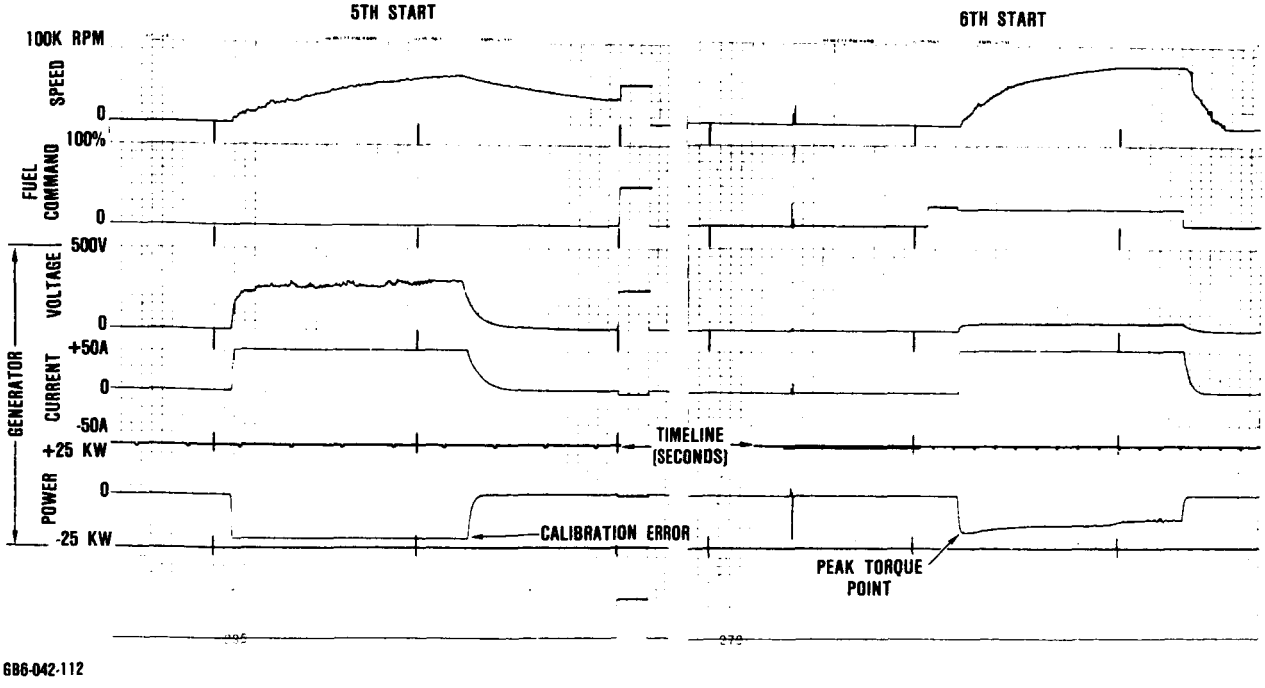

Figure 80. Strip Chart Recordings of SAGT-1A Engine Motorings.

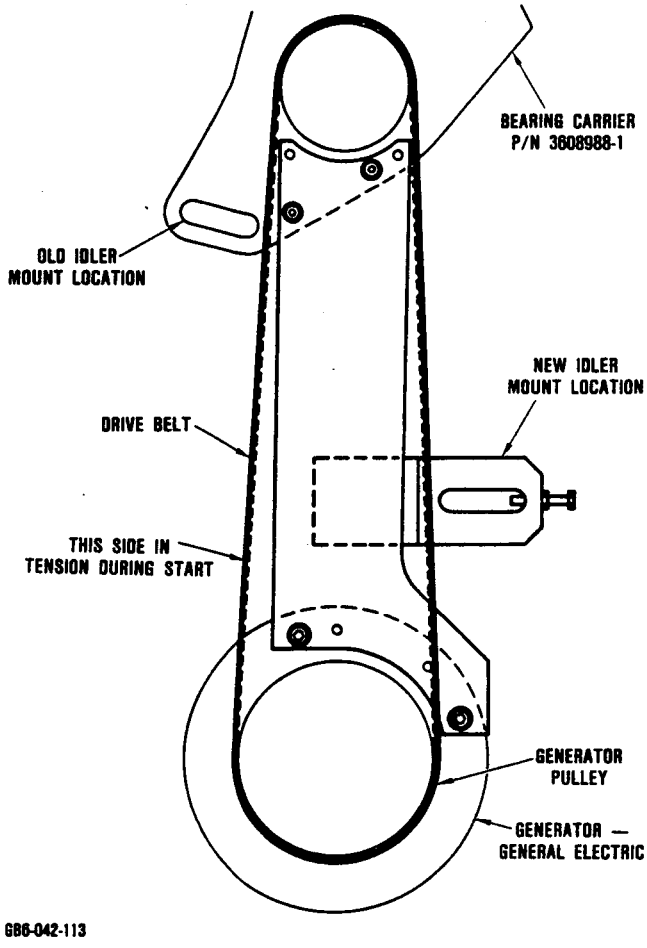

Figure 81. Engine Support Brace and Idler Mount Redesign.

The pulleys and belt were set up in a static load test facility as shown in Figure 82. A hydraulic load cylinder was used to apply the tensile load, and force was measured through a load cell. The belt stretch was measured by three dial indicators, one at the fixed end and two at the free end of the belt. Indicator locations are shown in Figures 83 and 84.

The average deflection for the 509-pound (2265-N) applied force was measured to be 24 mils (0.609 mm). Consequently, the deflection rate was calculated to be 9.4 mils (0.239 mm) for each 100 pounds (450 N) of tensile load applied to one side of the drive belt. Since the calculated start load is 340 pounds (1513 N), the resultant belt stretch is approximately 32 mils (0.813 mm). Therefore, the majority (98 percent) of the belt deflection noted during initial starts of the PCA was caused by the engine support frame deflection.

Since most of the deflection was in the engine support structure, the problem was resolved by placing a stiffening plate between the generator and the engine gearbox, as shown in Figure 81. The stiffening plate designed for this application is 3/8 inch (9.52 mm) thick. To assure zero deflection transmission of the load from the generator into the plate and from the plate into the engine gearbox, both joints were double pinned. This precludes relying on friction under the bolt heads to react the load. Since the belt only deflects 32 mils (0.813 mm) under load, spring-loaded idlers were not necessary. However, the idler was moved to the opposite side of the belt drive (i.e., the side of the belt that is unloaded during starts) because start torque transients are more severe than power-generation or shutdown transients.

4.2.2 Initial System Performance Test

After the engine was secured to the support structure, the stabilizing brace was installed on the PCA. This installation consisted of bolting the brace to the induction motor body, line drilling and tapping mounting holes into the gearbox adapter, and line drilling, reaming, and inserting four 0.25-inch (6.35-mm) steel reaction pins, two at each end. These four reaction pins were pressed into the engine gearbox adapter and the motor body, achieving a snug fit to the brace. This design permits removal of the brace while still eliminating any deflection between the engine and the motor. The installed stabilizer brace and the new idler location are shown in Figure 85.

4.2.2.1 Test Results

Build 51C motorings substantiated that the stabilizer brace shown in Figure 85 did indeed

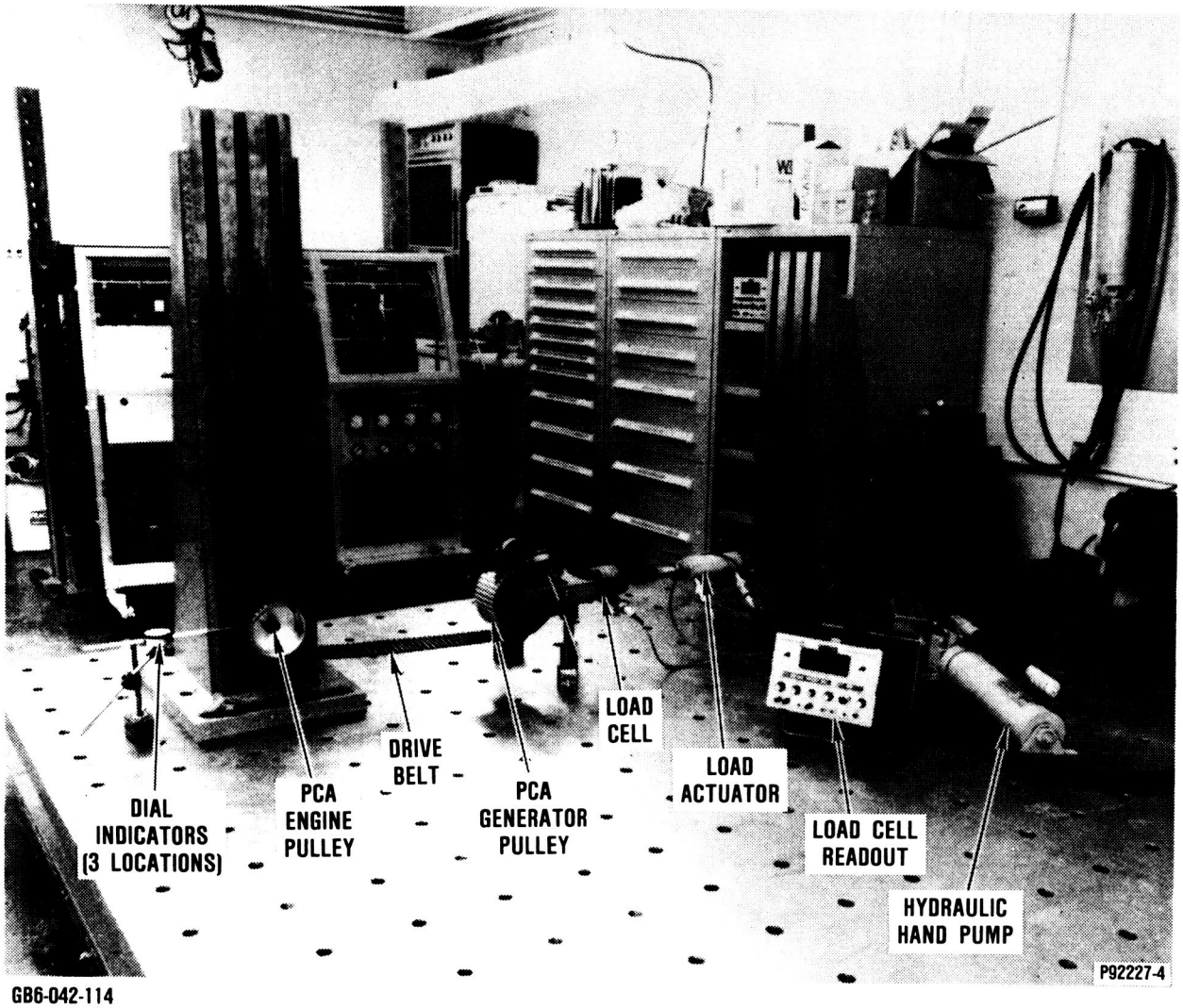

Figure 82. Drive Belt Load/Deflection Test Setup.

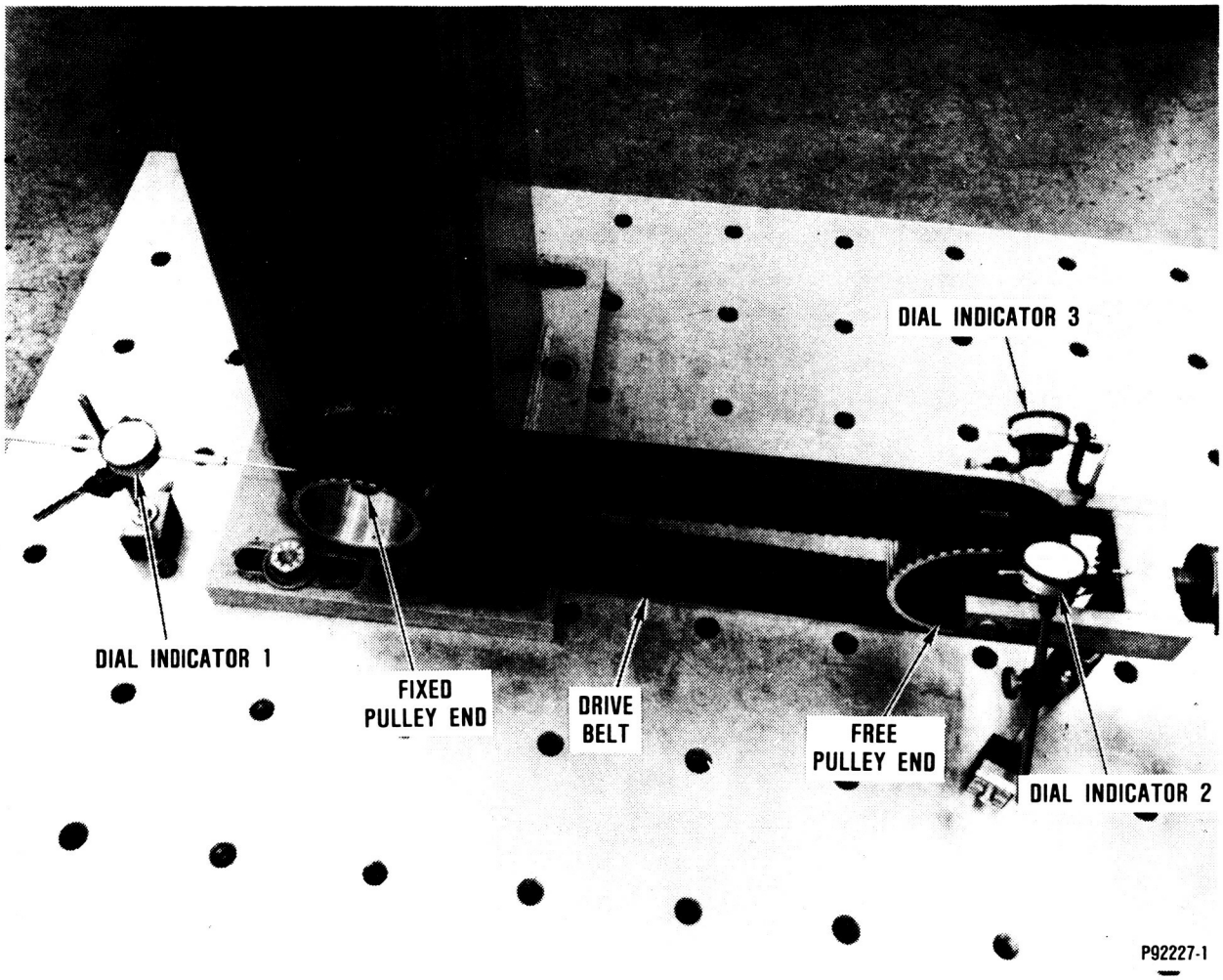

Figure 83. Locations of Load/Deflection Test Dial Indicators 1, 2, and 3.

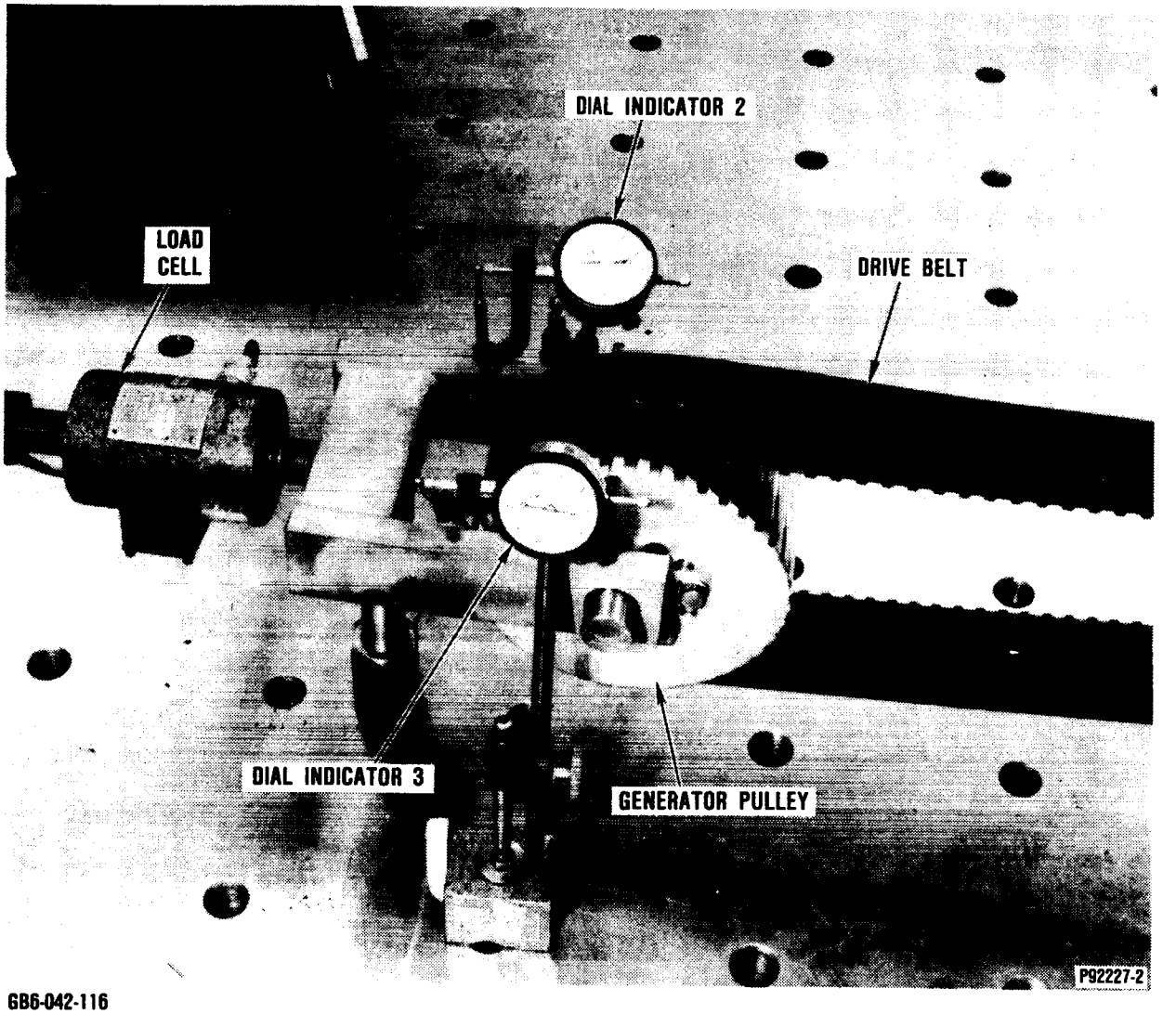

GB6-042-116

Figure 84. Locations of Load/Deflection Test Dial Indicators 2 and 3 (Free End).

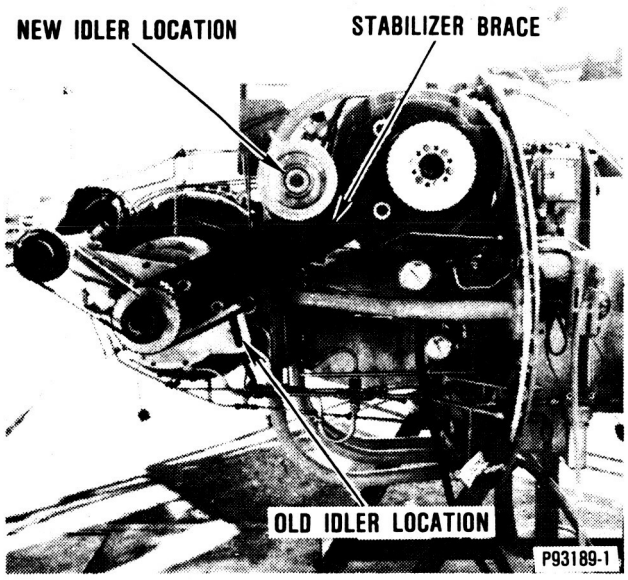

GB6-042-118

Figure 85. View of PCA Showing the Stabilizer Brace and New Idler Location.

solve the rotor dynamics problem experienced in the first motorings of the PCA system (Build 49). After the engine parameters were checked during motoring and the shaft motion was recorded on tape, the PCA system was started for the first time.

Three starts were made to generator synchronous speed (89,900 rpm engine speed) with no problems. During the final run, which lasted 60 minutes, the operating characteristics were excellent as demonstrated below:

- Turbine Inlet Temperature 1610F (882C)
- Regenerator Inlet Temperature 1250F (677C)
- Turbine Shaft Motion 0.6 mil (0.0153 mm)
- Compressor Shaft Motion 1.1 mils (0.0279 mm)
- Time to Generate Power 12 seconds

The analog data for the last minutes of this run are shown in Figure 86. The chart shows some fluctuation in the PCA electrical power output, varying between 11.4 hp (8.5 kW) at the start to 8.04 hp (6 kW) after 60 minutes.

4.2.3 Fuel System Development Tests

4.2.3.1 Fuel Schedule

Subsequent to the initial performance test, several start attempts were made without achieving light-off. Intensive efforts to resolve this problem were concentrated on the fuel control unit (FCU) and the electronic control unit (ECU). The FCU was bench tested on two separate occasions and accepted for system tests. After several engine start attempts, it was determined that the ECU maximum fuel schedule required modification.

Accordingly, the maximum fuel schedule was increased in an attempt to achieve light-off. The original fuel schedule was based on the equation

$$W_fMAX = (T_{4.1}\ SETPOINT - T_{3.5})\ (P_{3-4})/1515$$

Prior to the next start, the schedule was increased threefold, as represented by the equation

$$W_fMAX = (T_{4.1}\ SETPOINT - T_{3.5})\ (P_{3-4})/505$$

Light-off was achieved, but an overtemperature fault shut the system down. The schedule was then readjusted to provide fuel at approximately twice the original schedule, or

$$W_fMAX = (T_{4.1}\ SETPOINT - T_{3.5})\ (P_{3-4})/800$$

This fuel schedule (see Figure 87) proved successful in subsequent tests.

4.2.3.2 Fuel Pump Motor

Several starts were made to generator synchronous speed (89,900 rpm engine speed). During hot restart attempts, the fuel pump motor repeatedly tripped the overheat switch.

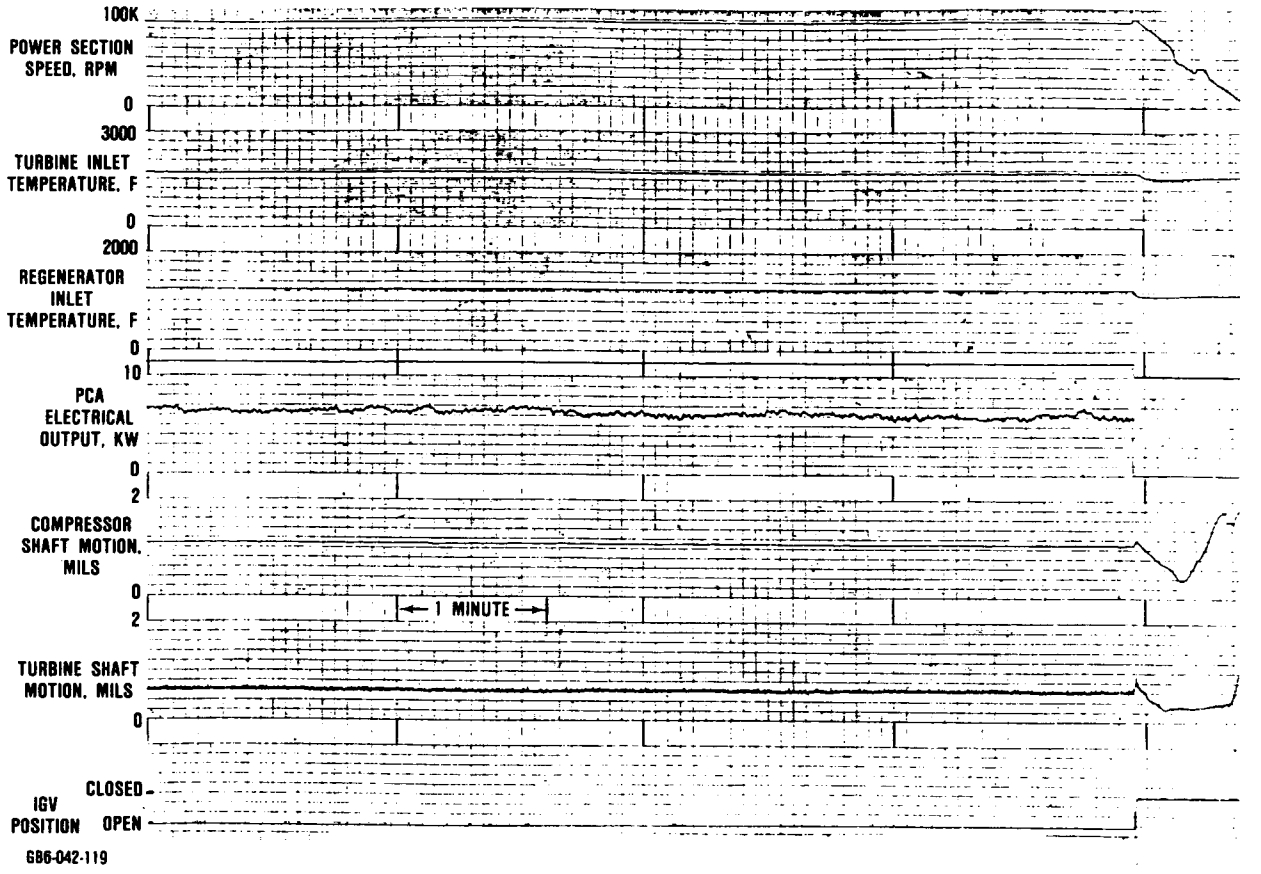

Figure 86. PCA Test (Build 51C AGT Engine) Operating Parameters.

The pump motor was intended to run in the horizontal position, whereas on the PCA it was mounted in the vertical position. This caused excess wear on the bushings, resulting in the motor overheating after a lengthy run. The fuel pump motor was therefore replaced with a motor that has been successfully used in 4 years of engine testing on the AGT101. This motor uses ball bearings to support the armature, which would make it more tolerant of running in the vertical position. Figure 88 shows the present (12 vdc) and former (110 vac) fuel pump motors mounted. Note that on the PCA installation, the fuel pump has been mounted upside down to prevent fuel from leaking into the motor. To accommodate the voltage operating change from one motor to the other (110 vac to 12 vdc), two other electrical changes were made to the PCA equipment.

4.3 System Demonstration Tests (Fuel Mode)

On January 16, 1986, a system demonstration test was successfully performed. The system was started to synchronous speed (89,700 rpm engine speed) and operated at 1600F (871C).

On January 24, 1986, a second system demonstration test was successfully performed. Three successive starts to synchronous speed were demonstrated. On the third successive start, the system was run for 30 minutes to achieve thermal equilibrium. Data taken during this run are presented in Table 19.

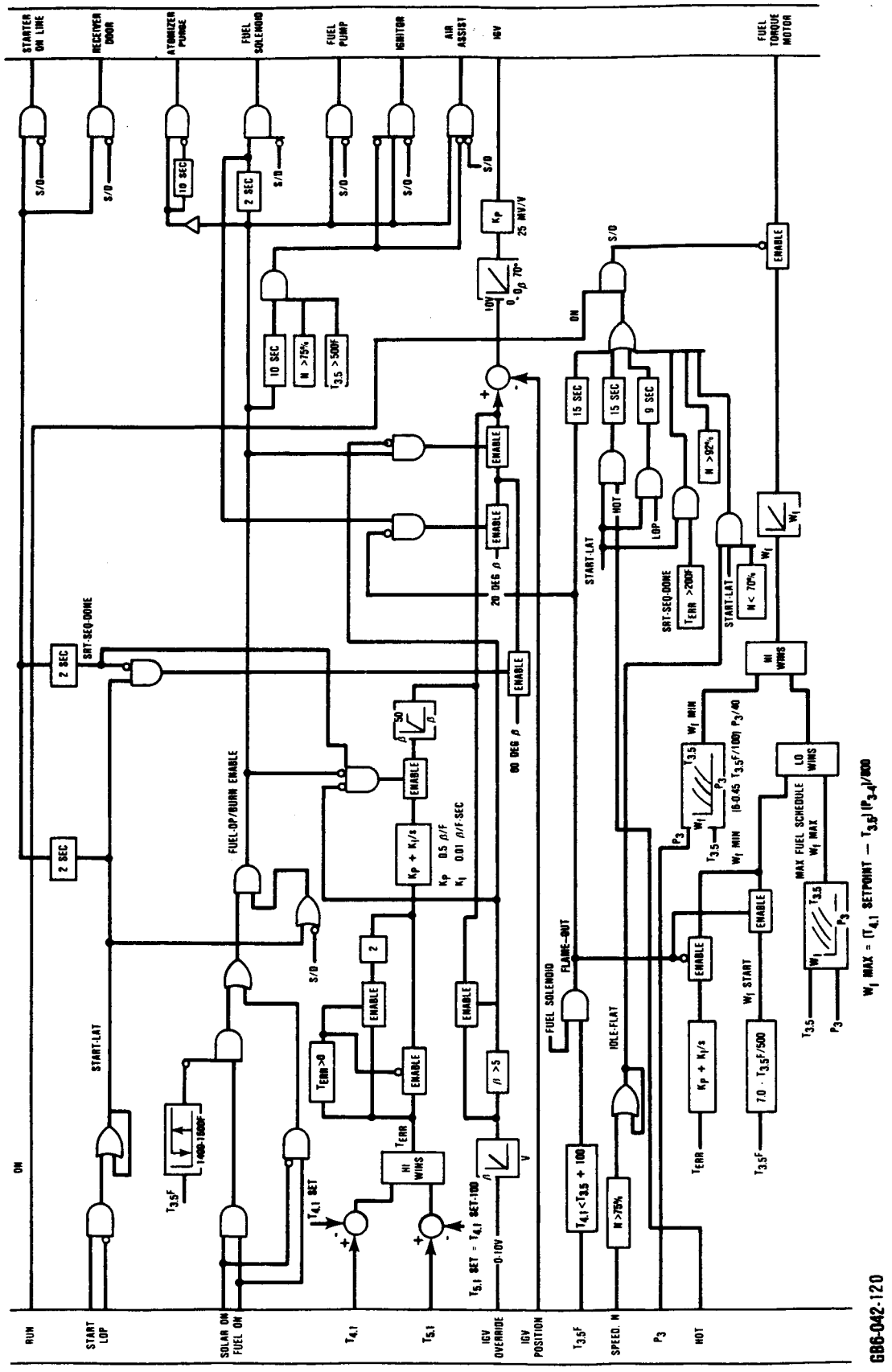

Figure 87. Updated Logic Diagram Reflects Maximum Fuel Schedule Change To Effect Repeatable Light-Offs.

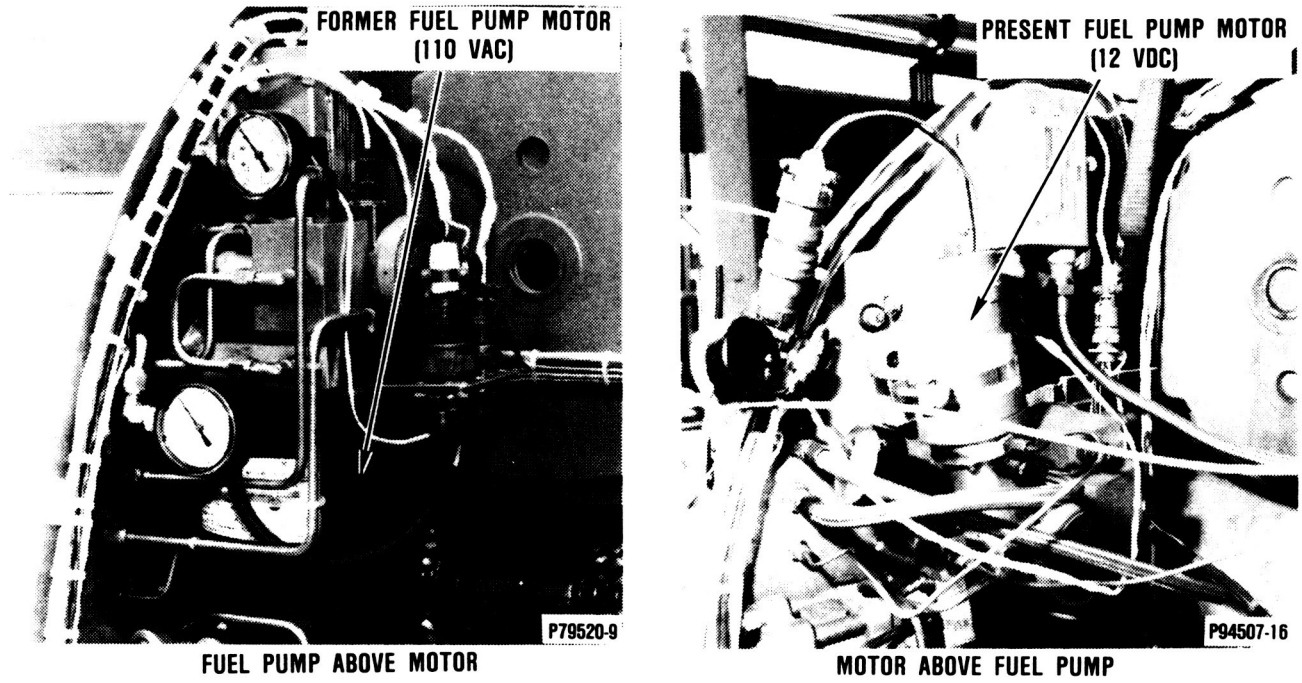

Figure 88. Fuel Control Changed To Improve Safety and Reliability.

Table 19. Maximum Outputs During Demonstration Test.

Parameter	Test Result
Engine Speed	89,700 rpm
Electrical Power	9.8 hp (7.3 kW)
$T_{Ambient}$	80F (26.7C)
$P_{Atmospheric}$	28.87 in. Hg (97.7 kPa)
Fuel Pulse	42 percent
$T_{4.1}$	1620F (882C)
$T_{5.1}$	1170F (631C)
$T_{3.7}$	1094F (590C)
$T_{6.0}$	460F (238C)
P_3	51 psia (353.5 kPa)
$T_{Oil\ Scavenge}$	206F (96.7C)

After the demonstration tests, a performance test was run to obtain accurate fuel flows. During this test, electrical power was approximately 9.4 hp (7 kW) and fuel flow was approximately 18 lb/hr (2.27 g/s) at steady-state conditions. These data indicate that engine speed may have to be lowered somewhat for peak power output in the solar mode on TBC-1.

This Page Intentionally Left Blank

5.0 CERAMIC ENGINE/PCA PERFORMANCE

The metal AGT101 was never intended to meet the performance goals set by the Department of Energy for solar-thermal to electric power conversion systems. The heat engine performance goal is 35 percent thermal efficiency for the near term and 41 percent for the long range. These efficiency levels can be attained if the metal engine (20 percent thermal efficiency based on the characterization test) is replaced with the ceramic AGT101, currently under development.

Assuming an 11-percent leakage level, thought to be a realistic goal by the end of 1986, performance of the all-ceramic engine has been predicted. The engine turbine inlet temperature was varied from 1900F (1038C) to 2500F (1371C) as plotted in Figure 89. The data along the 11-percent leakage line indicate that 1-percent improvement is attained for each 100F (55.5C) rise in turbine inlet temperature. For operation at 2100F (1149C) in Albuquerque [5300-ft (1615-m) altitude] and 80F (27C) compressor inlet temperature, the engine thermal efficiency is estimated to be 33.5 percent, with a corresponding thermal input power of 76 kW and output power of 25.5 kW (aerodynamic). When engine development succeeds in decreasing leakage to even lower levels, the predictions plotted in Figure 89 show the engine thermal efficiency reaching the 41 percent goal at 3 percent leakage and 2300F (1260C). If leakage were decreased to 1.5 percent by using a fixed-boundary recuperator and operating at 2500F (1371C), a peak thermal efficiency of 44 percent is predicted. The trade-offs to achieve this configuration would involve increased weight, volume, and cost for the recuperator; heavily insulated ducting; and improved receiver designs, such as the one shown in Figure 90, to reduce radiation losses at elevated temperatures.

Another area of development involves the mechanical drive train used to convert engine aerodynamic output to electrical generator output. The system depicted in Figure 91 is intended to minimize mechanical losses by eliminating the speed-reducing gearbox and coupling the electric generator directly to the engine output shaft. This optimum mechanical configuration, however, would increase the

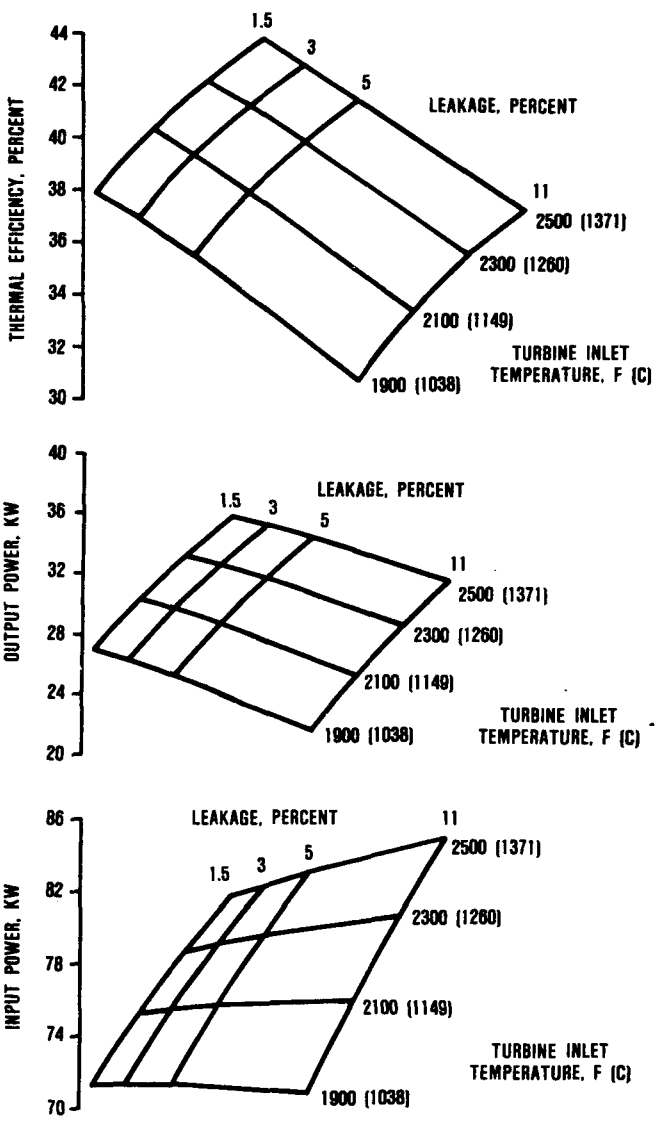

Figure 89. DOE Thermal Efficiency Goals Are Within the Ceramic AGT101 Capability.

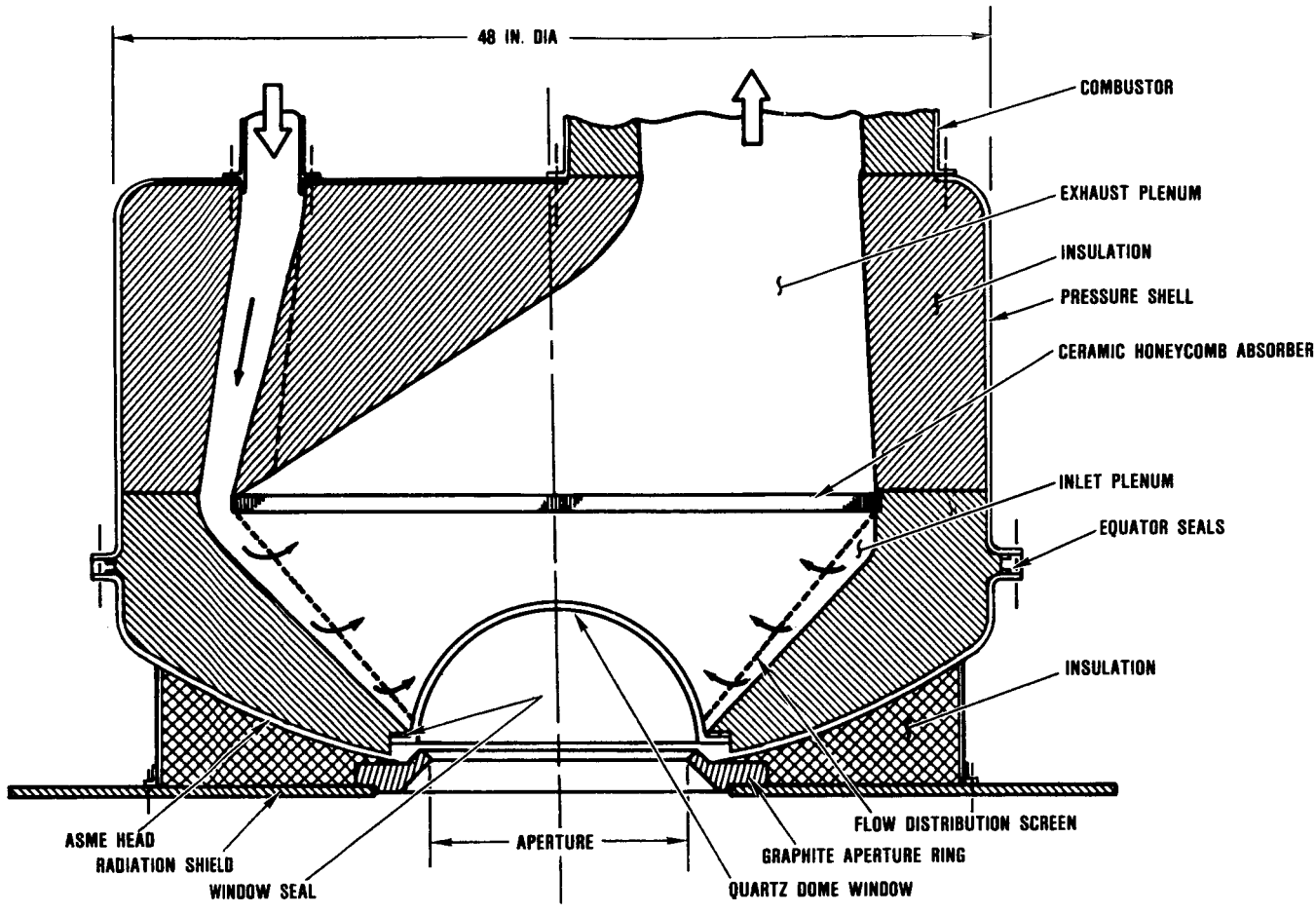

Figure 90. Advanced Receiver (Sanders Assoc., Inc.) Needs To Be Developed for SAGT Operation at Elevated Temperatures.

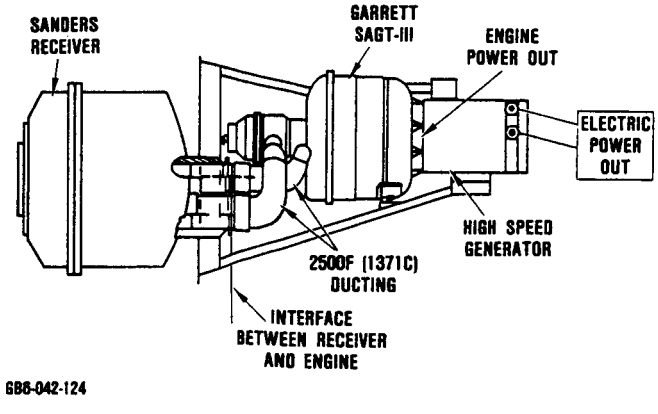

Figure 91. Developed Ceramic SAGT-III Can Meet DOE Efficiency Goals.

cost of the system in the area of electrical output conditioning due to the engineering cost associated with developing a high-speed generator and associated electrical equipment to change the high-frequency output to 60 cycle. This optimum system would also require a complex speed (frequency) control to control engine speed, as was envisioned for the Mod 'O' system (described in Appendix A).

A major goal for the optimum mechanical system should be to eliminate the lubrication system, thereby improving reliability and reducing maintenance costs. This could be accomplished by designing the power section and generator rotors with fully hydrodynamic bearing supports. GTEC bearings of this type

have demonstrated mean time between failures (MTBF) of 65,000 hours in commercial airline service (air cycle machines on the DC-10 aircraft).

5.1 Ceramic SAGT Test Predictions

To demonstrate near-term improvements attainable with the ceramic SAGT, it is proposed that the SAGT-1A described in Section 3.0 be retrofitted with the all-ceramic AGT101 when this power section becomes available. The ceramic AGT101 power section is completely interchangeable with the metal version used in the present SAGT program. The only required design change would involve the interconnecting ducts between the engine combustor and the receiver. To accommodate operation at 2100F (1149C), this ducting would require material changes in the shell, insulation, and bellows.

The predicted electrical output power for the ceramic SAGT-II PCA is shown in Figure 92. These data demonstrate that significant increases in efficiency and power output can be realized with the SAGT-II.

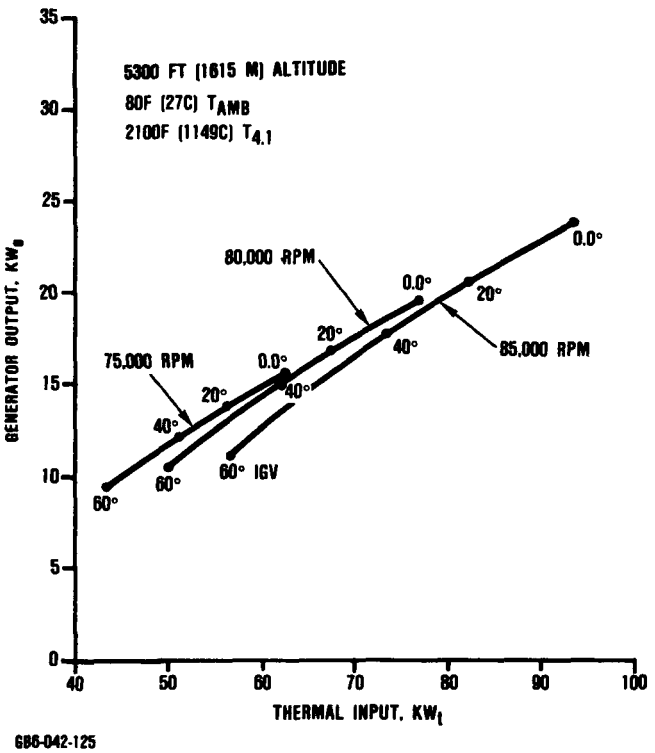

Figure 92. Predicted Electrical Output Power for Ceramic Versus Metal SAGT Shows Significant Increase.

This Page Intentionally Left Blank

6.0 ECONOMIC CONSIDERATIONS

In addressing the Department of Energy (DOE) cost goals for the heat engine in solar-dish electric-generator sets, certain basic assumptions are made:

1) The production quantities will be 10,000 units per year for 10 years.

2) The near-term goal (circa 1995) is $1000 per kWe.

3) The long-range goal (early 21st century) is $300 per kWe.

4) The automotive industry will mass produce a ceramic gas turbine engine by the year 2000.

Since there is a significant learning curve associated with the production of ceramic gas turbine parts, the sell price may be decreased sufficiently to meet the near-term DOE cost goals. Attaining the long-range cost goal, however, is solely dependent on the automotive industry beginning mass production of this type of engine. The SAGT production quantities would then represent a small fraction of the automotive production quantities, and the $6000-per-unit production cost (for a 20-kWe engine) appears to be a reasonable goal.

This Page Intentionally Left Blank

7.0 DESIGN LIFE

This section deals with design life limitations of the production solarized AGT with ceramic structures and turbine wheel. Since experience with ceramic gas turbine parts is limited, it is assumed that there are no inherent material problems (crack propagation, hot gas erosion, or excessive oxidation). The 100-hour test on ceramic structures showed no sign of distress in any of the parts.

Table 20 summarizes the projected field maintenance requirements for a production SAGT power section. The only parts requiring replacement and recoating are the regenerator seals. The estimated 5000-hour life of the regenerator system is based on the following considerations.

- System Design Logic - 90 percent of the AGT101 system is based on Ford 707 industrial engine experience since the mid-1960s.
  - NASA/Ford regenerator durability program achieved 10,000-hour core life.
  - Seal life in the 707, based on maximum wear location, was approximately 2500 hours.
    - 27-inch crossarm causing nonuniform pressure distribution under shoes
    - Processing difficulty with crossarm flatness over 27-inch span (heavy end loading)
    - Seal platform instability due to large thermal gradients in the 707 configuration
- AGT101/SAGT System Durability - AGT101 design has 4-inch crossarm lengths.
  - Provides uniform seal loading and good undershoe pressure distribution
  - Eliminates processing difficulties in crossarm, i.e., seal flatness
  - Hole in center of AGT101 seal increases section modulus, thus adding stability to crossarm
- Seal Life - Based on 707 experience and AGT101 design, a seal life of 5000 hours or more should be possible on AGT101 seals in the SAGT application.
  - A regenerator-seal durability test should be performed to verify seal life.

Table 20. Projected Field Maintenance Requirements for a Production SAGT Power Section.*

Component	Maintenance Required
Turbine Rotor	None
Compressor Rotor	None
Compressor Ball Bearing	None, based on B-10 life
	None, if changed to foil bearing
Seal at Ball Bearing	None, based on change to labyrinth
Foil Bearing	None
Regenerator Seals	Replace at estimated 5000 hours
Combustor Liner	Replace at estimated 5000 hours, if metallic
	None, if ceramic

*Based on 50,000-hour life goal.

Table 21 presents stress analysis results for the AGT101 and the SAGT-1 impellers. Comparison of the two reveals a significant stress

Table 21. Impeller Stress Comparison: AGT101 Versus SAGT-1.

Parameter	AGT101	SAGT-1
Disk Stresses, ksi (kPa)		
Avg. Tan	18.8 (129.6)	12.0 (82.7)
Bore Eff	44.3 (305.4)	28.0 (193.1)
Tan	40.4 (278.5)	25.9 (178.6)
Blade Stresses, ksi (kPa)		
Max Eff	31.6 (217.9)	20.2 (139.3)
Burst Ratio	1.68	2.44
Temperature, F (C)		
Maximum	374 (189)	270 (132)
Average	280 (138)	210 (99)
LCF Life Hours (Equivalent Cycle)	4800	119,000

margin for the SAGT impeller, resulting in a projected doubling of the required SAGT life for this impeller. Sand erosion or other surface deterioration of the impeller blades is not considered in the stress analysis. However, if this type of problem arises in the field, protective coatings such as titanium nitride may be applied to extend the useful life of the impellers.

The ball bearing life was projected based on the design data presented in Figure 93. These data indicate that approximately 8 percent of the bearings will fail by 50,000 hours. However, if the production design were configured using all foil bearings, the bearing life would increase significantly. The GTEC-patented foil bearing has exhibited excellent durability in production applications of turbomachinery. An MTBF of 65,000 hours has been established by such equipment in service on the McDonnell-Douglas DC-10 aircraft.

The all-hydrodynamic bearing design also eliminates the need for a buffer seal to prevent oil leakage into the impeller area of the rotor. The seal used in the metal SAGT-1A is a dual carbon ring seal having a projected life of only 4000 hours. This seal would have to be replaced with a labyrinth seal to increase life, but the trade-off is increased leakage, i.e., lower efficiency. These problems are avoided with an all-hydrodynamic bearing design.

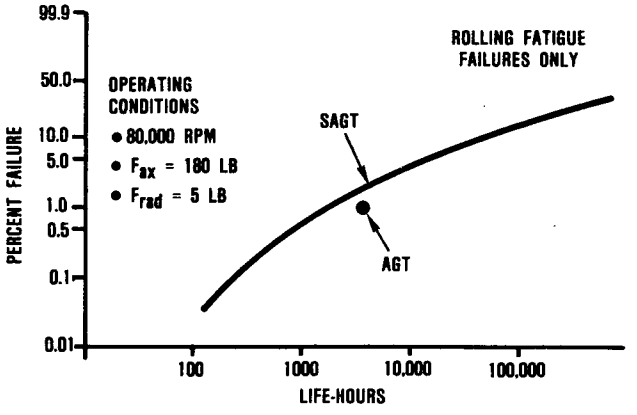

Figure 93. Ball Bearing B_{10} Life Meets SAGT-1A Design Life Requirements.

8.0 CONCLUSIONS

The design, fabrication, assembly, and testing of a small hybrid Brayton Engine/ Power Conversion Assembly (PCA) were paced by the development of the AGT101 gas turbine power section. The major development problems in the AGT101 program (NASA/DOE Contract DEN3-167) were rotor instability and internal leakage. After reliable, mechanically sound operation was assured, the SAGT-1A test program was completed with only minor modifications to the PCA. The following conclusions were drawn:

- Mechanical operation of the system required only minor development.
- Power section efficiency was low due to high internal leakages (15 percent versus a design goal of 5 percent).
- Overall reliability was high, including the fuel, ignition, control, and electrical systems.

This Page Intentionally Left Blank

APPENDIX A

MOD "O" SYSTEM DESCRIPTION

The development of the Mod "O" Power Conversion Unit (PCU) was undertaken by Garrett Turbine Engine Company (GTEC) in February 1980 under Contract DEN3-181 administered by the NASA Lewis Research Center (NASA/LeRC) and funded by the United States Department of Energy (DOE). Work proceeded through the design and analysis portion of the statement of work. The results of this effort are reported herein. The program was then redirected by the administering agency to use the AGT101 power section for the Brayton Engine/Generator Set (BE/G).

The Mod "O" System has the following features:

- GTEC Model GTP36-51 turbocompressor hardware
- Single-can combustor utilizing an air-blast atomizer
- Formed tube/fin recuperator
- Hydraulic starter
- Aircraft-type, 400-Hz, 3-phase generator
- Rectifier/regulator

Figure 94 is a schematic of the Mod "O" PCU. After filtration, ambient inlet air is compressed by the compressor, then heated by the recuperator. The air is further heated either by the solar receiver (solar-only operating mode) or the combustor (fuel-only mode), or by both (hybrid mode). The air then passes to the turbine where work is extracted. Some of the turbine exhaust gas heat is recovered in the recuperator before the gas is exhausted to the atmosphere. Turboshaft power is transmitted to the generator through the gearbox. The constant but nonsteady-frequency ac voltage output of the generator is converted to a constant dc voltage output by the rectifier.

Engine control was designed to be accomplished in the following manner. For all operating modes, the turbine inlet temperature would be maintained at 1500F (816C); studies have shown that this will result in the best partial-power efficiency. In the solar-only mode, the available solar power input would be matched to the engine by varying the engine airflow by increasing or decreasing engine speed. Engine speed would be controlled by loading or unloading the generator, accomplished by varying the current output of the rectifier. In the hybrid mode, the 1500F (816C) turbine inlet temperature would be maintained by varying the fuel flow. Engine speed would be maintained at an operator-selected set point by varying the generator load with the control rectifier.

ENGINE COMPONENTS

Turbocompressor

Design changes to the basic GTEC Model GTP36-51 turbocompressor for use in the Mod "O" PCU would be minimal. A new compressor housing and turbine discharge duct would be required, together with minor reworking of the turbine plenum. No modifications would be required to the rotating components, bearings, supports, or seals. Therefore, no change in critical speeds from those of the basic GTEC Model GTP36-51 is anticipated. The critical speeds are:

- First Critical Speed - 9500 rpm
- Second Critical Speed - 35,000 rpm
- Third Critical Speed - 132,000 rpm

The steady-state operating range for the Mod "O" turbocompressor would be 49,000 to 70,000 rpm. Since this range is safely between the second and third critical speeds, no problems are anticipated.

Mod "O" Unique Engine Components

Combustor - The combustion system for the Mod "O" PCU must accommodate a greater range of operation than is currently required

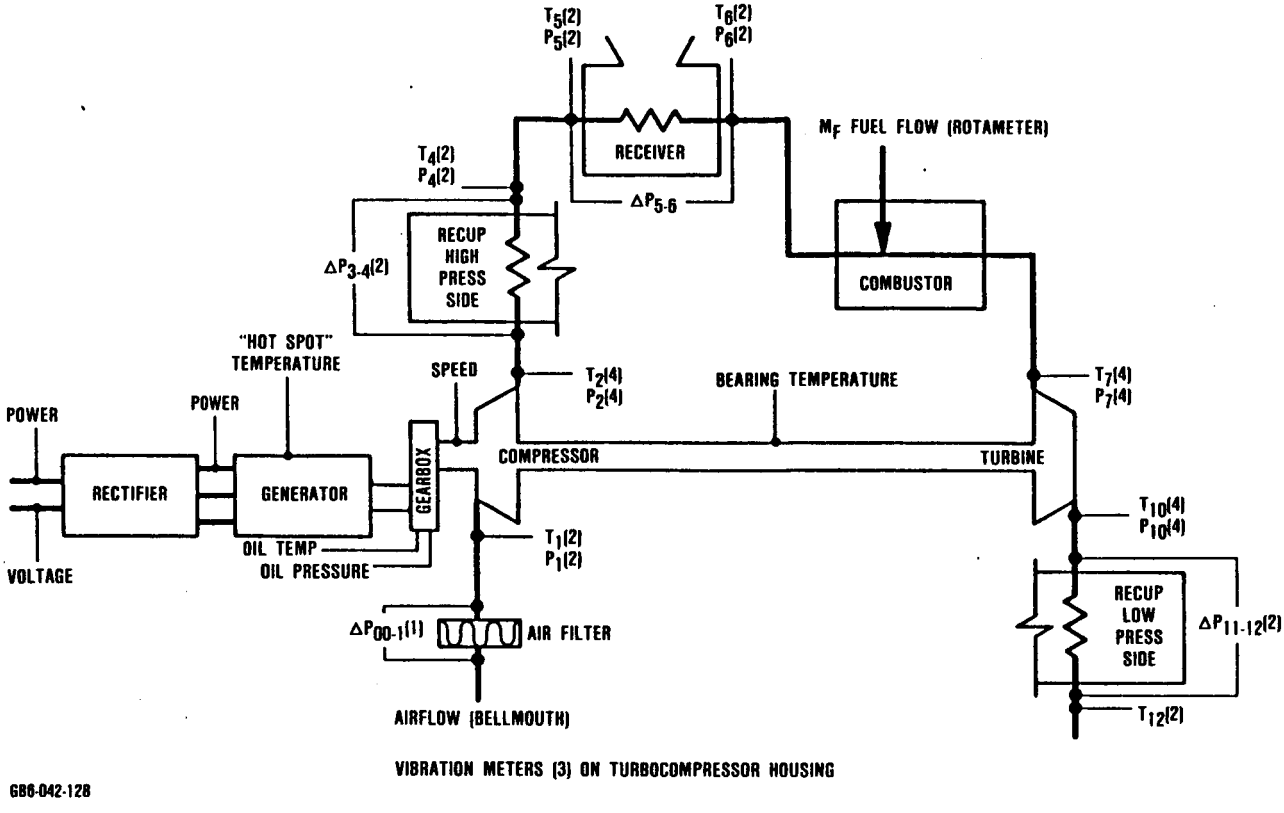

Figure 94. Schematic of Mod "O" PCU Defines Performance Rating Points and Instrumentation.

for basic applications. The combustor must possess the ignition and stability characteristics necessary to achieve an engine start to full speed and must also have superior lean-flame stability limits to allow operation at conditions imposed during high-heat inputs from the solar collector.

The combustor must also exhibit high combustion efficiency over the entire range of operation without forming carbon or undesirable emissions and with pressure-drop characteristics that are consistent with the engine cycle requirements. In addition, the combustor must have design features that will promote long service life with minimum maintenance. The high combustor inlet temperature dictates the need for special fuel handling concepts to prevent thermal decomposition of the fuel and subsequent fuel atomizer malfunction.

Combustor operating goals are summarized below:

- Combustion Efficiency - 99.6 percent at loaded operating conditions; 92.0 percent minimum at idle conditions
- Pressure Drop - 2 percent
- Combustor Discharge Temperature Maximum Variation - 250F (121C) above average
- Skin Temperature - 1700F (927C) maximum
- Smoke Generation - Minimal
- Carbon Formation - Minimal

The combustor operating design point conditions are presented below:

- Inlet Pressure, psia (kPa) - 30 (259)
- Inlet Temperature, F (C) - 1100 (593)
- Airflow, lb/sec (kg/s) - 0.634 (0.288)
- Outlet Temperature, F (C) - 1500 (816)
- Fuel Flow, lb/hr (kg/hr) - 24.25 (1.78)
- Fuel/Air Ratio - 0.01062

The combustion system (Figure 95) consists of the combustor with a single air-blast atomizer, an ignitor, and a 4-joule high-voltage ignition unit.

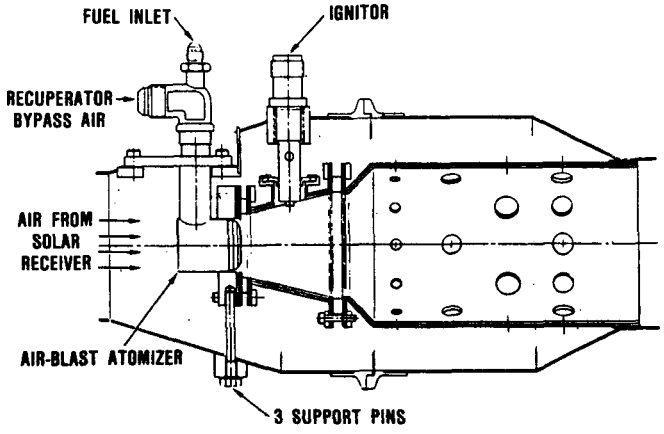

GB6-042-129

Figure 95. Solar Hybrid Mod "O" Combustor Meets Design Requirements.

The combustor has the same design features as those incorporated in the combustor for the GTEC Model GT601 recuperated gas turbine engine. Scaling this combustor for application to the Mod "O" engine resulted in the following dimensions:

- Outside Diameter - 3.6 inches (91.4 mm)
- Length - 9.5 inches (241.3 mm)

A thermal barrier coating (see Figure 96) would be used to meet the maximum wall temperature requirement. The coating consists of a compliant layer of stainless steel "Feltmetal" brazed to the inside of the combustor wall with a layer of Zirconia ceramic plasma-sprayed to the "Feltmetal." This coating is currently used on the GTEC Model GT601 combustor.

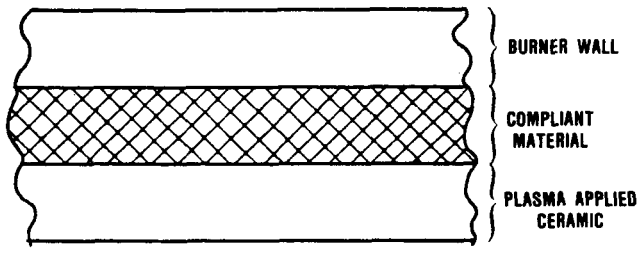

GB6-042-130

Figure 96. Hybrid Engine Combustor Wall Construction.

The fuel atomizer (Figure 97) is a pure air-blast type designed to prevent the following problems:

- Poor atomization at low fuel-flow rates
- Possible fuel decomposition in both the fuel delivery line and the internal flow passages of the atomizer housing due to the high combustor inlet temperature

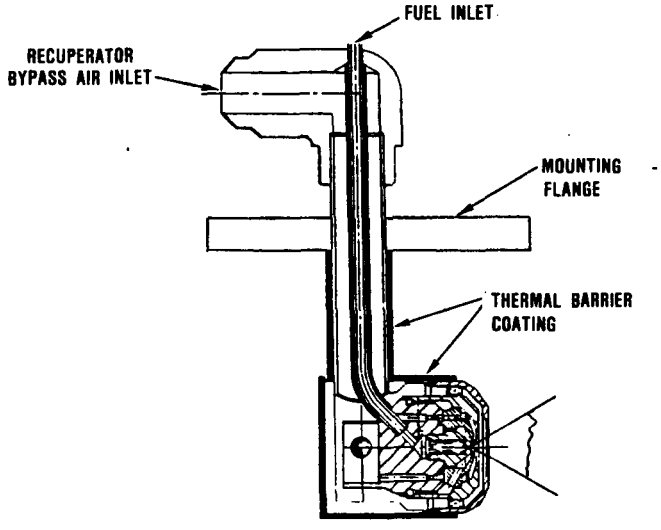

GB6-042-131

Figure 97. Air-Blast Atomizer Prevents Low-Flow Atomization and Premature Vaporization.

The atomizer is a modification of an existing air-blast type, suitably mounted and protected thermally with a plasma-sprayed Zirconia ceramic coating on the outer shell of the atomizer housing and the outside diameter of the fuel delivery tube. An atomizer of this type was demonstrated by the vendor at the minimum fuel-flow and air-blast-pressure conditions.

As noted above, the combustor design was based on the GT601 combustor, which has a pilot zone, a primary zone, and a secondary zone. During ignition and maximum power conditions, the combustion reaction occurs in both the pilot and primary zones. At idle conditions, the reaction occurs primarily in the pilot zone. The equivalence ratios in the pilot zone at maximum power and idle conditions are 0.9 and 0.26, respectively.

Preliminary airflow distribution for the Mod "O" combustor is shown in Figure 98, with a pilot-zone equivalence ratio of 0.9 at the maximum fuel augmentation condition.

Recuperator - The Mod "O" recuperator consists of two core assemblies that are currently used in the recuperator of the GTEC Model GT601 gas turbine engine. This recuperator is a formed tube/fin heat exchanger specifically designed to handle the rapid start-up of a gas turbine engine. A cross section of this recuperator (Figure 99) shows the triangular end sections, counterflow core, and high-pressure inlet and exit ports. The low-pressure exhaust gases are not contained in integral manifolds, but are ducted to and from the recuperator by means of external ductwork which is mechanically attached to the inlet and exit face of the core. A core assembly is shown in Figure 100.

In the Mod "O" application, two recuperator cores are arranged in parallel as shown in Figure 101. Sheet-metal ducts are used to form a common inlet and exit manifold for the exhaust gases. The high-pressure gas is split into two parallel streams and ducted to the two ports on top of the recuperator. The high-pressure gases leaving the recuperator are ducted in a similar manner.

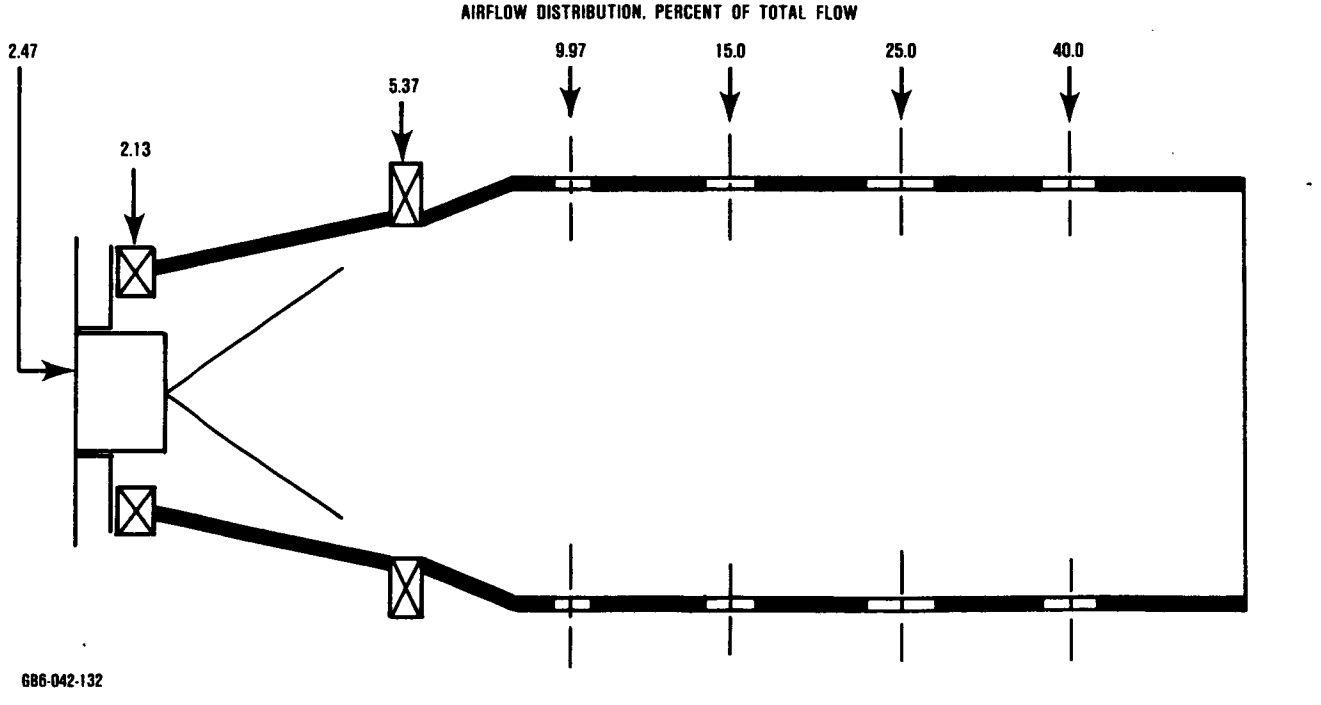

Figure 98. Preliminary Airflow Distribution Design for the Mod "O" Combustor.

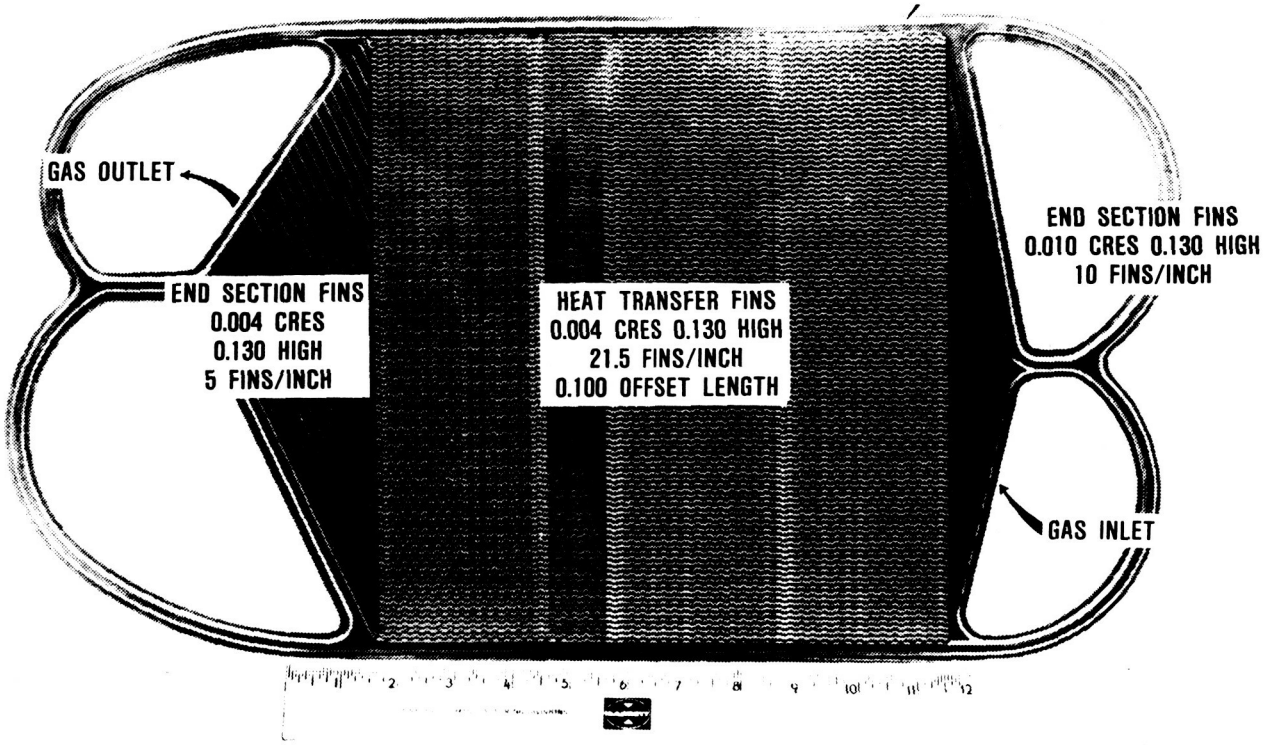

GB6-042-133

Figure 99. Cross Section of GT601 Recuperator Design for Rapid Start-Ups.

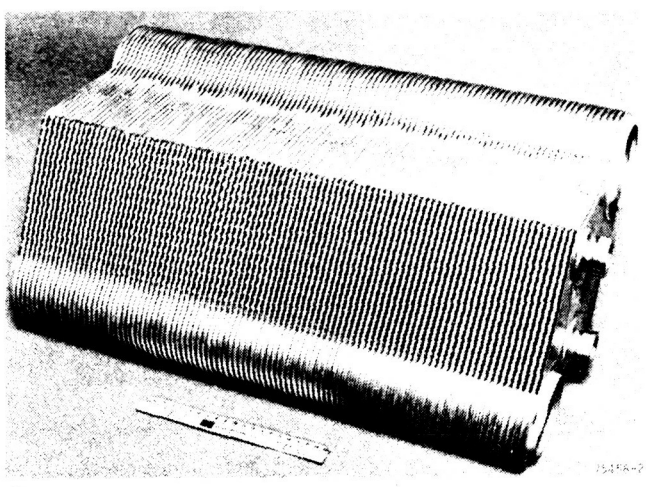

GB6-042-134

Figure 100. Two GT601 Recuperator Core Assemblies Will Meet Mod "O" Performance Requirements.

This selected configuration is similar to the one employed in the current GTEC Model GTP36-51 recuperated gas turbine engine. The recuperator cores are shown installed in the GTP36-51 engine in Figures 102 and 103. This engine has been operated successfully for several years in this configuration.

Recuperator performance at the Mod "O" design point is described in Table 22. The effectiveness is reduced to 0.89 from the original design requirements of 0.94. However, the pressure drop has also been reduced from the design value of 4.0 percent to 2.0 percent. These two factors combine to give a bus bar engine efficiency of 24.6 percent for the proposed recuperator versus 26.5 percent for the production formed-tube/fin recuperator.

Table 22 also compares the two approaches on the basis of cost. The development cost

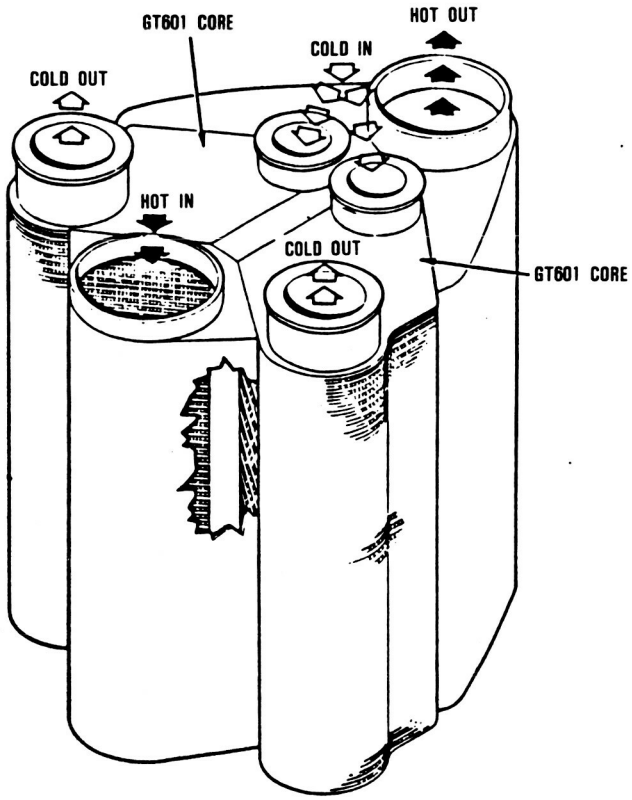

GB6-042-135

Figure 101. Mod "O" Dual GT601 Recuperator Installation Illustrates Sound Design Approach.

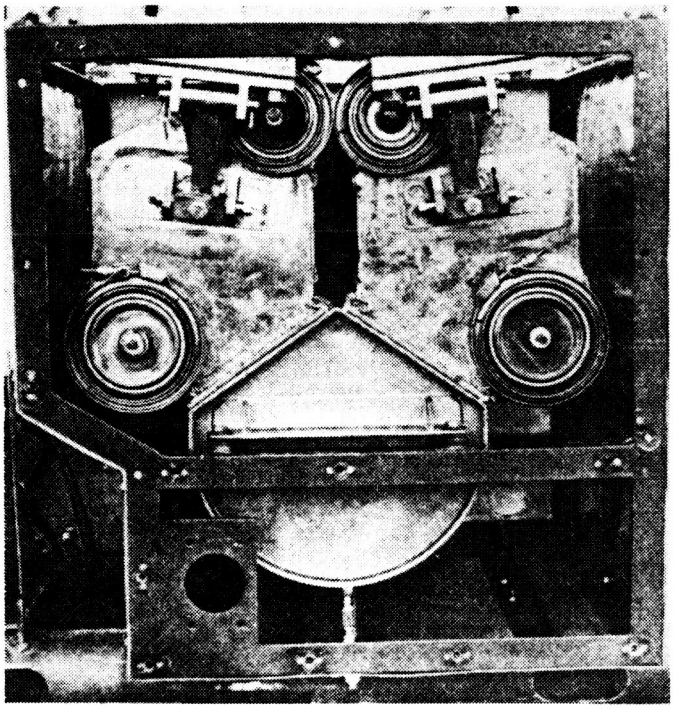

GB6-042-136

Figure 102. GTP36-51 Recuperator Installation, End View.

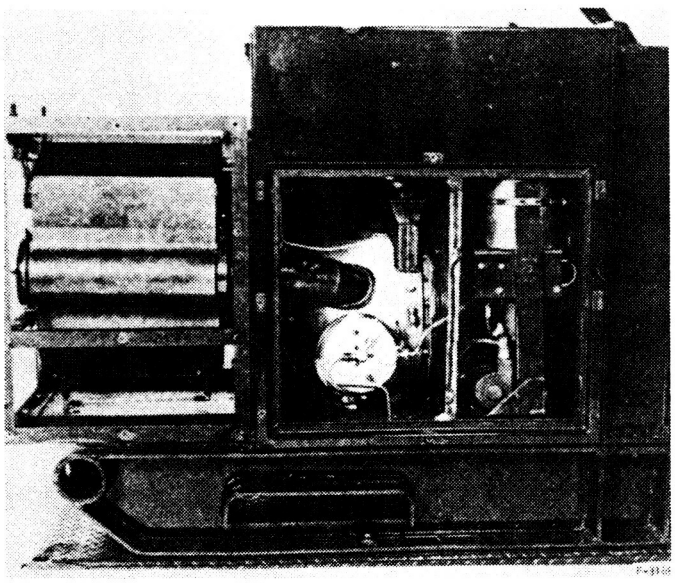

GB6-042-137

Figure 103. GTP36-51 Recuperator Installation, Side View.

(i.e., Mod "O" program costs) of the proposed configuration is taken as 1.0. Relative to that value, the cost for the production design is 1.72.

PERFORMANCE

The reference engine design and off-design operating conditions were generated with the aid of a steady-state off-design computer program. This computer tool permits engine performance analysis at other than design operating conditions for fixed hardware, e.g., varying power level, turbine inlet temperature, engine speed, ambient pressure, and temperature.

Table 22. Dual GT601 Recuperators Meet Design Goals at Lower Cost.

Parameter	Dual 601 Cores	Production Recuperator
Performance		
Effectiveness	**0.89**	**0.94**
P/P, percent	**2.0**	**4.0**
Weight, lb (kg)	**300 (136)**	**320 (145)**
Bus Bar Cycle Eff., percent	**24.6**	**26.5**
Relative Development Costs	**1.0**	**1.72**

The computer program uses analytical models of the following:

- Compressor
- Turbine
- Recuperator
- Receiver, combustor, and ducting
- Heat loss from the ducting and other components
- Heating of the compressor inlet air due to gearbox heat rejection

The computer program also models bearing friction losses and air cooling of the hot end bearing and the tube carrying fuel to the combustor.

Compressor and turbine performance maps were generated from test data. The recuperator was modeled using tested heat-transfer and friction-pressure-drop coefficient data. A pressure-drop map for the receiver was generated analytically. Each duct section and the combustor pressure drop were scaled with the square of the duct section or combustor-inlet corrected flow, to obtain the pressure drop at conditions other than the reference design conditions.

Duct heat losses were calculated at the reference design conditions assuming various thicknesses of Fiberfax insulation. Because they are assumed to be pure conduction, these duct heat losses were scaled in direct proportion to the temperature change across the duct-insulation wall to obtain the heat loss at conditions other than the reference design conditions.

Since compressor inlet air is used to cool the gearbox, this air will be warmer than ambient by approximately 3F (1.67C), resulting in a slight reduction in cycle efficiency. The amount of this temperature increase was calculated assuming that all the power loss due to gearbox inefficiency will be absorbed by the compressor inlet air.

Full-Power Performance

Full power is defined as the power output for a thermal power input to the engine (Q_E) of 72.7 kW_t. The turbine inlet temperature (T_7) was to be held constant at 1500F (816C) for all conditions. For this Q_E and T_7, Figure 104 shows the variation in cycle shaft power (CSP) as the ambient temperature changes, for operation at both sea level and 5000-foot (1525-m) altitude. The ambient temperature extremes for sea level are 10F (-12C) and 140F (60C), and for 5000-foot (1525-m) altitude, -20F (-29C) and 110F (43C). Figure 105 shows engine speed as a function of ambient temperature for Q_E = 72.7 kW_t and T_7 = 1500F (816C). As ambient temperature decreases, speed decreases and CSP increases, as shown by Figures 104 and 105. Over the ambient temperature extremes, CSP varies from 27.3 to 19.5 kW and speed varies from 58,900 to 69,900 rpm.

The engine will be rated at 80F (27C) ambient temperature at sea level and Q_E = 72.7 kW_t. Performance of the PCU at these reference design conditions is summarized in Table 23.

More complete performance tabulations for the reference design conditions are presented in Figure 106. This data sheet lists additional performance parameters, as well as temperature, pressure, and airflow at pertinent engine locations. The nomenclature used in Figure 106 is defined in Figure 94.

C-2

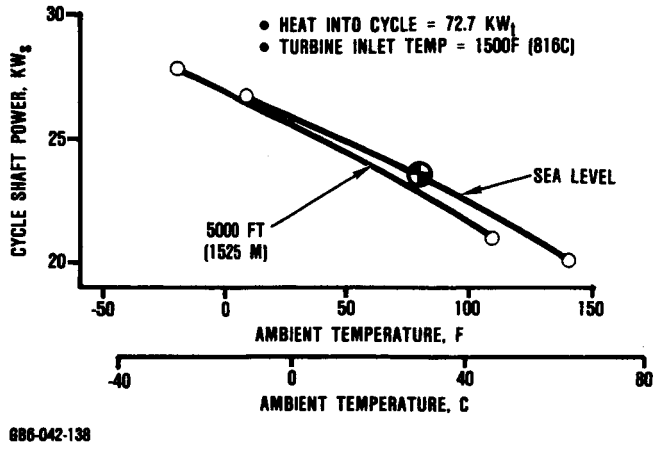

Figure 104. Cycle Shaft Power Depends on Ambient Temperature and Altitude.

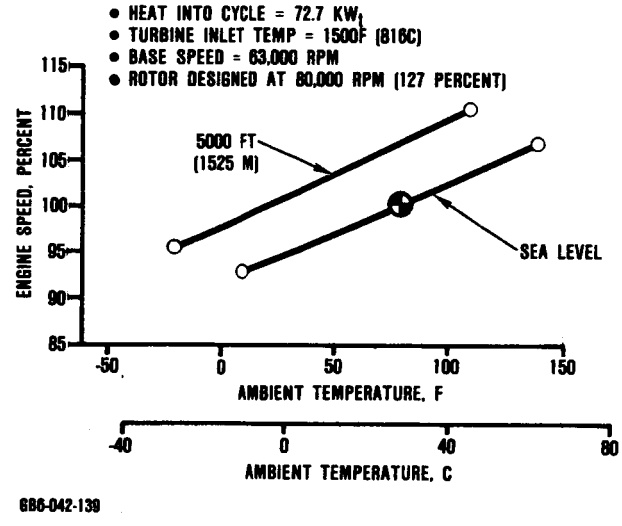

Figure 105. Engine Speed Is Related to Ambient Temperature at Constant Thermal Input.

The CSP is 21.7 kW_m, which results in a cycle efficiency at the engine shaft (CSP/Q_E) of 29.8 percent. The gearbox is 98-percent efficient and results in a shaft-power loss of 0.43 kW_m. The shaft assessory load is defined as the power required to run the lube pump, in this case 73 watts. Generator efficiency is 89 percent and results in a power loss of 2.33 kW. A loss of 0.660 kW is incurred in the rectifier, which is 96.5-percent efficient. The electric accessory load includes power to run the controls (28 watts) and power for the fuel pump (50 watts). The net electric power (NEP) at the ac bus is 17.0 kW_e. The corresponding efficiency of overall engine thermal input to dc bus bar (NEP/Q_E) is 23.4 percent.

Heat losses for the ducts and the recuperator at the reference design conditions of sea level, 80F (27C), and Q_E = 72.7 kW_t are tabulated below, together with insulation thicknesses.

Duct	Insulation Thickness, inches (mm)	Heat Loss, kW
Comb-Recup	1.0 (25.4)	0.004
Recup-Recvr	1.5 (38.1)	0.232
Recvr-Comb-Turb	2.0 (50.8)	0.356
Turb-Recup	1.5 (38.1)	0.463
Recup-Atm	1.0 (25.4)	0.015
Recuperator	2.0 (50.8)	0.265

Heat losses from engine components other than those listed above are negligible.

In the performance analysis, the recuperator heat loss was divided by four and each portion added to the four ducts that directly mate to the recuperator, i.e., all the ducts listed above except the receiver-combustor-turbine duct. Thus, the heat losses for these ducts as shown in Figure 107 are larger than those cited above. Figure 107 lists the performance data based on use of the more effective production recuperator, which results in higher CSP, NEP, and efficiency (23.0 kW_e, 18.1 kW_e, and 24.9 percent, respectively) than for the PCU with the existing recuperator (cf. Figure 106).

Table 23. Mod "O" PCU Performance Summary for 80F (27C), Sea Level.

Parameter	Efficiency, percent	Power Loss, kW	Power
Thermal Input			72.7 kW_t
Cycle Shaft Power (CSP)			21.7 kW_m
Cycle Efficiency (CSP/Q_E)	29.8		
Gearbox Efficiency	98	0.434	
Shaft Accessory Load (SAL)		0.073	
Generator Efficiency	89	2.33	
Rectifier Efficiency	96.5	0.660	
Electric Accessory Load (EAL)		0.078	
		3.575	
Module Electric Power (MEP), dc			18.1 kW_e
Module Efficiency (MEP/Q_E)	24.9		
Inverter Efficiency	94	1.087	
Net Electric Power (NEP), ac			17.0 kW_e
System Efficiency (NEP/Q_E)	23.4		

Partial-Power Performance

Turbocompressor - As Q_E decreases, engine airflow and therefore engine speed must decrease to maintain T_7 at a constant 1500F (816C). This relationship is depicted in Figure 108, which shows speed as a function of Q_E for the ambient temperature range of 130F (54C) to -20F (-29C).

As speed decreases, however, the temperature drop across the turbine also decreases, resulting in a higher recuperator inlet temperature (T_{11}) on the low-pressure side. Thus, T_{11} increases as Q_E decreases. However, T_{11} can only be increased to 1300F (704C) before exceeding the recuperator design limit. Also, output voltage for the 400-Hz generator is maintained constant as the generator speed decreases by increasing the strength of the exciter magnetic field in the rotor. The result: Rotor winding current increases as generator speed decreases. The heat generated is a function of the square of these currents multiplied by the winding resistance; thus, the heat generated increases rapidly as generator speed decreases. Rapid heat dissipation cannot occur due to the rotor construction and small spacing (air gap)

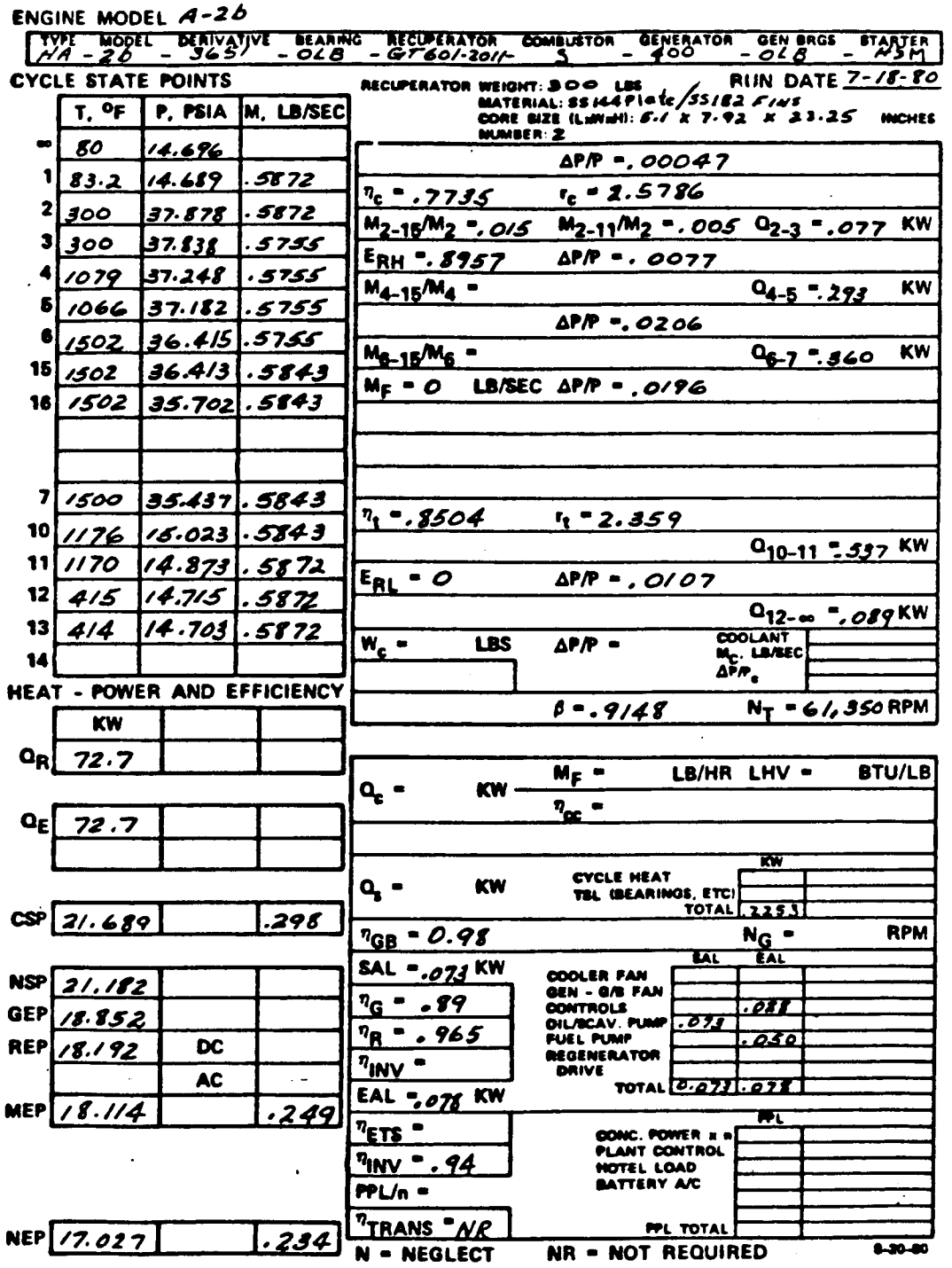

Figure 106. Performance Analysis Data Sheet for PCU with Existing Recuperator.

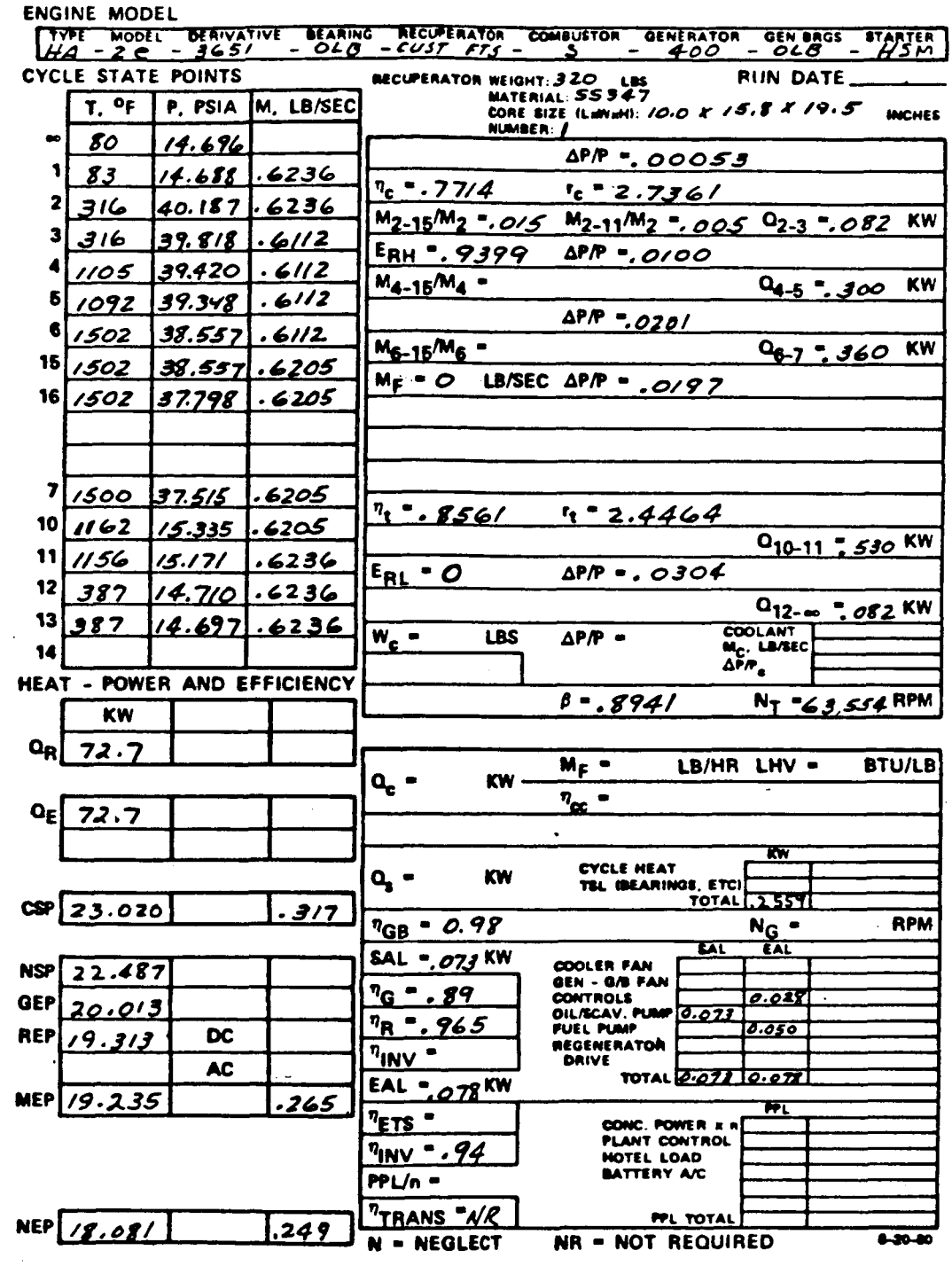

ENGINE MODEL

TYPE	MODEL	DERIVATIVE	BEARING	RECUPERATOR	COMBUSTOR	GENERATOR	GEN BRGS	STARTER
HA	2C	3651	OLB	CUST FTS	S	400	OLB	ASM

CYCLE STATE POINTS

	T, °F	P, PSIA	M, LB/SEC
∞	80	14.696	
1	83	14.688	.6236
2	316	40.187	.6236
3	316	39.818	.6112
4	1105	39.420	.6112
5	1092	39.348	.6112
6	1502	38.557	.6112
15	1502	38.557	.6205
16	1502	37.798	.6205
7	1500	37.515	.6205
10	1162	15.335	.6205
11	1156	15.171	.6236
12	387	14.710	.6236
13	387	14.697	.6236
14			

RECUPERATOR WEIGHT: 320 LBS
MATERIAL: SS347
CORE SIZE (L x W x H): 10.0 x 15.8 x 19.5 INCHES
NUMBER: 1

RUN DATE _____

ΔP/P = .00053

η_c = .7714 r_c = 2.7361

M_{2-15}/M_2 = .015 M_{2-11}/M_2 = .005 Q_{2-3} = .082 KW

E_{RH} = .9399 ΔP/P = .0100

M_{4-15}/M_4 = Q_{4-5} = .300 KW

ΔP/P = .0201

M_{6-15}/M_6 = Q_{6-7} = .360 KW

M_F = 0 LB/SEC ΔP/P = .0197

η_t = .8561 r_t = 2.4464

Q_{10-11} = .530 KW

E_{RL} = 0 ΔP/P = .0304

$Q_{12-\infty}$ = .082 KW

W_c = LBS ΔP/P = COOLANT M_c, LB/SEC; $\Delta P/P_c$

β = .8941 N_T = 63,554 RPM

HEAT - POWER AND EFFICIENCY

	KW		
Q_R	72.7		
Q_E	72.7		
CSP	23.020		.317
NSP	22.487		
GEP	20.013		
REP	19.313	DC	
		AC	
MEP	19.235		.265
NEP	18.081		.249

Q_c = KW M_F = LB/HR LHV = BTU/LB

η_{cc} =

Q_s = KW CYCLE HEAT TSL (BEARINGS, ETC) TOTAL .2557 KW

η_{GB} = 0.98 N_G = RPM

SAL = .073 KW

η_G = .89

η_R = .965

η_{INV} =

EAL = .078 KW

η_{ETS} =

η_{INV} = .94

PPL/n =

η_{TRANS} = N/R

	EAL	EAL
COOLER FAN		
GEN - G/B FAN		
CONTROLS		0.028
OIL/SCAV. PUMP	0.023	
FUEL PUMP		0.050
REGENERATOR DRIVE		
TOTAL	0.023	0.078

	PPL
CONC. POWER x n	
PLANT CONTROL	
HOTEL LOAD	
BATTERY A/C	
PPL TOTAL	

N = NEGLECT NR = NOT REQUIRED 8-30-80

GB6-042-140

Figure 107. Performance Analysis Data Sheet for PCU with Production Recuperator.

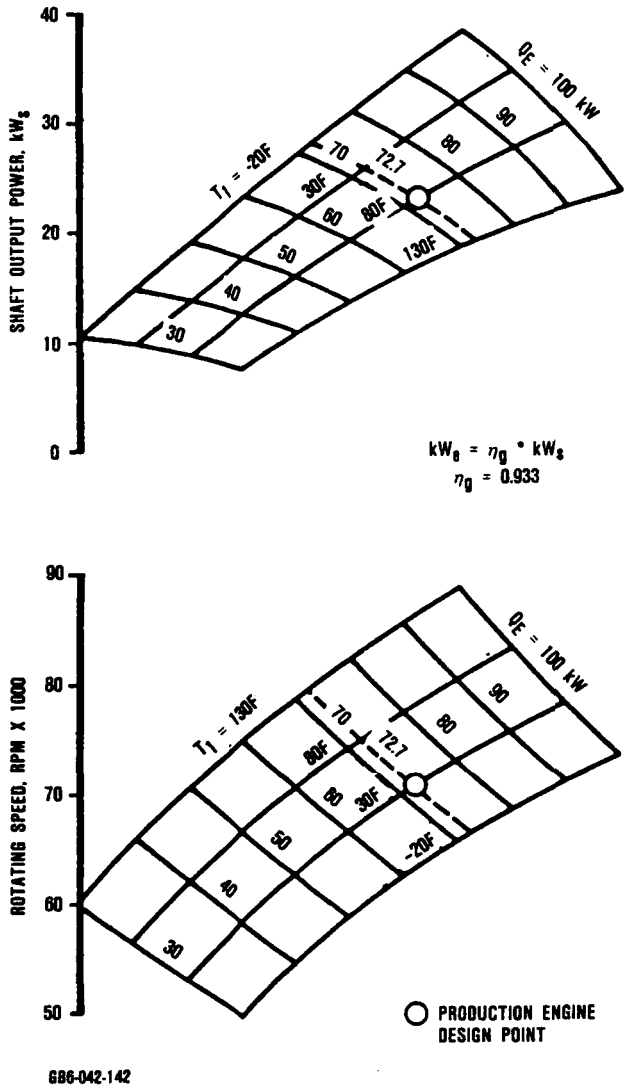

Figure 108. Engine Performance at Sea Level Indicates Required Speed Changes as Thermal Input and Ambient Conditions Change.

through which the rotor cooling air must flow. A lower limit on generator speed was therefore established (7000 rpm for the Bendix 28B135 generator) to prevent rotor overheating.

These considerations resulted in setting a lower speed limit of 78 percent of design speed (49,100 rpm) to prevent generator and recuperator overheating. The engine should not be operated below this speed.

As shown in Table 24, this lower limit of 78-percent speed does not significantly affect the amount of daily solar energy that can be collected and converted to electric power when the PCU is operated in the solar mode, i.e., no fossil-fuel augmentation. (Nearly all the daily insolation can be collected and converted when the PCU is operated in the hybrid mode.) Table 24 shows the Q_E required to operate the engine at 78-percent speed for a range of ambient conditions on a winter and a summer day. Also listed are the morning times when sufficient energy exists to begin engine operation at 78-percent speed and the afternoon times when the engine must be shut down to prevent speed from falling below 78 percent. The data presented in Table 24 assume no fossil-fuel augmentation. The times of day (in solar time, 24-hour clock) were calculated for a latitude of 40 degrees, and assume collector and receiver efficiencies of 0.9 and 0.85, respectively.

Also presented in Table 24 are estimates of the percent of total daily insolation that can be collected and converted into electricity. For both the winter day and the summer day, warmer ambient conditions result in a greater percentage of available solar energy being collected and converted into electricity.

Generator and Rectifier - The generator is most efficient when the turbocompressor speed is approximately 80,000 rpm. At that speed, the efficiency reaches 90 percent if the net shaft power, i.e., power out of the gearbox, is 20 kW. Generator efficiency decreases to between 86 and 87 percent as turbocompressor speed decreases.

CONTROL SYSTEM

The Mod "O" control system includes the electronic control unit (ECU), the sensors and solenoid, the harness to engine components, and the engine electrical components. The discrete analog ECU was designed to weigh 15

Table 24. Percent of Available Solar Energy Collected and Converted into Electricity: Solar-Only Operation at 40-Degree Latitude.

Ambient Condition	Minimum Q_E (kW_t)	Begin Engine Operation (solar time)	Terminate Engine Operation (solar time)	Percent of Available Solar Energy Collected and Converted into Electricity
Winter Day: December 21, Sunrise at 7.8 - Sunset at 16.3				
Sea Level, 10F (-12C)	42	8.6	15.4	90
5000 Feet,* -20F (-29C)	38	8.4	15.6	94
Sea Level, 80F (27C)	33	8.3	15.8	96
Summer Day: June 21, Sunrise at 4.9 - Sunset at 19.1				
Sea Level, 80F (27C)	33	5.9	18.2	95
Sea Level, 140F (60C)	27	5.6	18.4	97
5000 Feet,* 110F (43C)	24	5.5	18.5	98

*1525 meters

pounds (6.8 kg) and have outside dimensions of 10 x 14 x 8 inches (25.4 x 35.6 x 20.3 cm). Cooling would be accomplished by free convection, requiring that the ECU be housed in an enclosure. Power required by the ECU would be 110 vac (single phase).

The major design concepts of the logic diagram are shown in Figure 109 (temperature/speed control) and Figure 110 (mode selection logic). The ECU interfaces with all the other systems as shown in Figure 111, thereby creating a central processing unit that has full authority over all PCU functions.

The ECU design was accomplished by integrating the following logic statements:

When the power switch is moved to the ON position, the starter motor is engaged, provided the mode selector switch is in the Fuel Mode. A preset interval timer (Time Generator) starts when the starter motor is engaged. This is followed by arming of the temperature trim schedule provided the T_7 set point approximates 950F (510C) within 3 minutes after engine start. The fuel trim schedule is set to operate between T_7 values of 950F and 1500F (510C and 816C) within a 2-

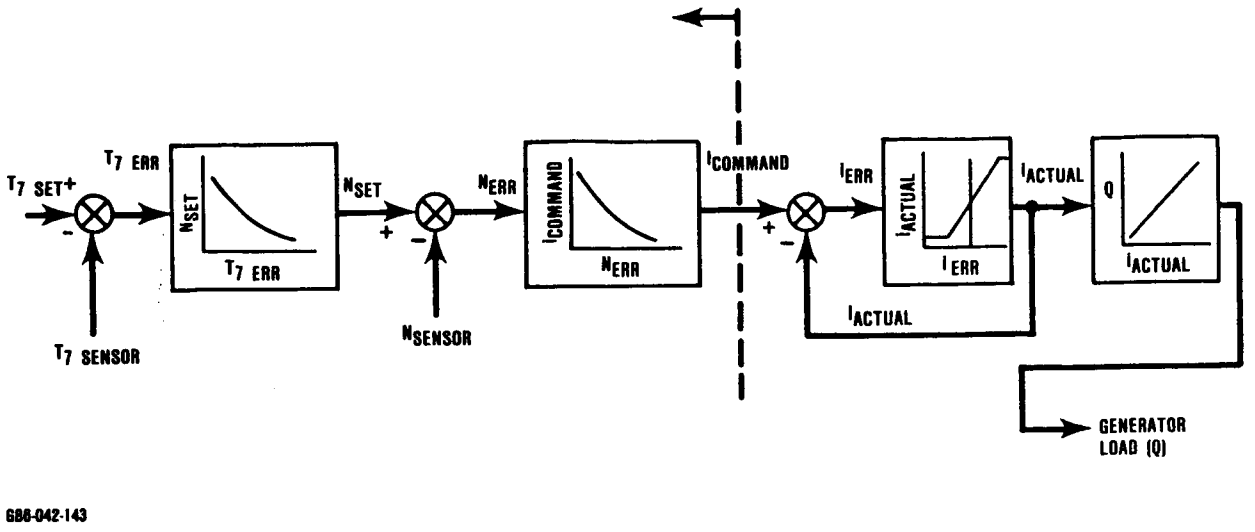

GB6-042-143

Figure 109. Turbine Inlet Temperature/Speed Control Scheme.

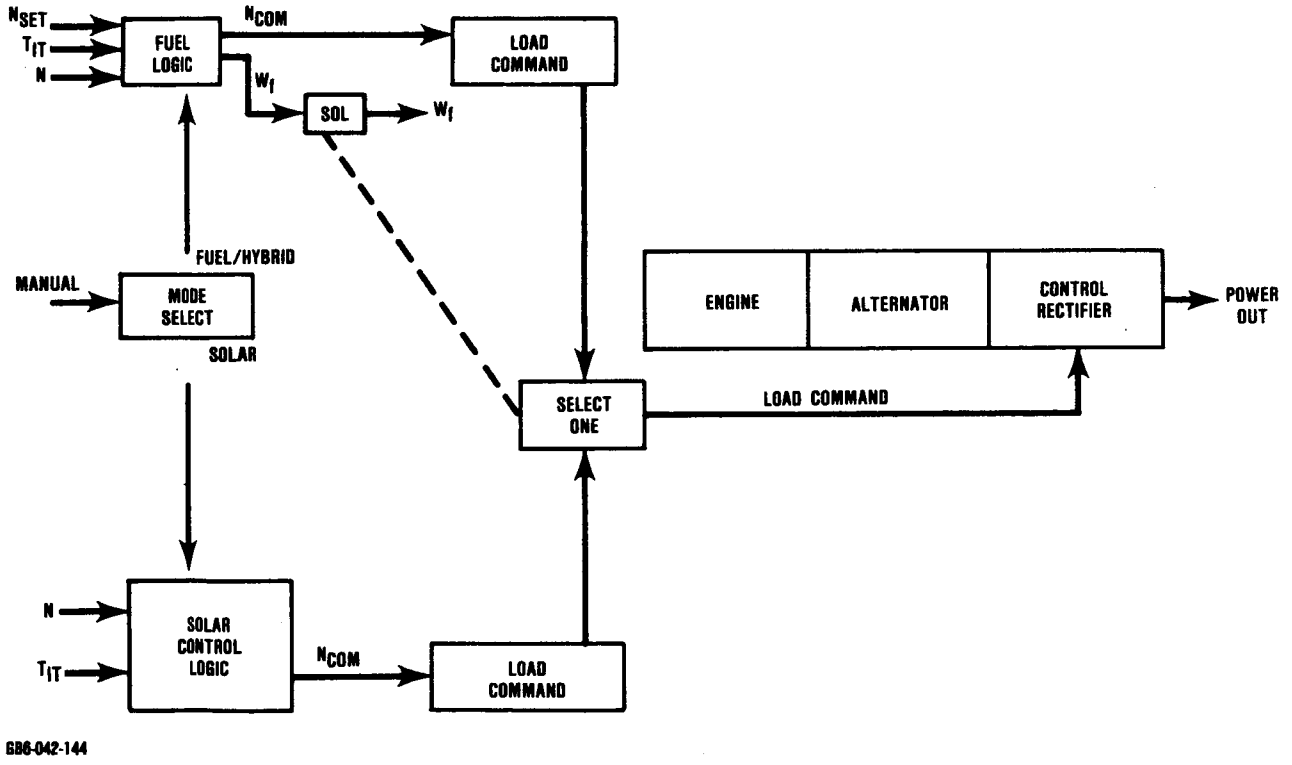

GB6-042-144

Figure 110. Mode Selection Adds Flexibility to Test Program.

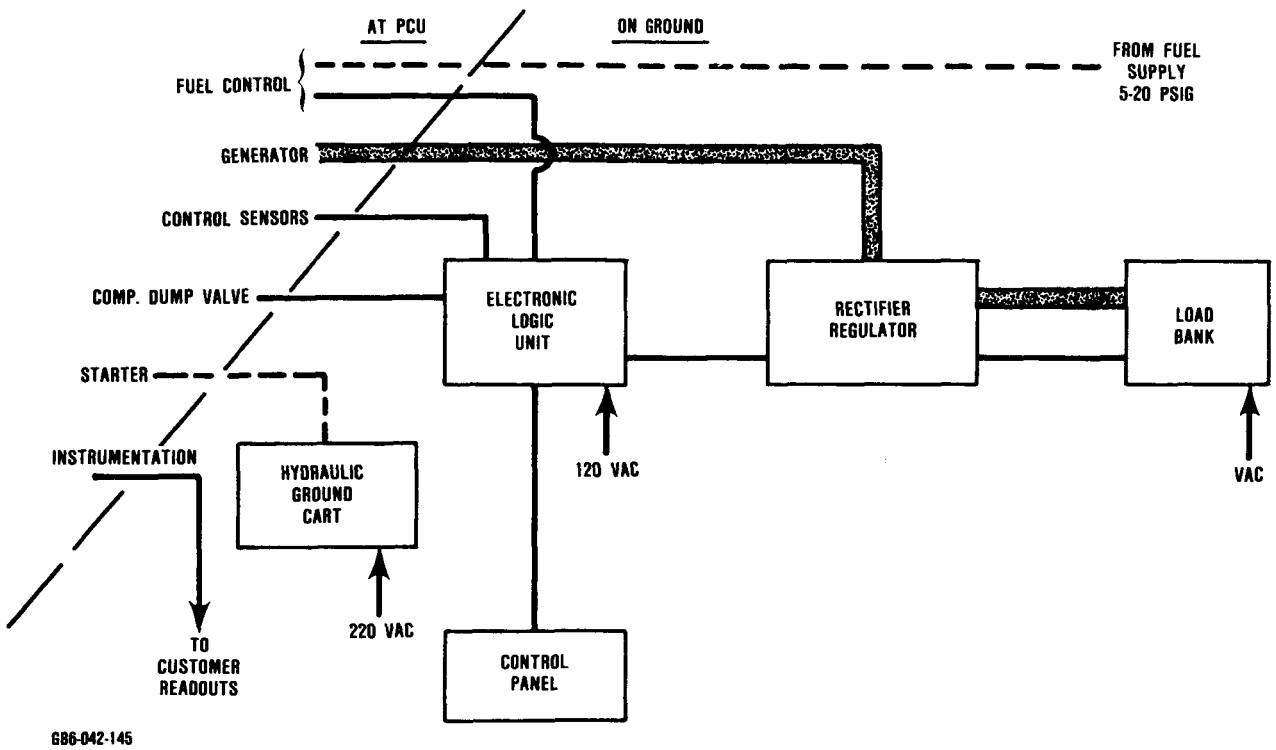

Figure 111. The ECU Interfaces with All Other Systems for Full Authority.

minute interval. The preset T_7 is compared with the actual T_7 prior to activation of the proportional governor control (K_p).

At 45-percent speed (N_t), the maximum fuel schedule is armed and is compared with the proportional gain. The smaller of the two is selected and becomes the acceleration schedule value that determines the amount of fuel supplied to the engine by the fuel control (pulse-width modulator). Also at 45-percent speed, the fuel solenoid and ignition unit are turned on. The ignition unit is allowed to run for 2 minutes, then is turned off by the timer.

If the engine is at 45-percent speed and T_7 is below 900F (482C), the no-flame fault is armed. This indicates a no-start condition, and after 10 seconds the engine will shut down.

The starter disengages when the engine speed reaches 60 percent and T_7 exceeds 700F (371C).

When the engine reaches 75-percent speed, the generator can be loaded. The current command is armed to control any faults that may occur in the electrical power system. The relays are switched to show any faults that may exist.

The integral control, which is a function of turbine inlet temperature, is compared with the minimum current set point, which is a function of speed. The higher of the two is selected and becomes the value representing the amount of fuel to be delivered by the pulse-width modulator. At this point, it should be noted that the acceleration schedule is not in effect, and the engine is running on integral control.

Most of the input signals required for shutdown protection are conditioned signals. If any one of the faults occurs, there is a 50-millisecond time delay.

If a fault occurs, the load on the generator is dropped, the concentrator is defocused, the fuel solenoid is shut off, and the ignitor is turned off. Each individual fault has its own driver, and if the fault occurs it is displayed on the panel.

Actual speed and temperature are displayed on the appropriate meters while the engine is operating.

The constant turbine inlet temperature/variable speed control concept is shown in Figure 109. Actual turbine inlet temperature is compared with the set-point temperature [1500F (816C)] to provide an error signal. This signal is conditioned to generate a speed set point which is compared with actual speed. The resulting error signal generates a current command signal, which is sent to the control rectifier as shown in Figure 111. The control rectifier modifies the output current until it equals the current command. An increase or decrease in the actual current results in a corresponding increase or decrease in generator load. A change in load effects a change in engine speed, thereby closing the speed control loop. A change in speed effects an opposite change in temperature, i.e., increased speed causes decreased temperature and vice versa, which results in closure of the temperature loop.

The control portion of the rectifier is a transistorized chopper circuit. The circuit is a duty-cycle modulator whose output voltage is the product of its input voltage and the duty cycle.

Rated output current from the control rectifier is 94 amperes at 213 volts. This load current can be varied electronically by the input current command from the engine controller. A command voltage varying from zero to 10 volts scales to a load current ranging from zero to 100 amperes dc. The control logic compares the output dc current with the current command and automatically adjusts the chopper duty cycle to attain the commanded current.

When the concentrator is oriented to the sun and insolation has increased so that the receiver is hot enough to start engine operation, the engine control will receive a signal and initiate the start sequence. The starter motor will engage and accelerate the turbocompressor to approximately 65-percent speed. After T_7 increases, the engine should be self-sustaining at this speed and the starter motor will disengage. Since the control logic normally attempts to increase T_7 to 1500F (816C) by reducing N_t, the N_t logic must contain a low N_t limit that is greater than the self-sustaining speed to allow the start cycle to continue. As insolation increases, T_7 will increase to 1500F (816C) and, with further increases, the speed set point will be continuously readjusted upward to maintain a constant T_7.

A preset interval timer will start when the starter motor is engaged. The engine control will turn off the starter if the engine does not become self-sustaining before expiration of the time interval. This prevents starter motor damage, which might result, for instance, from a reduction in insolation during start-up, allowing the motor to continue running.

In a normal shutdown, both insolation and the N_t set point decrease in order to maintain T_7 at 1500F (816C). When the N_t set point reaches approximately 65-percent speed, T_7 will begin to decrease and, with further decreases in insolation, the engine output power will continue to drop until the engine is no longer self-sustaining. At this point, the engine will decelerate to zero speed.

Two failure conditions -- turbine overspeed and receiver outlet or turbine inlet overtemperature -- require special provisions. Should an overtemperature or overspeed condition be sensed, the control will transmit a signal to turn the concentrator away from the sun and thus shut down the PCU.

The control sensors and solenoid are described in Table 25. These components are all existing production parts and will be used to monitor and protect the PCU equipment.

Table 25. Control Sensors and Solenoid Are Existing Production Parts.

Item	Characteristic	Previous Usage	GTEC P/N
Low Oil Pressure Switch	20 psi (138 kPa) set point on delivered pressure	GTCP36-50/-100	3876001-2
High Oil Temperature Switch	300F (149C) set point	GTCP36-100E	3888030
Speed Sensor	Electromagnetic-type sensing element	GTCP36-200	3876017 Mod
Turbine Inlet Temperature Sensor	C/A* 0 to 1600F (-18 to 871C)	GTCP36-50/-100	3876003
Recuperator Hot Side Temperature Sensor	C/A* 0 to 1500F (-18 to 816C)	GTCP36-50/-100	3876003
Fuel Shut-Off Solenoid	Normally closed 2-way	GTCP36-50/-100	692545-1

*Chromel/alumel.

Control System Analysis

An analog computer simulation of the Mod "O" engine, controls, and solar receiver was performed to study control loop performance and stability in the fuel, solar, and hybrid modes of operation. A particular area of concern was crossover from the fuel-only to the hybrid to the solar-only mode because oscillation between modes might occur during certain cloud-cover conditions.

The analog computer analysis verified the control concept as originally configured, except with regard to the method for instigating crossover from the hybrid to the solar-only mode. The original concept proposed the use of a speed error exceeding ±2 percent from the speed set point as a method for instigating crossover. This method caused large T_7 errors and control system instability. Efforts to reduce the temperature error by reducing the speed hysteresis band resulted in cycling between the solar-only and hybrid mode during crossover.

Since T_7 control is used in all three operating modes, it is the logical and convenient parameter to use in detecting the need for switching modes. Therefore, modes are switched when saturation of the T_7 control mode occurs. For example, during hybrid operation, as insolation is increasing in the morning, fuel flow is cut back to the minimum allowed; the minimum fuel flow is dependent on the combustor blowout fuel flow. T_7 then rises as insolation further increases (T_7 is no longer being controlled by the fuel control loop). When the control detects that T_7 has reached 1550F (843C), fuel is shut off and the solar T_7 control loop is activated, thereby effecting a fuel-to-solar crossover. Conversely, while insolation is decreasing during the afternoon, the T_7 control loop ceases to reset speed when minimum speed is reached (i.e., T_7

control loop saturation in the solar mode). T_7 then rapidly drops to 1425F (774C) and fuel is once again turned on. Simulation of this method demonstrated a stable crossover.

Figure 112 is a schematic of the essential elements of the control system. In the solar-only operating mode, T_7 is maintained at approximately 1500F (816C) by commanding the control rectifier to load and unload the generator and thus vary turbocompressor speed as insolation varies. In the hybrid operating mode, T_7 is maintained at approximately 1500F (816C) by varying the fuel flow, and speed is maintained at an operator-selected set point by varying the generator load with the control rectifier.

An important parameter in the control analysis is the minimum combustor fuel flow ($W_{f_{min}}$), i.e., the flow required to sustain stable combustion. This parameter influences selection of the upper and lower T_7 set points; the smaller the $W_{f_{min}}$ value is, the closer

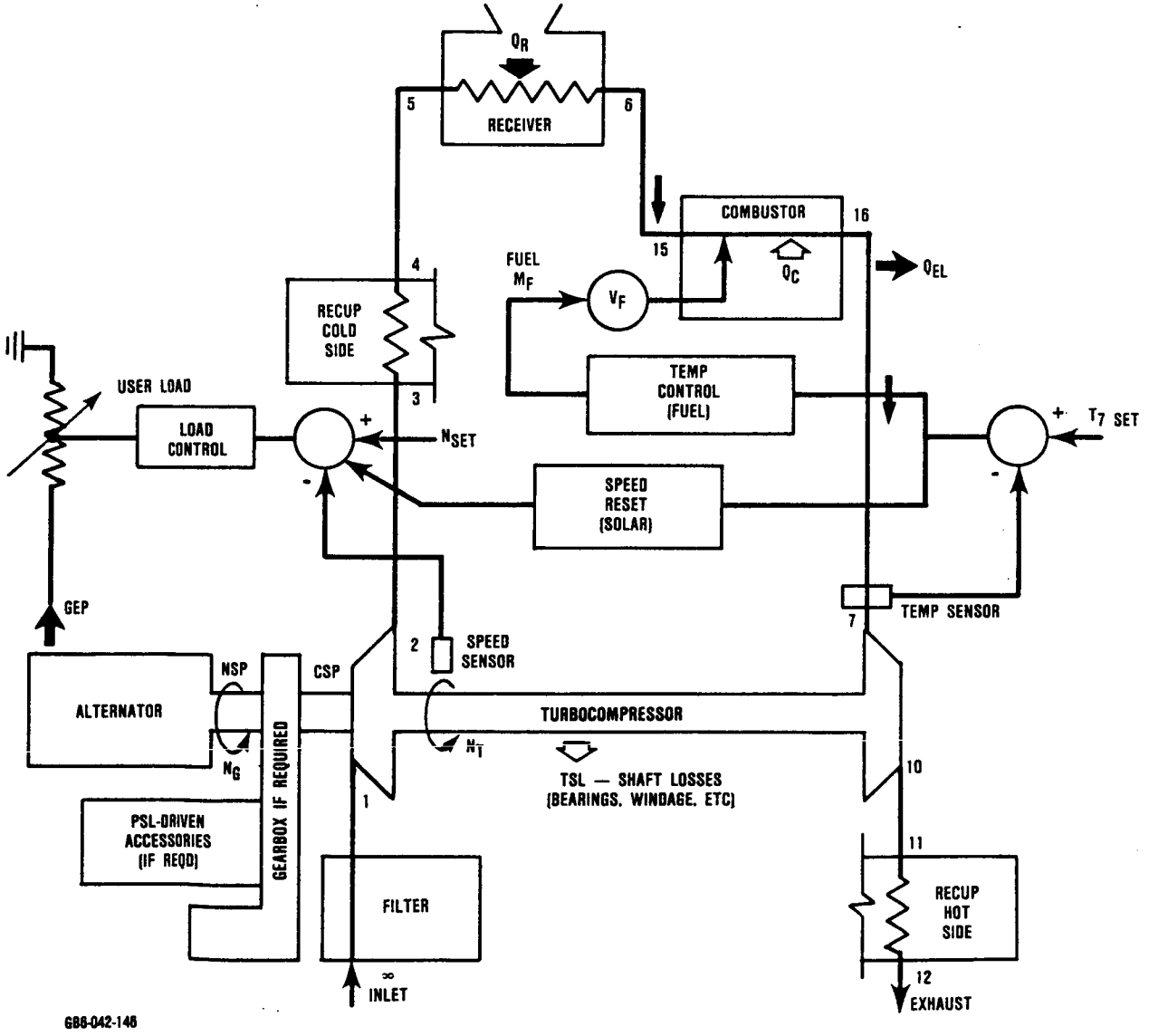

Figure 112. Brayton Engine/Generator Diagram Used for Control Loop Analysis.

together are these set points. Since $^{W}f_{min}$ is difficult to predict analytically, it was to be determined experimentally in a combustion test rig.

One initial result of the control analysis was establishment of the relationship between engine speed and the partial derivative of T_7 with respect to combustor fuel flow i.e., $\partial T_7/\partial W_f$. As shown in Figure 113, $\partial T_7/\partial W_f$ is inversely proportional to engine speed. For the minimum turbocompressor speed of 78 percent, $\partial T_7/\partial W_f$ is equal to 58F/lb/hr (83C/kg/hr). Thus, if $^{W}f_{min}$ is 1 lb/hr (0.454 kg/hr) at 78-percent speed, T_7 will increase or decrease by approximately 68F (38C) when the combustor is turned on or off at this $^{W}f_{min}$. The difference between the upper and lower T_7 set points must therefore be greater than 68F (38C) to prevent system instability when the system is changing from the solar-only to the hybrid mode or vice versa. If the difference between the upper and lower T_7 set points were less than 68F (38C) and if T_7 were to drop to its lower set point due to decreasing insolation, the combustor would turn on and the T_7 upper set point would immediately be exceeded. The combustor would then turn off and T_7 would fall below the lower T_7 set point, causing the combustor to again turn on. Thus, the combustor would alternately be turned on and off if the difference between the upper and lower T_7 set points were less than 68F (38C) for $^{W}f_{min}$ = 1 lb/hr (0.454 kg/hr) at 78-percent speed. If $^{W}f_{min}$ is equal to 2 lb/hr (0.91 kg/hr), then the difference between the upper and lower T_7 set points must be greater than 136F (76C).

Further examination of Figure 113 reveals that the difference between the upper and lower T_7 set points can be decreased by raising the minimum engine speed, if $^{W}f_{min}$ does not change. For example, if $^{W}f_{min}$ is held constant at 2 lb/hr (0.91 kg/hr), raising the minimum engine speed from 78 to 85 percent of design speed would reduce the required difference between the upper and lower T_7 set points from 136F (76C) to 114F (63C).

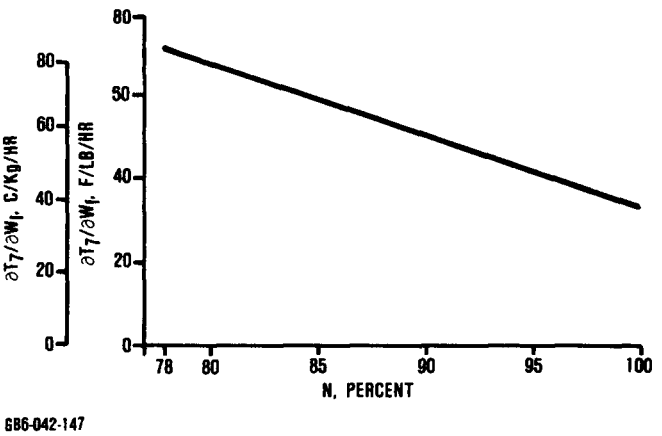

Figure 113. Effect of Raising Minimum Speed To Reduce $\partial T_7/\partial W_f$ Temperature Control Parameter.

Figure 114 illustrates a cloud transient for sea level, hot day. When a small cloud partially blocks the sun, Q_E drops from 44 kW_t to 30 kW_t and remains there for approximately 30 seconds. $^{W}f_{min}$ is 1 lb/hr (0.454 kg/hr), and the upper and lower T_7 set points are 1555 and 1445F (846 and 785C), respectively.

This analog computer simulation (Figure 114) shows a stable crossover from the solar-only to the hybrid operating mode. The T_7 trace shows that fuel is turned on to 1 lb/hr (0.454 kg/hr) when T_7 drops to 1445F (785C). At this point, T_7 jumps to 1543F (839C) and $\partial T_7/\partial W_f$ equals 33F/lb/hr (40C/kg/hr).

Figure 115 shows the cycling that occurs between the solar-only and hybrid modes when $W_{f_{min}}$ is 2 lb/hr (0.91 kg/hr) and the upper and lower T_7 set points are 1550 and 1420F (843 and 771C), respectively. Subsequent investigation revealed that the upper T_7 set point must be raised to 1580F (860C) to prevent cycling when the $W_{f_{min}}$ is 2 lb/hr (0.91 kg/hr).

CONTROL PANEL

The primary function of the control panel is to monitor the engine, the generator, and such components as the starter, the ignition system, and the fuel system. Layout of the control panel is shown in Figure 116. The

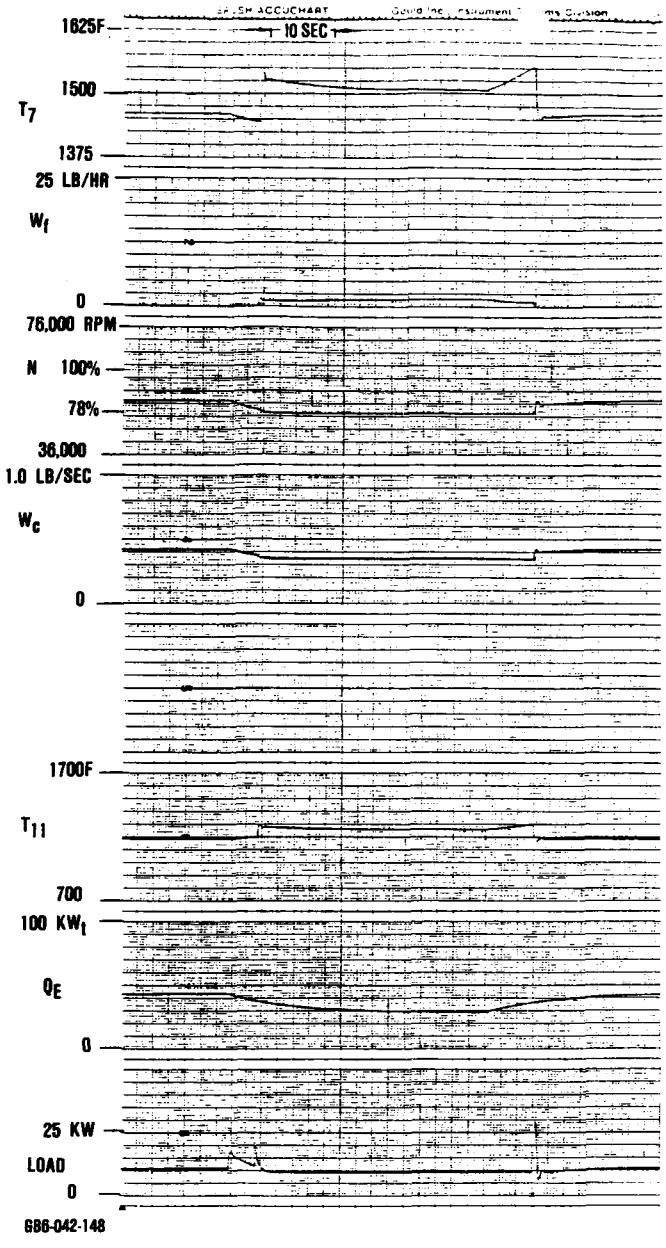

Figure 114. Stable Crossover During Cloud Transient.

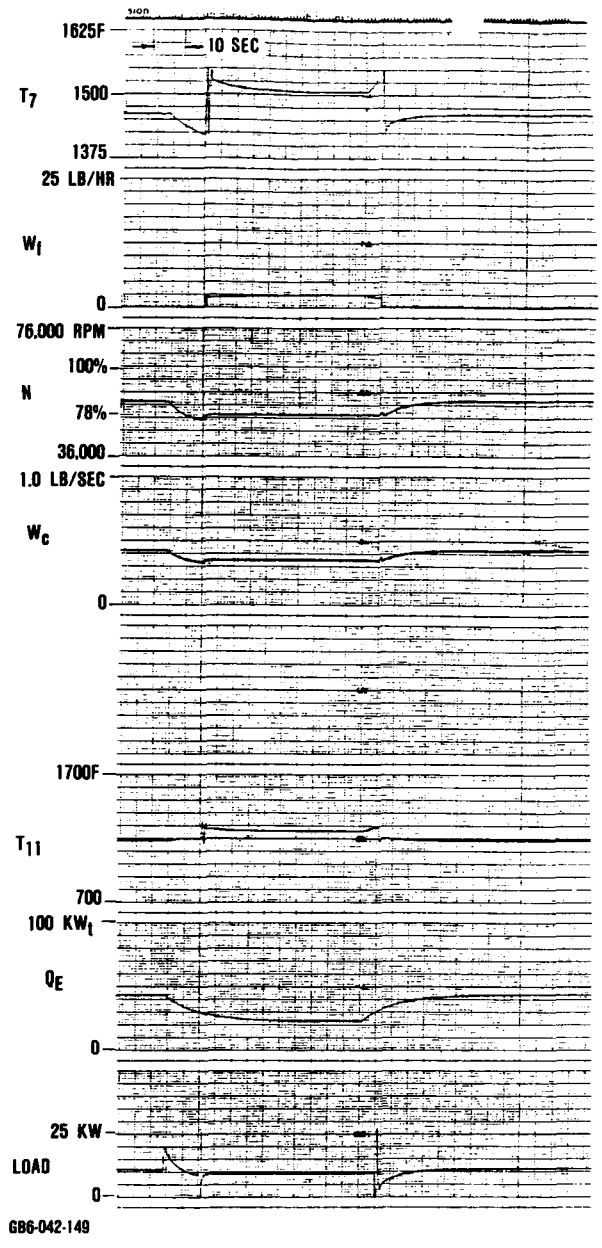

Figure 115. Cloud Transient Showing Tendency for Instability.

meters on the top of the panel monitor engine speed, turbine inlet temperature, recuperator temperature, and receiver temperature. Manual controls designated SPEED SET and T_7 SET are provided for selecting different set-point values during operation. Since the system is designed to operate at a constant T_7 of 1500F (816C), the T_7 SET control will be covered by a removable box to discourage arbitrary changes to T_7.

Engine fault protection is provided by fault lamps that light when the faults occur. Fault protection is provided for:

Table 26. Generator and Voltage Regulator Were Specified.

Parameter	Description
Generator	
Manufacturer	Bendix 28B135-129
Type	Self-excited, 3-phase, brushless
Rating	25 kva at 120/208 volts, SL, 60C inlet air
High Efficiency	89 percent at design point
Availability/Previous Usage	In production/generator sets and Sikorsky A/C
Cooling Air	Integral fan
Lightweight	49 lbs (22.2 kg)
Small Size	6.5 in. dia. x 12.5 in. long (16.5 x 31.75 cm)
Speed Range	7000 to 10,000 rpm
Frequency Range	350 to 500 Hz (400 Hz nominal)
Voltage Regulator	
Manufacturer	Bendix 20B100-2
Type	Solid state
Regulated Voltage	115/200 volts (nominal)
Compact Size	3 x 4 x 2.75 in. (7.62 x 10.16 x 6.35 cm)
Weight	1 lb (0.454 kg)

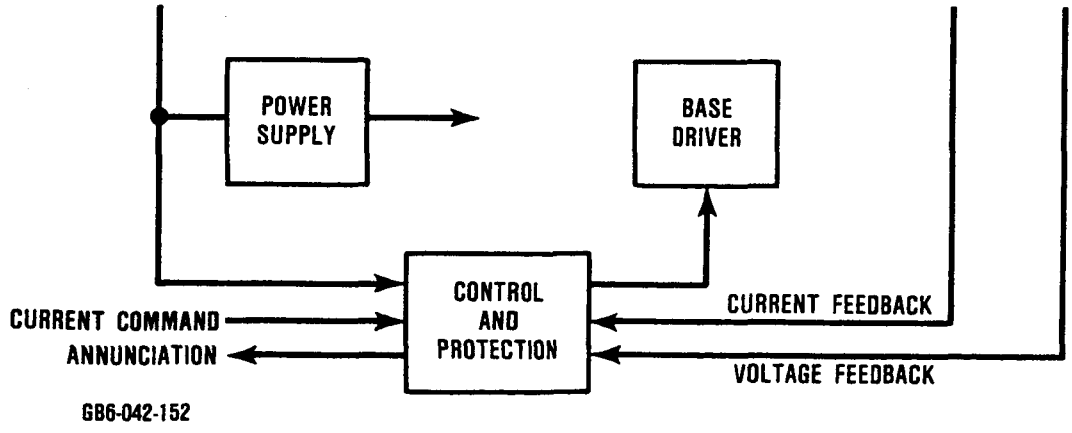

Figure 118. Rectifier/Regulator Subsystems Were Designed for Control and Protection.

Figure 119 is a schematic of the rectifier/regulator power flow path, which includes full-wave bridge rectification of the ac generator three-phase power, dc filters for limiting ripple voltage, and the transistor/regulator pulse-width-modulated load control. Pulse frequency is 5 kHz and pulse width is varied from 20 µsec to 180 µsec to control the output power to the parasitic load bank. Table 27 lists the characteristics of the power transistors used in the rectifier/regulator.

Figure 120 is a logic diagram of the transistor/regulator base drive control for generating pulse-width modulation of the rectifier/regulator output as a function of the power command signal from the ECU. Overcurrent, overtemperature, or undervoltage will cause a loss of base drive to the transistor regulator, interrupting power output from the rectifier/regulator unit.

Table 27. Power Transistor Characteristics Comply with System Needs.

Parameter	Description
Manufacturer	Fuji Electric Co., Inc.
Type	Power Darlington
Voltage Rating	520 V_{ceo} (sustained)
Current Rating	100 A_c (continuous)
Switching Time	
Rise	1.0 microsecond
Fall	1.0 microsecond
Gain	100 at 100 A_c
Saturation Voltage	2.0 V_{ce} at 100 A_c

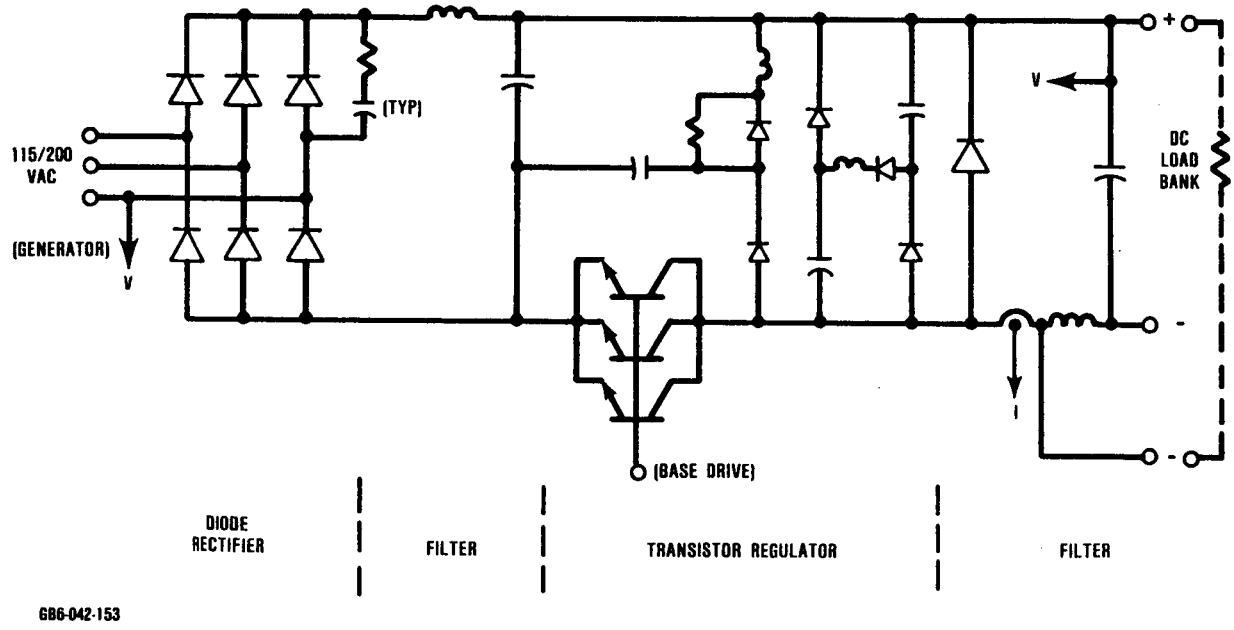

Figure 119. Power Flow Path Through Rectifier/Regulator to Load Bank.

The rectifier/regulator provides switched output signals to the ECU for initiating system shutdown in the event of rectifier/regulator overcurrent, overtemperature, or input undervoltage as shown in Figure 121. Relay switching was selected to ensure electrical isolation of the ECU from the rectifier/regulator.

The basic features and characteristics of rectifier/regulator performance are listed below:

- Input
  - 108/187 to 132/229 volts rms
  - 350 to 500 Hz
  - 25 kva maximum
- Shunt Output
  - 250 volts dc, nominal
  - 0 to 100 amps dc
- Series Output
  - 200 volts dc, nominal
  - 0 to 125 amps dc
- Protection
  - Input undervoltage <100/173 volts rms
  - Output voltage limited to 270 volts dc
  - Output current limited to 175 amps dc
  - Overtemperature
- Accuracy
  - ±2 percent of current command

The curves in Figure 122 show the high efficiency and power-factor capabilities of the rectifier/regulator. Effective conversion of generator output is related to both factors. At a 20-kW output load, efficiency and power factor are as follows:

- Rectifier/Regulator Efficiency = 96.5 percent
- Input kva = 22.0
- Input Power Factor = 0.94

Figure 123 is a layout of the rectifier/regulator components. Included is a diagram of the protective enclosure, which is rated for outdoor service. Transient load capacity is 40 kW for 5 seconds, sufficient to accommodate a transient which may occur during crossover from the solar to the hybird mode.

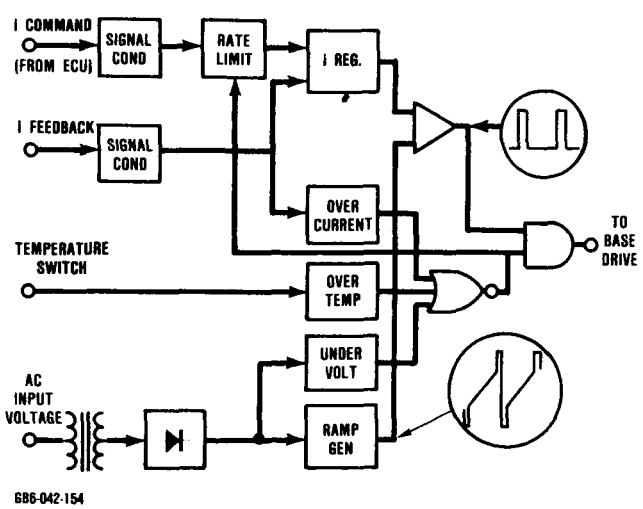

Figure 120. Logic Block Diagram Defined for Electrical System.

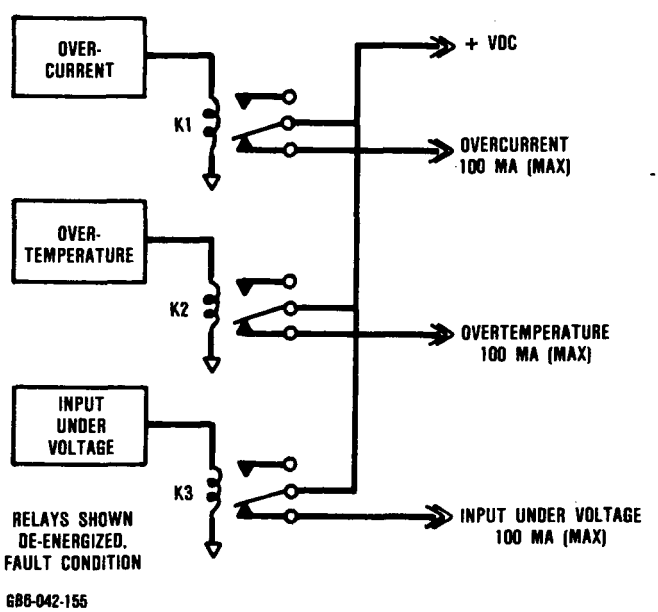

Figure 121. Rectifier/Regulator Protective Circuits Are Incorporated in Design.

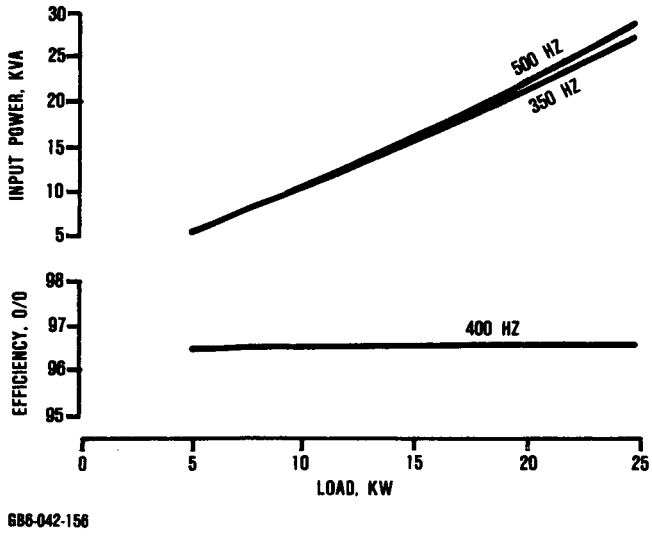

Figure 122. Rectifier/Regulator Performance Is Capable of High Efficiencies.

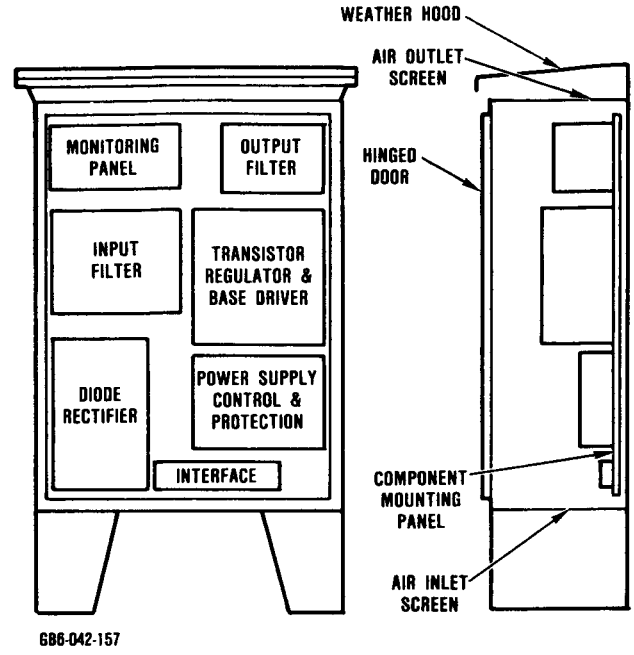

Figure 123. Rectifier/Regulator Assembly Is Housed in Protective Enclosure.

APPENDIX B

AGT101 PROGRAM SUMMARY

PROGRAM DESCRIPTION

As part of the U.S. Department of Energy (DOE) Gas Turbine Highway Vehicle System Program, Garrett Turbine Engine Company (GTEC) and Ford Motor Company are engaged in the development of an advanced gas turbine (AGT) engine for automotive application. The program is authorized under DOE/NASA Contract DEN3-167, with the NASA Lewis Research Center (NASA/LeRC) providing program management and technical direction. Program effort is directed at providing the United States automotive industry with the high-risk, long-range technology necessary to produce gas turbine engine power trains for automobiles that will have reduced fuel consumption and reduced environmental impact. Status and technical progress through May 1986, which completes 6-1/2 years of the program, are summarized in this appendix.

The program was initiated on October 1, 1979. Design reviews of the Reference Power-Train Design (RPD) and the initial development engines were held on schedule in early 1980, representing successful completion of Contract Milestone 1. The RPD is a design that could be considered for production evaluation. Figure 124 depicts the program schedule since inception, with critical milestones identified. Note that the present contract is directed toward power section development, with emphasis on ceramic component development. The program has since been extended and is now scheduled for completion by June 1987.

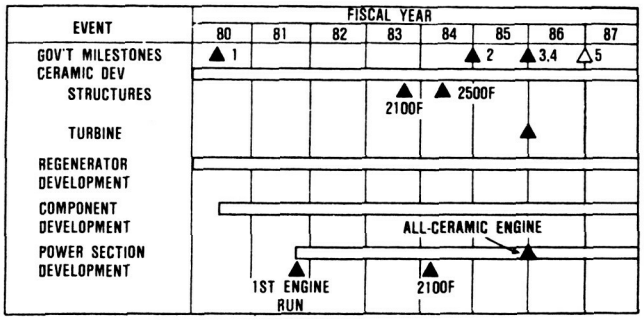

Figure 124. AGT101 Program Schedule.

ENGINE DESCRIPTION

Design Features

The AGT101 engine (see Figure 125) is flat rated at 100 hp (74.6 kW) with a minimum SFC of 0.3 lb/hp-hr (0.18 kg/kW-hr). The single-

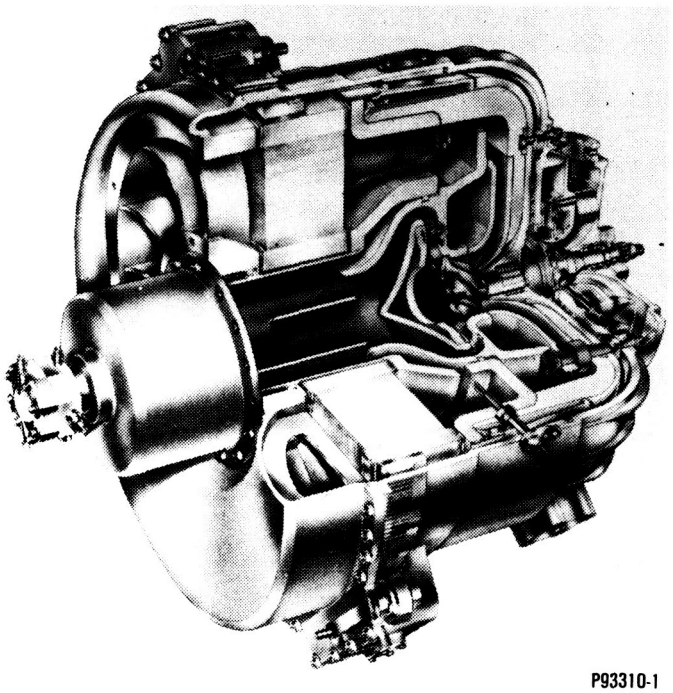

Figure 125. AGT101 Power Section.

shaft rotating group is composed of a radial turbine, a centrifugal compressor, and output gear supported by an air-lubricated foil-journal bearing and an oil-lubricated ball bearing. The maximum (steady state) engine speed is 100,000 rpm, and idle speed is approximately 50,000 rpm.

Ambient air enters the engine through variable inlet guide vanes and passes through the single-stage compressor. The compressed air, at approximately 365F (185C), is routed around the full engine perimeter to the high-pressure side of the ceramic rotary regenerator. This feature provides increased thermal efficiency by minimizing heat loss. The partially heated air passes through the regenerator core where it is further heated (at idle) to approximately 1940F (1062C), and then passes to the combustor.

The combustion system features a fixed-geometry, lean-burn, low-emission combustor. Work conducted by NASA and GTEC indicates that this lean-burn combustion system has high potential for meeting emission standards. Combustor air rises in temperature to a maximum of 2500F (1371C) with the addition of fuel, is ducted to the ceramic stator, and is then expanded across the radial turbine rotor. Turbine exhaust gases at 2000F (1093C), which is the maximum temperature at idle, are ducted through the low-pressure side of the rotary regenerator and out the engine exhaust at a maximum temperature of 510F (266C) at maximum power.

The all-ceramic hot-section structural components are symmetrical except for one housing that separates high- and low-pressure regenerator flow. The symmetrical design provides a more uniform stress distribution and simplifies component manufacturing.

Engine Testing

As shown in Figure 126, the all-ceramic AGT101 engine has evolved through a series of iterative steps. The all-ceramic engine was initially designed, and metallic components substituted (except the regenerator), to ac-

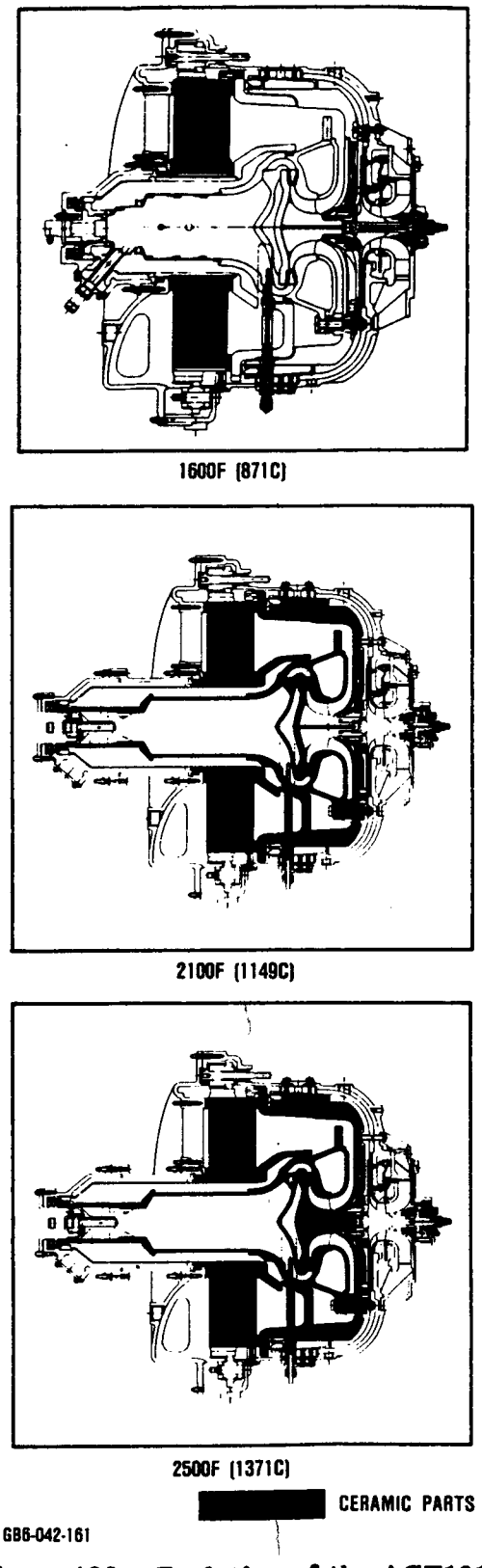

Figure 126. Evolution of the AGT101.

commodate early power-section testing and evaluation at 1600F (871C). This unit began test in June 1981 and successfully completed Contract Milestone 2 of the program, performance characterization.

As the ceramic structures have been developed, they have been introduced into the power section along with a cooled dual-alloy metallic turbine rotor, permitting testing at 2100F (1149C). Testing of the 2100F (1149C) power section started in February 1984. Subsequently, the dual-alloy rotor was replaced by a ceramic rotor, and engine testing in the all-ceramic configuration began in January 1986. This testing will continue throughout the remainder of the program.

Table 28 summarizes the AGT101 engine testing. Engines with a "C" suffix are ceramic engines. Through 1984, three engines had accumulated test time. In 1985, a fourth engine, S/N 004C, was introduced to aid in test support and performance evaluation. With the resolution of mechanical problems in 1984 (Reference 3), testing has been dedicated to ceramic engine evaluation as evidenced by engine S/N 002C accumulating the most time.

Table 28. AGT101 Accumulated Engine Test Time.

Power Section S/N	Builds	Starts	Operating Time, hours
001	37	232	118
002	4	70	21
002C	16	103	145
003	52	333	118
004C	4	40	8
Total	113	778	410

Significant testing was accomplished in 1985, including numerous full-speed (100,000 rpm) and 2100F (1149C) runs, development start cyclic tests, baseline performance tests at 2100F (1149C), and ceramic combustor engine tests. These tests are detailed in the discussion that follows.

Initial evaluation of all ceramic component interfaces at 2100F (1149C) and full-pressure loading was accomplished. With operation at 100,000 rpm and 2100F (1149C), the engine develops its maximum pressure ratio (5:1), thereby loading all the interfaces. No evidence of contact stress was evident at any component interface. Mechanical operation of the engine was smooth and repeatable from build to build and from engine to engine.

As described in a succeeding section of this appendix (see Ceramic Development), start transient testing followed a progressive sequence from slow thermal ramps to increasingly faster ramps, becoming more indicative of actual engine requirements. As ceramic components were qualified through these start conditions in the screening rigs, engine testing also progressed. Figure 127 shows the required-to-run line superimposed on actual engine test data for a typical development start [ambient to 1800F (982C) in 15 seconds]. The development start is indicative of engine operation requirements today, and subjects the ceramic components to better than 85 percent of the maximum stress observed during a normal start. After achieving 1800F (982C)

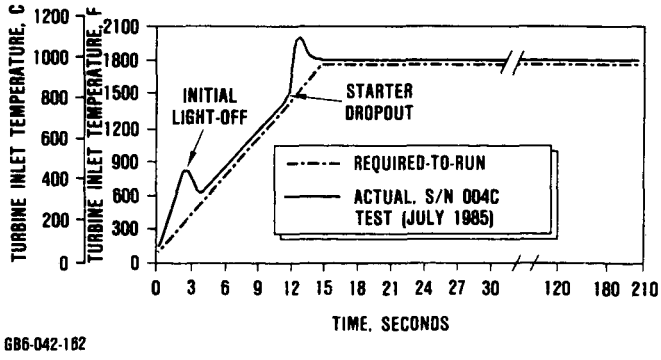

Figure 127. Development Start for AGT101 [2100F (1149C)].

and 60,000 rpm, the engine is held at these conditions for approximately 6 minutes before proceeding with the testing. The 6-minute hold period allows the ceramic components to reach thermal (stress) equilibrium. S/N 002C and S/N 004C have accumulated over 50 development starts with no component distress. All future testing will be conducted using either the development or normal start conditions.

Performance data at 2100F (1149C) were also obtained for S/N 002C over the speed range of 60,000 to 100,000 rpm. Because of the ceramic composition of the engine parts, only a limited number of sensors could be installed. Using the limited amount of available data as a starting point in the engine performance model, the unknowns (leakages) are varied until the best data match is obtained. During this iterative calculation, energy and mass balance is maintained. Based on this approach, the internal leakage was calculated to be 21 percent (Figure 128), a level consistent with a standard sea-level performance of 43.4 shp (32.4 kW). Although the engine configuration was far from optimum, the test results represent the baseline performance from which improvements are directed and comparisons made.

After the successful rig test of a ceramic combustor in 1985, this component was added for 2100F (1149C) engine evaluation. As shown in Figure 129, the liner mates to the transition duct, with the dome, swirler, and spacer axially located on the liner. The lean-burn fuel nozzle is located on the engine centerline. Successful start transients to 1800F (982C) were accomplished with no component distress.

Ceramic Development

With a view to meeting the final objectives for the all-ceramic gas turbine engine, the AGT101 program identified two major ceramic-material goals. These goals have been categorized as "proof of design" and "materials capability demonstration." "Proof of design" is defined as a ceramic component design

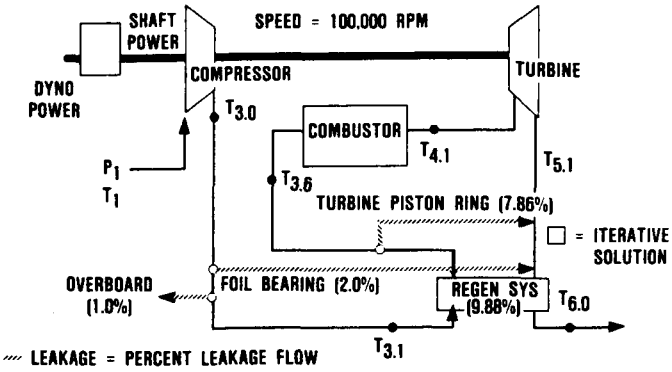

	TEST DATA	CALCULATED VALUES
DYNO POWER	30.07 HP (22.4 KW)	30.08 HP (22.4 KW)
SHAFT POWER	—	43.4 HP (32.4 KW)
P_1	14.096 PSI (97.2 KPa)	14.096 PSI (97.2 KPa)
T_1	85F (29.4C)	85F (29.4C)
$T_{3.0}$	445F (229C)	466F (241C)
$T_{3.1}$	502F (261C)	501F (261C)
$T_{3.6}$	1383F (751C)	1404F (762C)
$T_{4.1}$	2139F (1171C)	2139F (1171C)
$T_{5.1}$	—	1597F (869C)
$T_{6.0}$	680F (360C)	658F (348C)

GB6-042-163

Figure 128. Engine Test Data Setup Model.

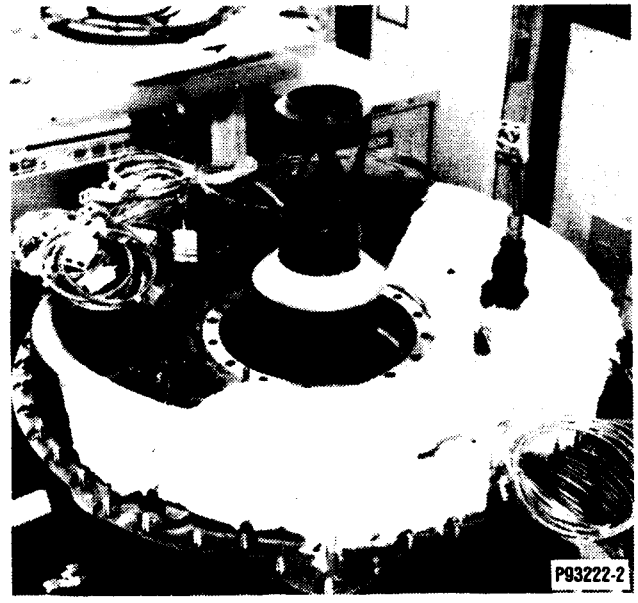

GB6-042-164

Figure 129. Ceramic Combustor Installed in AGT101.

that has been consistently subjected to 1.25 times the "normal engine start" thermal transient and mechanically induced stresses without incurring fracture. This start transient, illustrated in Figure 130, is accomplished in component thermal and mechanical screening and test rigs. "Materials capability demonstration" is defined as the material or materials capable of withstanding the harsh gas turbine environment of the AGT101 [turbine inlet temperatures to 2500F (1371C)] for a period of 200 hours without failure or significant strength degradation.

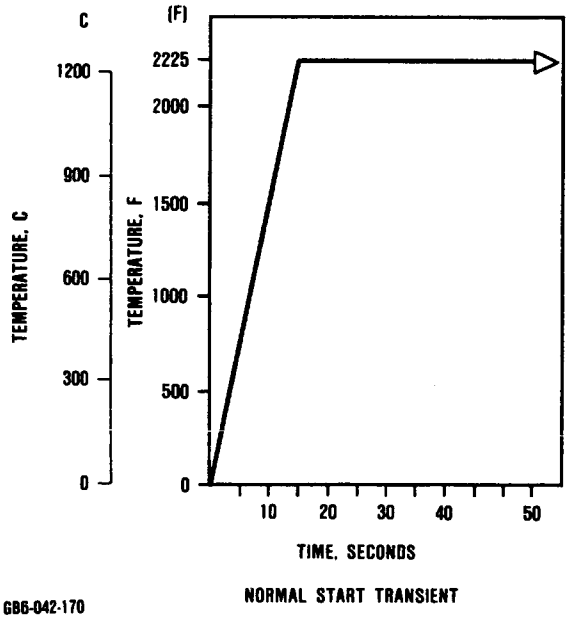

Figure 130. AGT101 Normal Start Transient.

To achieve "proof of design," the AGT101 program has evaluated a number of ceramic materials and processes from several U.S. and foreign suppliers. The material selection criteria are shown in Figure 131 with initial material selection based primarily on the flexibility of the fabrication approach, strength and strength retention at room and elevated temperatures, and component availability. A

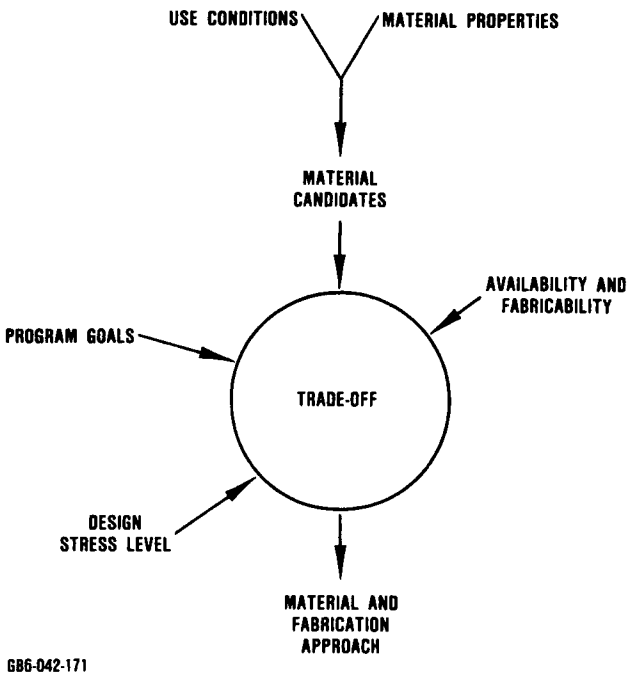

Figure 131. Material Selection Criteria.

list of the ceramic materials being evaluated in the AGT101 program is presented in Table 29, together with the supplier and the associated forming process.

SUMMARY

Ceramic engine testing at 2100F (1149C) and component testing at 2500F (1371C) have progressed throughout the program and continue to demonstrate the "proof of design" for the AGT101. Maximum speed operation at 2100F (1149C) has been successfully demonstrated on numerous occasions with no evidence of contact stress or distress to the ceramic components. Initial baseline performance has been established at 2100F (1149C). Internal leakage appears to be a key development need. Ceramic combustor rig tests and engine tests were successfully conducted, including start-transient and steady-state operation.

Improvements in material properties are progressing for both silicon carbide and sin-

tered silicon nitride. Ceramic rotor fabrication efforts continue at Ford and AiResearch Casting Company. In addition, Kyocera and NGK-Locke have produced ceramic rotors which have passed pre-engine qualification tests. A 100-hour endurance test of the all-ceramic AGT101 engine is planned for the near future.

Table 29. Numerous Ceramic Materials Were Evaluated.

Source	Material	Forming Process
AiResearch Casting Company	Reaction Bonded Silicon Nitride (RBSN)	Slip Cast (Injection Molded)
	Sintered Silicon Nitride (SSN)	Slip Cast (Injection Molded)
	Sintered Reaction Bonded Silicon Nitride (SRBSN)	Slip Cast (Injection Molded)
Ford Motor Company	Sintered Reaction Bonded Silicon Nitride (SRBSN)	Slip Cast
Carborundum	Sintered Alpha Silicon Carbide (SASC)	Isopressed, Injection Molded, Slip Cast, Extruded
Kyocera Corporation	Sintered Silicon Nitride (SSN)	Slip Cast
NGK-Locke	Sintered Silicon Nitride (SSN)	Isopressed, Injection Molded, Slip Cast
	Magnesium Aluminum Silicate (MAS)	Extruded
Corning	Lithium Aluminum Silicate (LAS)	Slip Cast

APPENDIX C

ABBREVIATIONS, ACRONYMS, AND SYMBOLS

A_c	Amps, Collector
AC	Alternating Current; also ac
AGT	Advanced Gas Turbine or Automotive Gas Turbine
AMB	Ambient; also amb
AS	Aluminum Silicate
ASME	American Society of Mechanical Engineers
ASTM	American Society for Testing and Materials
atm	Atmosphere
BE/G	Brayton Engine/Generator; also E/G, PCU, or PCA
Btu	British Thermal Unit
C	Degrees Centigrade
CFDC	Combined Federal Driving Cycle
CFM	Cubic Feet Per Minute; also cfm
CG	Center of Gravity; also cg
cm	Centimeter
CRES	Corrosion-Resistant Steel
CSP	Cycle Shaft Power (kW_m)
D	Dimensional
DC	Direct Current; also dc, Vdc, or VDC
DOE	U.S. Department of Energy
E_r	Recuperator Temperature Effectiveness (Dimensionless)
E_{RH}	Recuperator Effectiveness, High-Pressure Side
E_{RL}	Recuperator Effectiveness, Low-Pressure Side
EAL	Electric Accessory Load
ECU	Electronic Control Unit
EFF	Effective
ERDA	Energy Research and Development Administration
F	Degrees Fahrenheit
F_{ax}	Axial Force
F_{rad}	Radial Force
F/A	Fuel-Air Ratio
F/B	Foil Bearing
FCU	Fuel Control Unit
FPS	Feet Per Second; also fps
GE	General Electric
GEP	Generator Electric Power Output (kW_e)
GTEC	Garrett Turbine Engine Company

hp	Horsepower
HP	High-Pressure Side, Air Side
Hz	Hertz
I	Insolation (kW/m^2)
I_d	Diametral Moment of Inertia
I_p	Polar Moment of Inertia
IGV	Inlet Guide Vane
J	Joule
K_p	Proportional Governor Control
KG	Kilogram; also kg
kPa	Kilopascal; also KPa
KSI	Thousands of Pounds Per Square Inch; also ksi
KVA	Kilovolt Ampere; also kVa
kW	Kilowatt
kW_e	Kilowatt, Electrical
kW_m	Kilowatt, Mechanical
kW_t	Kilowatt, Thermal
LAS	Lithium Aluminum Silicate
LB	Pound; also lb
LCF	Low Cycle Fatigue
LeRC	Lewis Research Center
LHV	Lower Heating Value
LOP	Low Oil Pressure
LP	Low-Pressure Side, Gas Side
m	Meter
M	Working Fluid Mass Flow (lb/sec); numeric subscripts refer to stations identified on Figure 3-55
M_W, M_F, M_C	Mass Flow (lb/sec)--Water, Fuel, Coolant
ma	Milliampere
MAS	Magnesium Aluminum Silicate
MEP	Module Electric Power Output (kW_e)
mm	Millimeter
MOR	Modulus of Rupture
MPa	Megapascal
MPS	Meters Per Second; also mps
MTBF	Mean Time Between Failures
N	Newton
N_e	Engine Speed; also N_E or N
N_G	Rotational Speed of Generator (rpm)
N_{reg}	Regenerator Speed
N_t	Rotational Speed of Turbocompressor (rpm)
$N/\sqrt{\theta}$	Corrected Speed
NASA	National Aeronautics and Space Administration
NC	Normally Closed
NEMA	National Electrical Manufacturers Association
NEP	Net Electric Power Output (kW_e)
NSP	Net Shaft Power to Generator (kW_m)

P	Pressure (psia); numeric subscripts, when used, refer to stations identified on Figure 3-55
P_{BAR}	Barometric Pressure
P_{IN}	Inlet Pressure
P_{REG}	Regenerator Drive Pressure
PCA	Power Conversion Assembly; also BE/G
PCU	Power Conversion Unit; also BE/G
P/N	Part Number
P-P	Peak-to-Peak (Displacement)
PPL	Parasitic Plant Loss
PS	Static Pressure
PSI	Pounds Per Square Inch
PSIA	Pounds Per Square Inch, Absolute
PSIG	Pounds Per Square Inch, Gage
PSL	Parasitic Shaft Power Loss to Driven Accessories (kW)
PT	Total Pressure
Q	Entropy Function
Q_C	Thermal Power from Combustor (kW_t)
Q_E	Thermal Power to Engine = $Q_R + Q_C$ (kW_t)
Q_{EL}	Heat Loss from Engine Surfaces (kW_t)
Q_R	Thermal Power from Receiver (kW_t)
Q_t	Heat Flow or Thermal Power (KW_t)
r_c	Radius of Compressor
R_e	Reynold's Number
RBSN	Reaction Bonded Silicon Nitride
RCVR	Solar Receiver Door
REG	Regulator
REP	Rectified Electric Power Output (kW_e)
RMS	Root Mean Squared
RPD	Reference Power-Train Design
RPM	Revolutions Per Minute; also rpm
SAE	Society of Automotive Engineers
SAGT	Solarized Automotive Gas Turbine
SAL	Shaft Accessory Load
SASC	Sintered Alpha Silicon Carbide
S/D	Shutdown
SEC	Second; also sec or s
SFC	Specific Fuel Consumption
Si_3N_4	Silicon Nitride
SL	Sea Level
S/N	Serial Number
SRBSN	Sintered Reaction Bonded Silicon Nitride
SSN	Sintered Silicon Nitride
T	Temperature; numeric subscripts, when used, refer to stations identified on Figure 3-55
$T_{4.1}$	Turbine Inlet Temperature; also TIT, T_{IN}, or T_7
TAN	Tangential
TBC	Test Bed Concentrator

TDT	Turbine Discharge Temperature
TIR	Total Indicator Reading
TIT	Turbine Inlet Temperature; also $T_{4.1}$, T_{IN}, or T_7
TSL	Rotating Group Losses (Bearings, Seals, Windage)
T-T	Total-to-Total
V	Volts
V_{ce}	Volts, Collector to Emitter
V_{ceo}	Volts, Collector to Emitter with Base Open
V_f	Voltage, Fuel Control
VAC	Volts, Alternating Current; also vac
VDC	Volts, Direct Current; also vdc
VIGV	Variable Inlet Guide Vane
W_a	Airflow
W_c	Coolant Flow
W_f	Fuel Flow
WT	Weight
β	Cycle Pressure Loss Fraction (Dimensionless, i.e., $[\beta = (1 - \sum \Delta P/P) = (r_T/r_C)]$
η	Efficiency
η_C	Compressor Efficiency
η_G	Generator Efficiency
η_{COMB}	Combustor Efficiency
η_{CSP}	Engine Cycle Shaft Power Efficiency = CPS ÷ Q_E
η_{ETS}	Electrical Transport System Efficiency
η_{GB}	Gearbox Efficiency
η_{GEP}	Engine Electric Power Efficiency at Generator Terminals = GEP ÷ Q_E
η_{INV}	Inverter Efficiency
η_{MEP}	Module Electric Power Efficiency = MEP ÷ Q_E
η_{NEP}	Net Electric Power Efficiency of Plant = NEP ÷ Q_E
η_R	Rectifier Efficiency
η_T	Turbine Efficiency
η_{TRANS}	Transformer Efficiency
θ	Temperature/Pressure Corrections
$\mu\epsilon$	Microinch (Inch x 10^{-6})

REFERENCES

1. Anderson, D.H., C.A. Fucinari, C.J. Rahnke, and L.R. Rossi, Annual Summary Report, No. 2630-1, Automotive Gas Turbine Ceramic Regenerator Design and Reliability Program, ERDA Contract No. E(11-1) 2630, September 15, 1976.

2. Cook, J.A., C.A. Fucinari, J.N. Lingscheit, and C.J. Rahnke, Annual Summary Report, No. 2630-18, Automotive Gas Turbine Ceramic Regenerator Design and Reliability Program, ERDA Contract No. E(11-1) 2630, October 15, 1976.

3. Kidwell, J.R., and D.M. Kreiner, "AGT101-Advanced Gas Turbine Technology Update," Paper Presented to the American Society of Mechanical Engineers (ASME), 85-GT-177, March 1985.

BIBLIOGRAPHY

Advanced Gas Turbine (AGT) Powertrain System Initial Development Progress Report, NASA CR-165130, August 1980.

Carruthers, W.D., D.W. Richerson, and K.W. Benn, 3500 Hour Durability Testing of Commercial Materials, Interim Report, NASA CR-159785, July 1980.

Ceramic Gas Turbine Engine Demonstration Program, Interim Report No. 17, May 1980, pp. 4-1 to 4-49, prepared under Contract N00024-76-C-5352.

Conceptual Design Study of Improved Automotive Gas Turbine Powertrain--Final Report, NASA CR-159580, May 1979.

Finger, D.G., Contact Stress Analysis of Ceramic-Metal Interfaces, Final Report, Contract N00014-78-C-0547, September 1979.

Johnson, I.A., et al., Aerodynamic Design of Axial Flow Compressors, NASA SP 36, 1965.

Menzik, Z., and M.A. Short, Quantitative Phase Analysis of Synthetic Si_3N_4 by X-Ray Diffraction: An Improved Procedure, Ford Motor Co. Scientific-Research Staff Technical Report No. SR-72-98.

Rice, R.W., S. Freiman, J.J. Mecholsky, R. Ruh, and Y. Harada, in Ceramics for High Performance Applications II (J.J. Burke, E.N. Lenoe, and R.N. Katz, eds.), Brook Hill Publishing Co., Chestnut Hill, Massachusetts, 1978.

Rice, R.W., and J.J. Mecholsky, in The Science of Ceramic Machinery and Surface Finishing II (B.J. Hockey and R.W. Rice, eds.), NBS Special Publication 562, 1979, pp. 351-378.

Richerson, D.W., J.J. Schuldies, T.M. Yonushonis, and K.M. Johansen, in Ceramics for High Performance Applications II (J.J. Burke, E.N. Lenoe, and R.N. Katz, eds.) Brook Hill Publishing Co., Chestnut Hill, Massachusetts, 1978.

Richerson, D.W., T.M. Yonushonis, and G.Q. Weaver, in Ceramic Gas Turbine Demonstration Engine Program Review (J.W. Fairbanks and R.W. Rice, eds.), MCIC Report MCIC-78-36, March 1978, pp. 193-217.

Stanitz, J.D., and V.D. Prian, A Rapid Approximate Method for Determining Velocity Distribution on Impeller Blades of Centrifugal Compressors, NACA TN 2421.

1. Report No.	2. Government Accession No.	3. Recipient's Catalog No.
CR-179559		

4. Title and Subtitle	5. Report Date
Brayton Cycle Solarized Advanced Gas Turbine: Final Report	December 1986
	6. Performing Organization Code
7. Author(s)	8. Performing Organization Report No.
Engineering Staff of Garrett Turbine Engine Company, A Division of The Garrett Corporation	31-6190
	10. Work Unit No.
9. Performing Organization Name and Address	11. Contract or Grant No.
Garrett Turbine Engine Company (GTEC) P.O. Box 5217 Phoenix, Arizona 85010	DEN3-181
	13. Type of Report and Period Covered
12. Sponsoring Agency Name and Address	Contractor Report February 1980-March 1986
U.S. Department of Energy Office of Conservation and Solar Applications Washington, DC 20545	14. Sponsoring Agency Code DOE/NASA/0181

15. Supplementary Notes

Final Report Under Interagency Agreement
Project Manager, Mr. Thomas N. Strom, Transportation Propulsion Division, NASA Lewis Research Center, Cleveland, Ohio 44135

16. Abstract

This report describes the development of a Brayton Engine/Generator Set for solar thermal to electrical power conversion, authorized under DOE/NASA Contract DEN3-181. The program objective was to design, fabricate, assemble, and test a small, hybrid, 20-kW Brayton-engine-powered generator set. The generator set, also called a power conversion assembly (PCA), is designed to operate with solar energy obtained from a parabolic dish concentrator, 11 meters in diameter, or with fossil energy supplied by burning fuels in a combustor, or by a combination of both (hybrid mode). The PCA consists of the Brayton cycle engine, a solar collector, a belt-driven 20-kW generator, and the necessary control systems for automatic operation in solar-only, fuel-only, and hybrid modes to supply electrical power to a utility grid.

The original configuration of the generator set, known as the Mod "0" System, incorporated the recuperated GTEC Model GTP36-51 gas turbine engine for the PCA prime mover. However, subsequent development of the GTEC Model AGT101 under DOE/NASA Contract DEN3-167 led to selection of the regenerated AGT101 as the power source for the PCA. Performance characteristics of the AGT101-powered PCA, thermally coupled to a solar collector (provided by Sanders Associates, Inc.) for operation in the solar mode, are presented in the report.

The PCA was successfully demonstrated in the fuel-only mode at the GTEC Phoenix, Arizona, facilities prior to its shipment to Sandia National Laboratory in Albuquerque, New Mexico, for installation and testing on a test bed concentrator (parabolic dish). Considerations relative to Brayton-engine development using the all-ceramic AGT101 when it becomes available, which would satisfy the DOE heat engine efficiency goal of 35 to 41 percent, are also discussed in the report.

17. Key Words (Suggested by Author(s))	18. Distribution Statement
Solar - Energy Brayton - Cycle Development Program Energy - Conservation	Unclassified - Unlimited Star Category 85 DOE Category UC-96

19. Security Classif. (of this report)	20. Security Classif. (of this page)	21. No. of Pages	22. Price*
Unclassified	Unclassified	120	

* For sale by the National Technical Information Service, Springfield, Virginia 22161